



University of Ioannina

Faculty of Sciences

Department of Physics

**Microstructural Characteristics and Dynamic
Behavior of Cu-Zr Metallic Glasses**

Lagogianni Alexandra

PhD Thesis

IOANNINA, 2014

«Η έγκριση της διδακτορικής διατριβής από το Τμήμα Φυσικής της Σχολής Θετικών Επιστημών, του Πανεπιστημίου Ιωαννίνων δεν υποδηλώνει αποδοχή των γνώμων του συγγραφέα Ν. 5343/32, άρθρο 202, παράγραφος 2»

Ημερομηνία αίτησης της κ. Λαγογιάννη Αλεξάνδρας: 345/16-2-2009

Ορισμός Τριμελούς Συμβουλευτικής Επιτροπής από τη Γ.Σ.Ε.Σ : 348/27-4-2009

Μέλη Τριμελούς Συμβουλευτικής Επιτροπής:

Επιβλέπων:

Ευαγγελάκης Γεώργιος, Καθηγητής Φυσικού, Πανεπιστημίου Ιωαννίνων

Μέλη:

Κομνηνού Φιλομήλα, Καθηγήτρια Φυσικού, Αριστοτελείου Πανεπιστημίου Θεσσαλονίκης

Παπαγεωργίου Δημήτριος, Αναπληρωτής Καθηγητής ΤΜΕΥ, Πανεπιστημίου Ιωαννίνων

Ημερομηνία ορισμού θέματος: 348/27-4-2009

Θέμα : «Μικροσκοπικά δομικά χαρακτηριστικά και δυναμική συμπεριφορά μεταλλικών υάλων»

ΟΡΙΣΜΟΣ ΕΠΤΑΜΕΛΟΥΣ ΕΞΕΤΑΣΤΙΚΗΣ ΕΠΙΤΡΟΠΗΣ από τη Γ.Σ.Ε.Σ:
437/7-4-2009

Ευαγγελάκης Γεώργιος, Καθηγητής Φυσικού, Πανεπιστημίου Ιωαννίνων

Κομνηνού Φιλομήλα, Καθηγήτρια Φυσικού, Αριστοτελείου Πανεπιστημίου Θεσσαλονίκης

Παπαγεωργίου Δημήτριος, Αναπληρωτής Καθηγητής ΤΜΕΥ, Πανεπιστημίου Ιωαννίνων

Λέκκα Χριστίνα , Επίκουρος Καθηγήτρια ΤΜΕΥ, Πανεπιστημίου Ιωαννίνων

Μπάκας Θωμάς, Καθηγητής Φυσικού, Πανεπιστημίου Ιωαννίνων

Κοσμιδής Κωνσταντίνος, Καθηγητής Φυσικού, Πανεπιστημίου Ιωαννίνων

Καμαράτος Ματθαίος, Αναπληρωτής Καθηγητής Φυσικού, Πανεπιστημίου Ιωαννίνων

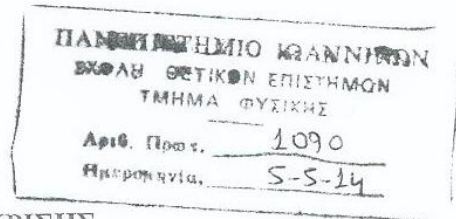
Έγκριση Διδακτορικής Διατριβής με βαθμό «άριστα» στις 2-5-2014

Ο Πρόεδρος του Τμήματος Φυσικής

Η α.α Γραμματέας του Τμήματος

Ιωάννης Ρίζος, Καθηγητής

Ευγενία Νάκου



ΠΡΑΚΤΙΚΟ

ΔΗΜΟΣΙΑΣ ΠΑΡΟΥΣΙΑΣΗΣ ΚΑΙ ΚΡΙΣΗΣ ΔΙΔΑΚΤΟΡΙΚΗΣ ΔΙΑΤΡΙΒΗΣ

Σήμερα, 2/ 5/ 2014, ημέρα Παρασκευή και ώρα 10.00, στην αίθουσα διαλέξεων του Τμήματος Φυσικής, πραγματοποιήθηκε η διαδικασία δημόσιας παρουσίασης και κρίσης ενώπιον της επταμελούς Εξεταστικής Επιτροπής της διδακτορικής διατριβής που εκτόνησε η υποψήφια κ. Αλεξάνδρα Λαγογιάννη στα πλαίσια του Προγράμματος Μεταπτυχιακών Σπουδών στη Φυσική.

Την επταμελή Εξεταστική Επιτροπή, που όρισε με σχετική απόφασή της η Γενική Συνέλευση με Ειδική Σύνθεση του Τμήματος Φυσικής σύμφωνα με το άρθρο 8.2 του Κ.Μ.Σ. (συν. αρ. 437 / 07-04-2014) αποτελούν οι:

1. Γ. Ευαγγελάκης Καθηγητής Τμήματος Φυσικής Π.Ι. (επιβλέπων)
2. Κ. Κοσμίδης, Καθηγητής Τμήματος Φυσικής Π.Ι.
3. Θ. Μπάκας, Καθηγητής Τμήματος Φυσικής Π.Ι.
4. Μ. Καμαράτος, Αναπλ. Καθηγητής Τμήματος Φυσικής Π.Ι.
5. Φ. Κομνηνού, Καθηγήτρια Τμήματος Φυσικής ΑΠΘ.
6. Χ. Λέκκα, Επικ. Καθηγητής Τμήματος Μηχανικών Υλικών Π.Ι.
7. Δ. Παπαγεωργίου, Αναπλ. Καθηγητής Τμήματος Μηχανικών Υλικών Π.Ι.

Η υποψήφια παρουσίασε και υποστήριξε δημόσια ενώπιον των μελών της Εξεταστικής Επιτροπής (η κ. Κομνηνού συμμετείχε με τηλεδιάσκεψη) την εκπονηθείσα διδακτορική διατριβή με τίτλο: «Δομικά χαρακτηριστικά και δυναμική συμπεριφορά μεταλλικών υάλων Cu-Zr»

Εν συνεχεία, τα μέλη της Επιτροπής δήλωσαν ομόφωνα ότι έμειναν ιδιαίτερα ικανοποιημένοι από την παρουσίαση και από τις απαντήσεις της υποψήφιας στις ερωτήσεις που του υποβλήθηκαν και έκριναν ομόφωνα ότι η εργασία είναι άρτια, άριστου επιπέδου και επιστημονικά ορθή.

Με βάση τα παραπάνω, η Επιτροπή εγκρίνει τη διδακτορική διατριβή, την βαθμολογεί με βαθμό Άριστα και εισηγείται την έγκρισή της από το Τμήμα Φυσικής καθώς και την απονομή στη κ. Αλεξάνδρα Λαγογιάννη του Διδακτορικού Διπλώματος στη Φυσική.

Τα μέλη της Εξεταστικής Επιτροπής

1. Γ. Ευαγγελάκης Καθηγητής Τμήματος Φυσικής Π.Ι. (επιβλέπων)
2. Κ. Κοσμίδης, Καθηγητής Τμήματος Φυσικής Π.Ι.
3. Θ. Μπάκας, Καθηγητής Τμήματος Φυσικής Π.Ι.
4. Μ. Καμαράτος, Αναπληρωτής. Καθηγητής Τμήματος Φυσικής Π.Ι.
5. Φ. Κομνηνού, Καθηγήτρια Τμήματος Φυσικής ΑΠΘ.
6. Χ. Λέκκα, Επικ. Καθηγητής Τμήματος Μηχανικών Υλικών Π.Ι.
7. Δ. Παπαγεωργίου, Αναπληρωτής. Καθηγητής Τμήματος Μηχανικών Υλικών Π.Ι.

Το ερευνητικό έργο συγχρηματοδοτήθηκε από την Ευρωπαϊκή Ένωση - Ευρωπαϊκό Κοινωνικό Ταμείο (ΕΚΤ) & Εθνικούς Πόρους, στα πλαίσια του προγράμματος με τίτλο «ΗΡΑΚΛΕΙΤΟΣ ΙΙ» το οποίο εντάσσεται στο Ε.Π.Ε.Δ.Β.Μ του Υπουργείου Παιδείας Διά Βίου Μάθησης και Θρησκευμάτων.



The research Project is co-funded by the European Union - European Social Fund (ESF) & National Sources, in the framework of the program “HRAKLEITOS II” of the “Operational Program Education and Life Long Learning” of the Hellenic Ministry of Education ,Life Long Learning and religious affairs .



Consultative jury

Evangelakis G., Professor of Physics Department, University of Ioannina

Komninou Ph., Professor of Physics Department, Aristotle University of Thessaloniki

Papageorgiou D., Assoc. Professor Department of Materials Science and Engineering,
University of Ioannina

Examining jury

Evangelakis G., Professor of Physics Department, University of Ioannina

Komninou Ph., Professor of Physics Department, Aristotle University of Thessaloniki

Papageorgiou D., Assoc. Professor Department of Materials Science and Engineering,
University of Ioannina

Lekka Ch., Assist. Professor of Department of Materials Science and Engineering,
University of Ioannina

Bakas T., Professor of Physics Department, University of Ioannina

Kosmidis K., Professor of Physics Department, University of Ioannina

Kamaratos M., Assoc. Professor of Physics Department, University of Ioannina

Abstract

This dissertation is devoted to the study of the relationship between the microstructure and the characteristic properties of Cu-Zr Metallic Glasses by means of computer simulations. The role of stoichiometry and the structural evolution upon cooling during the Glass formation process, as well as the microscopic mechanisms acting for the accommodation of mechanical solicitation was exhaustively studied in model 3D, 2D and 1D systems. In all cases it came out that the microstructure is dominated and characterized by tiny Icosahedral clusters that appear to play fundamental role for the stability, the glass formation and the mechanical response under tensile deformation of these systems. In particular, it was found that in all stoichiometries studied, Cu-centered 13-atom icosahedral clusters (ICO) are the basic structured unit present in the systems, while their number and their Cu content increases with Cu concentration. In addition, it came out that the solidification process upon cooling correlates with the ICO number evolution.

In addition, it was found that the mechanical response of bulk MG exhibits no strain rate sensitivity (SRS), while the accommodation of the deformation is strongly correlated with the number of nearly perfect Icosahedral (ICO) clusters present in the system, which enrich in Cu under strain, while their number drops continuously until fracture. In the case of systems with free surfaces it came out that their microstructure is again marked by the presence of ICOs whose number evolves similarly with the bulk case in the elastic region, to reach a plateau value after yielding. Moreover, positive strain rate sensitivity was found in this case, thus allowing for larger ductility than their bulk counterparts.

In the cases of 1D and 2D nanosized $\text{Cu}_{50}\text{Zr}_{50}$ Metallic Glasses (MG), it was found that the systems in ribbon geometry fail earlier than the systems in foil geometry, while in both

systems their mechanical behavior under tension is highly correlated with the evolution of icosahedral clusters.

Moreover, the case of building a metallic glassy thin film directly from icosahedral clusters, following processes similar to those occurring during cluster deposition was also addressed. The electronic and chemisorption characteristics of the deposited clusters that are closely related to the clusters' geometrical characteristics, such as size, shape, and structure, were taken into account in the study of the stability of $\text{Cu}_x\text{Zr}_{100-x}$ ($0 < x < 100$) icosahedral clusters (ICO), of four different sizes (147, 309, 561, 923 atoms) that were softly landed on the surface of the $\text{Cu}_{50}\text{Zr}_{50}$ metallic glass. From the calculated clusters' geometrical characteristics of the equilibrated systems, i.e. gyration radii, locations ICOs' center masses, etc., it came out that the deposited clusters become stable and preserve their initial structural symmetry as the number of Zr atoms and the clusters' size are increasing. Moreover, it was found that significant alterations in the resulting surface energies are induced upon ICOs deposition, depending on ICOs' size and their stoichiometry. The Cu-based ICOs were found to increase the surface energies by as much as 30% in the case of 923 atoms ICO.

Περίληψη

Η παρούσα διδακτορική διατριβή επικεντρώνεται στην σχέση μεταξύ της μικροδομής και των χαρακτηριστικών ιδιοτήτων των Μεταλλικών Υάλων Cu-Zr μέσω προσομοιώσεων σε ηλεκτρονικό υπολογιστή. Ο ρόλος της στοιχειομετρίας και η δομική εξέλιξη κατά την διάρκεια της ψύξης, διαδικασία στην οποία πραγματοποιείται η υαλοποίηση, καθώς επίσης και οι μικροσκοπικοί μηχανισμοί που λαμβάνουν χώρα κατά την διευθέτηση της μηχανικής παραμόρφωσης, μελετήθηκαν ενδελεχώς σε συστήματα τριών, δύο και μίας διάστασης, αντίστοιχα. Εξήχθηκε το συμπέρασμα ότι σε όλες τις παραπάνω περιπτώσεις συστημάτων, η μικροδομή χαρακτηρίζεται ως επί το πλείστον από μικροσκοπικά συσσωματώματα εικοσαεδρικής δομής τα οποία εμφανίζονται να παίζουν κυρίαρχο ρόλο τόσο στην σταθερότητα όσο και στην διαδικασία υάλωσης, καθώς επίσης και στην μηχανική απόκριση των συστημάτων κατά την επιβολή εφελκυστικής παραμόρφωσης.

Πιο συγκεκριμένα βρέθηκε ότι σε όλες τις υπό μελέτη στοιχειομετρίες, η κύρια δομική μονάδα ήταν τα εικοσαεδρικά συσσωματώματα δεκατριών ατόμων με άτομο χαλκού στο κέντρο, των οποίων τόσο ο αριθμός όσο και το ποσοστό τους σε άτομα χαλκού (άτομα κελύφους) αυξάνονταν καθώς αυξανόταν το ποσοστό χαλκού στην στοιχειομετρία του συστήματος. Επιπρόσθετα, αποδείχθηκε ότι η διαδικασία στερεοποίησης των συστημάτων συσχετίζεται άμεσα με την εξέλιξη του αριθμού αυτών των συσσωματωμάτων. Επίσης κατά την μελέτη της μηχανικής απόκρισης των συστημάτων όγκου (bulk) βρέθηκε ότι αυτά τα συστήματα δεν παρουσιάζουν ευαισθησία στον ρυθμό παραμόρφωσης (strain rate sensitivity) που τους επιβάλλεται, ενώ η διευθέτηση της μηχανικής παραμόρφωσης είναι ισχυρά συσχετισμένη με τον αριθμό των σχεδόν τέλειων εικοσαεδρικών συσσωματωμάτων που υπάρχουν στο σύστημα, τα οποία εμπλουτίζονται σε άτομα χαλκού, καθώς η παραμόρφωση αυξάνει, ενώ ο αριθμός τους διαρκώς μειώνεται μέχρι το

σημείο της θραύσης του υλικού. Στην περίπτωση των συστημάτων που είχαν ελεύθερες επιφάνειες, παρατηρήθηκε πάλι ότι η μικροδομή τους κυριαρχείται από εικοσαεδρικά συσσωματώματα και ο αριθμός τους εξελίσσεται με ανάλογο τρόπο με αυτό των συστημάτων όγκου, συγκλίνοντας σε μία σταθερή τιμή μετά το όριο διαρροής. Επίσης παρατηρήθηκε θετική ευαισθησία ρυθμού παραμόρφωσης, γεγονός που επιτρέπει στα συστήματα να επιδεικνύουν μεγαλύτερη ολκιμότητα από τα αντίστοιχα συστήματα όγκου που επιδεικνύουν μηδενική ευαισθησία στον ρυθμό παραμόρφωσης που τους επιβάλλεται.

Στις περιπτώσεις των συστημάτων με μία και δύο διαστάσεις, τάξης μεγέθους νανομέτρων, παρατηρήθηκε ότι τα συστήματα με γεωμετρία ταινίας (ribbon) καταρρέουν πρώτα σε σχέση με τα αντίστοιχα συστήματα με γεωμετρία φύλλου, ενώ και στις δύο περιπτώσεις συστημάτων η μηχανική τους απόκριση κατά την διάρκεια εφελκυσμού είναι ισχυρά συσχετισμένη με την εξέλιξη των εικοσαεδρικών συσσωματωμάτων.

Επιπρόσθετα, μελετήθηκε η περίπτωση 'δημιουργίας' υμενίου από μεταλλική ύαλο με ανάλογη διαδικασία με αυτήν που λαμβάνει χώρα κατά την πειραματική εναπόθεση εικοσαεδρικών συσσωματωμάτων σε επιφάνεια. Γνωρίζοντας ότι τα ηλεκτρονικά χαρακτηριστικά των εναποτιθέμενων συσσωματωμάτων είναι σθεναρά συσχετισμένα με τα γεωμετρικά χαρακτηριστικά τους, όπως το μέγεθός τους, την μορφή τους, την δομή τους, όσον αφορά στην σταθερότητα των $\text{Cu}_x\text{Zr}_{100-x}$ ($0 < x < 100$) εικοσαεδρικών συσσωματωμάτων, μελετήθηκαν τέσσερα διαφορετικά μεγέθη (147,309, 561,923 άτομα) εικοσαεδρικών συσσωματωμάτων τα οποία εναποτέθηκαν στην επιφάνεια μεταλλικής ύαλου με στοιχειομετρία $\text{Cu}_{50}\text{Zr}_{50}$. Από τα γεωμετρικά χαρακτηριστικά των συσσωματωμάτων που υπολογίστηκαν, όπως η γυροσκοπική ακτίνα, η σχετική αλλαγή των κέντρων μάζας τους, το ποσοστό των ατόμων τους που παρέμεινε πάνω από την επιφάνεια μετά την εναπόθεσή τους κτλ., παρατηρήθηκε ότι τα συσσωματώματα μετά την

εναπόθεσή τους, ήταν σταθερότερα και διατηρούσαν την αρχική γεωμετρική τους δομή , όσο το ποσοστό του ζirkονίου στα άτομα τους αυξάνονταν. Επίσης βρέθηκε ότι σημαντικές αλλαγές επήλθαν στις επιφανειακές τους ενέργειες λόγω της εναπόθεσης των συσσωματωμάτων, οι οποίες εξαρτιόνταν από το μέγεθος καθώς και την ίδια την στοιχειομετρία του συσσωματώματος που εναποθέταμε. Τέλος βρέθηκε ότι τα πλούσια σε άτομα χαλκού εικοσαεδρικά συσσωματώματα αύξαναν την επιφανειακή ενέργεια μέχρι και κατά 30%, ποσοστό το που βρέθηκε στην εναπόθεση συσσωματώματος με 923 άτομα και πλούσιο σε χαλκό.

Acknowledgements

First of all I would like to express my gratitude to my professor Prof. Evangelakis for introducing me to Molecular Dynamic Simulations and the fascinating world of Metallic Glasses. He has provided excellent guidance and has supported me, both scientifically and psychologically, in the most explicit way. All conversations with him were very constructive, and he has supplied to me lots of knowledge, yet without limiting my critical thinking.

Furthermore, I would like to thank the Assoc. Prof. D.G Papageorgiou and Assist. Prof. Ch. E Lekka for being so helpful and generous concerning several scientific issues. Discussions with Assoc.Prof. D.G Papageorgiou were extremely fruitful, and he has always been available to solve any simulation problem might appear during my work.

Additionally, I would like to thank Prof. Ph. Komninou from the Department of Physics of Aristotle University of Thessaloniki for her extremely useful advice on both scientific and career issues as well as for the encouragement she provided during my presentations at the conferences we met each other.

Moreover, I would like to express my gratitude to the other members of my committee from the Physics Department of Ioannina, namely Prof. C. Kosmidis, Prof. T. Bakas and Assoc. Prof. M. Kamaratos for all the valuable knowledge they passed on to me during the years of my studying at the Physics Faculty and for accepting to participate in my PhD defense committee..

In addition, I feel obliged to thank my colleague, Dr. Nikos Panagiotopoulos, my best friend during all my academic studies, for being a great partner, and for the infinite hours of hanging out and talking. I have been extremely lucky to interact with such a wonderful

person. This also stands for all guys in the lab, they created a beautiful environment and made every day special. It has been a pleasure working with all of them! I would also like to thank all my friends: Nikos, Marilena, Maria, Smaragda, Sarantis, Ioanna, Olga, Theano, George, Martha, Jason, Gregory, Almy, Loukas and lots of others for helping me conserving my sanity. I would need many pages to mention you all!

Last but not least, I am grateful to my parents Emmanuel and Kyriaki and to my brother Ioannis, for supporting me both emotionally and financially, from the first day of my life until now. Thank you so much for everything that you helped me achieve, and for everything that I hope to achieve in the future.

Λαγογιάννη Εμμανουήλ και Κυριακή, δεν μπορώ να περικλείσω μέσα σε μια δυο προτάσεις την απέραντη ευγνωμοσύνη που νιώθω, για όλα αυτά που μου έχετε προσφέρει, από την πρώτη μέρα της ζωής μου ως τώρα. Θεωρώ τον εαυτό μου ευλογημένο που είστε γονείς μου. Δεν μπορώ παρά να σας ευχαριστήσω μέσα από την καρδιά μου για όλα όσα με βοηθήσατε να καταφέρω ως τώρα.

Dedicated to my family

Αφιερωμένο στους γονείς μου

Εμμανουήλ και Κοριακή

Contents

Introduction	1
I. Chapter 1.....	20
1.1. Metallic glasses	22
1.2. History and progress of Metallic Glasses	24
1.3. Properties and Applications	25
1.4. Drawbacks	29
1.5. Glass forming ability of Metallic Glasses.....	30
1.6. References.....	34
II. Chapter 2.....	37
2.1. Introduction. (Aim of the present work).....	38
2.2. Why we selected CuZr as model system.....	41
2.2. Why Simulations- techniques	42
2.3. Molecular Dynamic Simulations (MD).	43
2.4. Basic concepts of Molecular Dynamic Simulation	45
2.5. Verlet algorithm	48
2.6. A short description of Statistical Mechanics-Ensembles.....	51
2.7. TBSMA – Potential model	57
2.8. Boundary conditions.	59
2.9. Basic thermodynamic properties extracted from trajectories of MD simulations.	60
2.10. Computational Tools for structural analysis	62
2.10.1. Radial Distribution Function	62
2.10.2. Common Neighbor Analysis (CNA)	64
2.11. References.....	67
III. Chapter 3.....	69
Relationship between microstructure, temperature and stoichiometry.....	70
3.1. RESULTS -Introduction	71
3.2. Preparation of the systems	72
3.3. Results.....	73
3.4. Concluding remarks.....	76
3.5. References.....	77

IV. Chapter 4.....	78
Correlation between microstructure and tensile deformation	79
4.1. Introduction	80
4.2. Computational details.....	81
4.3. Results.....	82
4.3.1. Bulk systems.....	82
4.3.2. Results	93
4.3.3. Conclusions.....	100
4.3.4. Cross-Correlation.....	101
4.3.5. References.....	110
V. Chapter 5.....	112
Mechanical behaviour of 1D and 2D nanosized systems.....	113
5.1. Introduction	114
5.2. Computational details.....	114
5.3. Results.....	115
5.3.1. 1D nanosized systems (ribbons).....	115
5.3.2. 2D nanosized systems (foils).....	116
5.4. Comparison of the microstructural alterations between foils and ribbons.....	118
5.5. Influence of the strain rate on foils.....	119
5.6. References.....	125
VI. Chapter 6.....	127
Clusters as <i>building blocks</i> of MGs	128
6.1. Introduction	129
6.2. Computational details.....	130
6.3. Results and discussion.....	132
6.3.1. Characterization of the microstructure.....	132
6.3.2. Energetic considerations	136
6.4. Concluding remarks.....	142
6.5. References.....	143

I. Chapter 1

1.1. Metallic glasses

The first thought that comes to mind is how a glass can be metallic. This arguable question arises from the fact that the word “glass”, in our daily life, commonly refers to the window glass, and a window glass is transparent, while metals are not. The term “glasses” is used to describe amorphous (from the greek word “amorphos”, ἀμορφος) or disordered non-crystalline materials (alloys), lacking of all characteristics of their crystalline counterparts, like structural periodicity, defects, slip planes, stacking faults etc. And the epithet “metallic” is used to describe the constituent elements of these alloys that are always metallic. Referring to their metallic nature they exhibit characteristics like non-directional metallic bonds, specular reflection and electrical conductivity, although less in comparison with crystalline alloys and elements.

Metallic glasses (MGs) exhibit short (SRO, below 0.5nm) or medium -range- order (MRO, between 0.5 and 3nm), but they lack of large-range –order (LRO, beyond 3nm). Usually they can be obtained from the liquid phase by undercooling, using efficiently high cooling rates (10^1 to 10^6 K/sec), to temperatures well below their glass transition temperature (T_g). Efficient cooling rate is the critical cooling rate that is required upon solidification to suppress nucleation and growth of crystalline phases and thus crystallization. At this cooling rate the atoms don't have enough time and energy to move towards more stable positions and coordinate themselves, and the resulting alloy enters an amorphous state where it can be regarded as a “frozen liquid”.

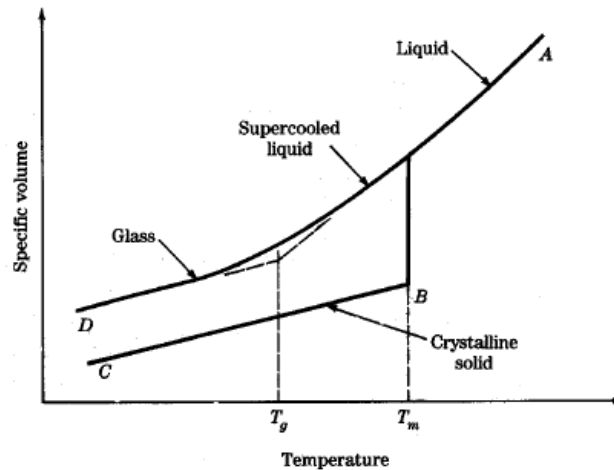


Fig.1.1. Evolution of specific volume versus temperature upon solidification.

Despite the fact that metallic glasses exhibit a clear similarity with liquids they have some main differences, for example their viscosity is by order of magnitudes higher compared to that of liquids. Moreover in liquids, atoms possess translational degrees of freedom, so they can diffuse easily compared to the atoms of a glass where their atomic mobility is suppressed and they behave like in a rigid solid. Nevertheless, their Gibbs free energy is higher than crystalline solids (less Gibbs energy leads to more stable states); therefore they are considered as to be metastable.

Another critical difference between liquids and glasses is that the former display independent structure and properties from thermal history, while the latter's structure and properties are strongly affected by the thermal history and the techniques-procedures applied for their preparation [1]. Metallic glasses can be obtained by a large variety of techniques like vapour-, electro-deposition techniques [2,3] sputtering [4], atomic condensation [5] or rapid liquid quenching [6,7]. The most commonly used technique is the rapid liquid quenching, which can be achieved by splat quenching, melt spinning, water

quenching or copper-mold casting; depending on the specific technique a different cooling rate is imposed [8].

1.2. History and progress of Metallic Glasses

The first ever reported metallic glass was the alloy $\text{Au}_{75}\text{Si}_{25}$ (%w), obtained by rapid solidification (at rates of 10^6 K/sec) from liquid, and it was in a publication in Nature on September 3, 1960 by Duwez, Klement and Willens [9, 10]. Unfortunately, the alloy had been transformed into a non equilibrium crystalline state after 24 hours at room temperature due to its low thermal stability. Additionally, the acquired high cooling rate for this solidification process limits the one dimension of the specimen and thus the early developed products by this technique were always in foil, ribbon, wire geometries or powders leading to a limited range of applications.

During the following decades an immense number of efforts have been devoted to the increase of specimens' sizes by means of techniques with slower cooling rates (water quenching) or by trying different combinations of metallic elements aiming in enhancing the glass forming ability of the alloys. In 1971 the first metallic glass, in rods geometry with diameter in the range of millimeters, was an alloy of Pd-Cu-Ni produced by casting at a cooling rate of 10^3 K/sec by Chen Willens.

That was the time that the arbitrary term "bulk" was established for describing metallic glasses of such dimensions (millimeters), known as Bulk Metallic Glasses (BMGs). Since then on, many alloys based on lanthanum, aluminum, copper [11], magnesium [12], and zirconium [13] were found to have excellent glass forming ability. The first commercial metallic glass, known as Vitreloy 1 $\text{Zr}_{41.2}\text{Ti}_{13.8}\text{Cu}_{12.5}\text{Ni}_{10}\text{Be}_{22.5}$ [14] was developed in Caltech in 1993, and this work

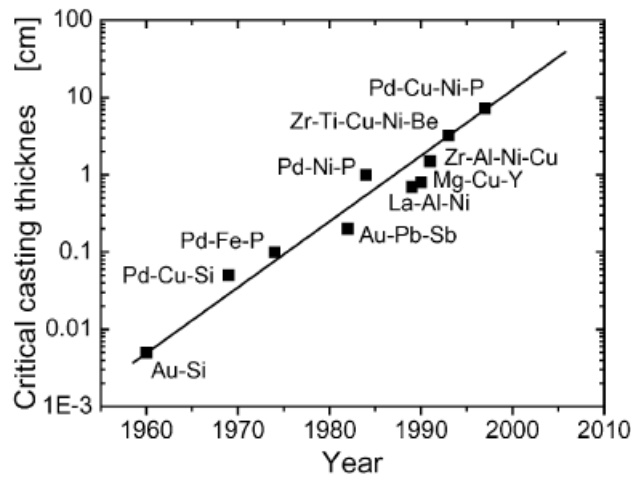


Fig.1.2. The evolution of critical casting thickness from 1960 till 2000.

accompanied from the work of Inoue's group was the starting point of the use of BMG in structural applications.

In conclusion, the appearance of a new class of materials was a fact, and the exhaustive study and progress until now has contributed not only in the understanding of the glassy nature generally, but it stimulated work on equilibrium and supercooled metallic liquids.

1.3. Properties and Applications

The absence of crystalline characteristics and long-range-order (LRO) endows the MGs with an attractive combination of properties that make them suitable candidates for many applications against other conventional engineering materials. More specifically the specific (fracture) strength of MGs has been found more than twice as high as that of crystalline materials, with the highest values around $600\text{MPa}/\text{gr}/\text{cm}^3$ [15]. They are considered as one of the best spring materials because they store high elastic energy per unit volume and mass, as a consequence of their high elastic strain. Also, MGs have high strength (twice that of steel, while they are lighter).

Due to their high hardness, corrosion and wear resistance [16, 17], low density and the ability to cast into a net-shape with a mirror finish and a complex shape, they are used for tooling, particularly as knife edges [18]. Also, jewels are produced from MGs because of their excellent polish-ability, abrasion and corrosion resistance [19].

Aiming in widening the industrial application fields of MGs they are commonly used for coatings because this technique is not affected by their limited size and brittleness [20]. MGs coatings can be deposited by several processes like plasma spraying [21] high velocity oxy-fuel (HVOF) spraying [22], cold gas dynamic spraying [23] and the resultant coatings are free from oxides, they have low porosity and high density and of course excellent mechanical properties. Table 1.1 gathers some basic applications of MGs, based on different combinations of their properties and thus different applications.

Current and possible applications of BMGs	
Application	Technical reasons
Golf clubs (commercialised)	High strength, high σ_y/E , σ_y^2/E
Knives for ophthalmology (commercialised)	High hardness, wear and corrosion resistance, high σ_y^3/E^2
Edges for sport goods (skis, skates)	High hardness, wear and corrosion resistance, high σ_y/E , ability to be sharpened
Precision mechanical elements	High strength, high hardness, wear and corrosion resistance, good abilities for surface finishing
Materials for digital master discs	Wear resistance, no grain structure
Dental materials	High strength, hardness, wear and corrosion resistance, castability, abilities for surface finishing
Wires for musical instruments	High strength, high workability
Jewellery (Pd and Pt-based alloys)	High hardness, wear and corrosion resistance, lustre, precious metal content
Machinery structural material (high performance springs)	High σ_y^2/E , high fatigue strength, high workability

Table.1.1. Applications of MGs due to specific mechanical properties [24].

A more recent application of metallic glasses, especially those of Ti-based, is in the field of medicine, as implants. Their improved corrosion properties, high fracture strength and wear resistance, increased elastic strain range and lower Young's modulus, make them favorable implant materials in trauma and orthopedic surgery [25,26] as well as for dental root implants [27,28].

Another attractive characteristic of MGs is that in a rather small temperature range, called supercooled liquid region, $\Delta T = T_x - T_g$ (corresponding to the crystallization and glass formation temperatures, respectively) they become soft and can be easily, deformed, stretched, bent, and formed into many complex shapes.

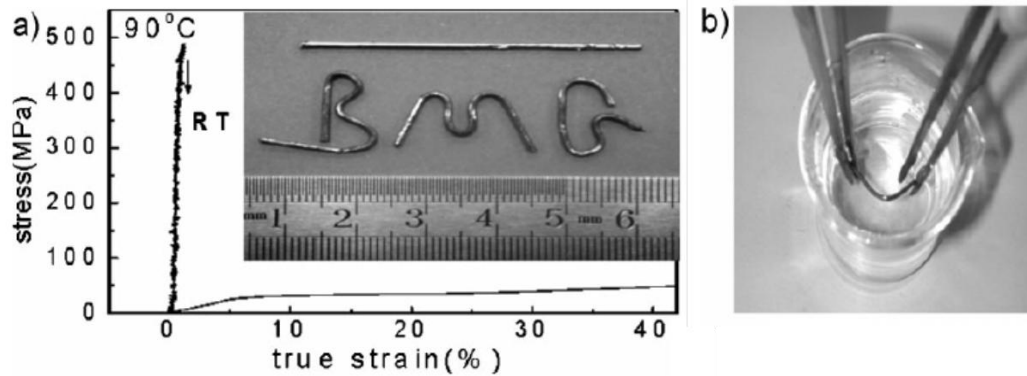


Fig.1.3. a) Stress–true-strain curve of $Ce_{70}Al_{10}Cu_{20}$ glassy rod (with 2 mm diameter) under compressive deformation at RT and at 90C. The inset photo shows letters formed by these glassy rods by simple manipulation in near-boiling water as shown in b) [29].

This polymer-like thermoplastic behavior, combined by the incredible ability of shaping in very-fine microstructures (even in nanoscale), within the supercooled liquid region, is unusual for conventional metallic materials and it is of great importance for MEMS (micro-electromechanical) devices where high-precision parts are needed [30-32]. The reason that make MGs suitable candidates for such applications is that compared with most polymers, when returned to room temperature after thermoplastic treatment, they maintain metallic-nature behavior, such as high strength and good electric conductivity.

Another very interesting feature of MGs, provided both from experimental and theoretical results, is that many of their mechanical properties are strongly correlated with others. In Fig.1.4 displays the strong linear correlation between the fracture strength and Young

Modulus and Fig.1.5 the correlation shear stress at yielding and shear modulus at room temperature of various Bulk Metallic Glasses, BMGs.

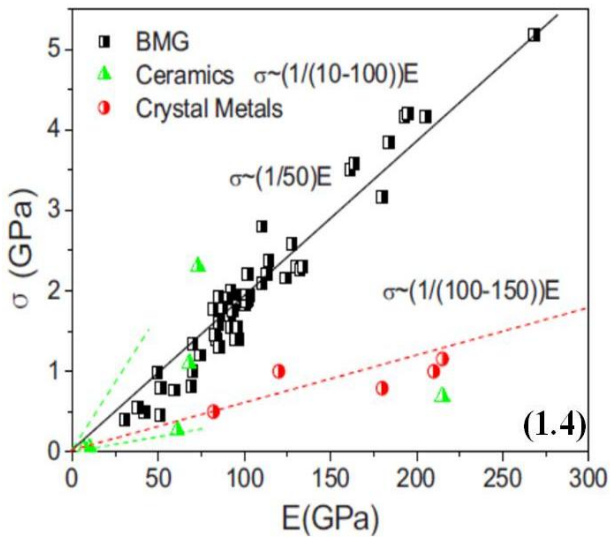


Fig.1.4. Left picture corresponds to the correlation between fracture strength Young modulus [33].

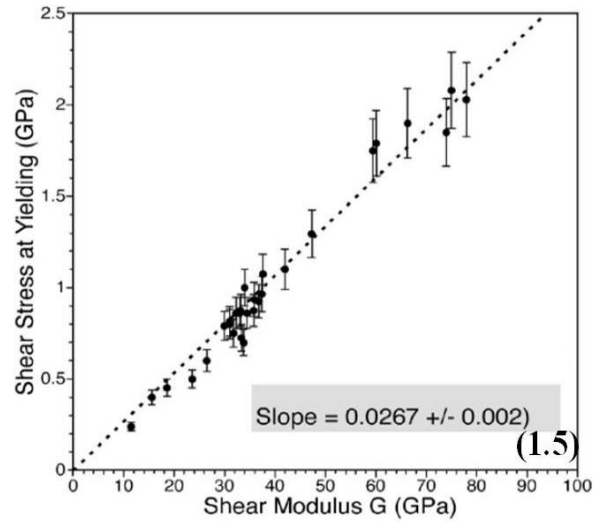


Fig.1.5. Right picture shows the high correlation between shear and stress and shear modulus [34].

The next figure displays a diagram about the correlations between elastic modules, glass formation and structural and mechanical properties.

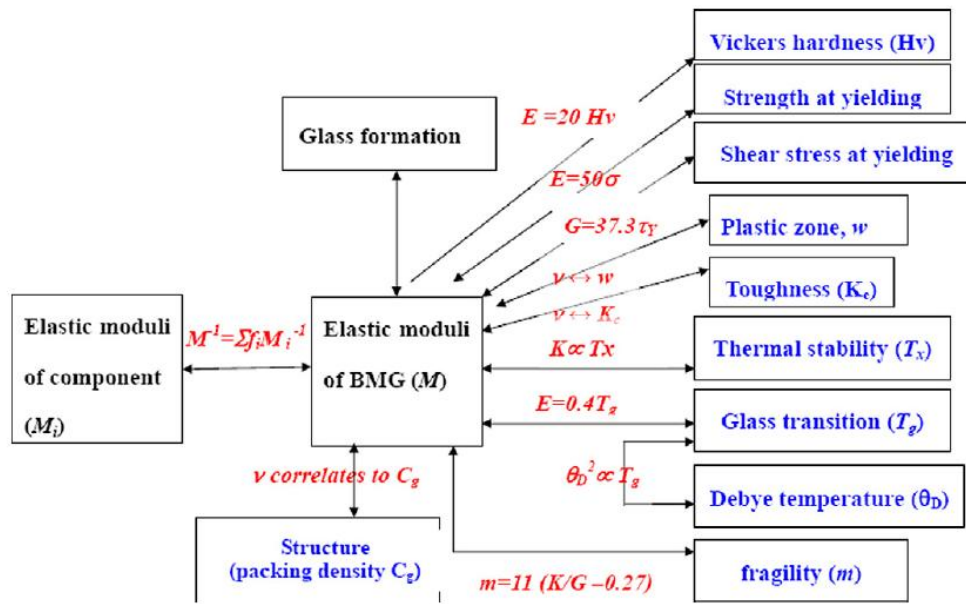


Fig.1.6. Correlations between the elastic moduli, glass formation, structure and properties of the metallic glasses [35].

1.4. Drawbacks

Similarly with all the materials, metallic glasses display their own drawbacks that restrict their applications. One of their basic flaws is that they exhibit low plasticity at room temperature and more specifically their plastic strain at compression is extremely low (~2%), while at uniaxial tension is almost zero [36-38]. In the effort to deform MGs they fail catastrophically through the formation of what's termed "shear Bands". Shear bands are regions where a large strain is accumulated in a very-thin region (typically 10–20nm thick), exhibiting strain softening or thermal softening [36-40].

Another critical issue is their production cost which is generally much higher than the one of conventional crystalline alloys and it is due to the fact that their melting and processing often requires high-purity elements and expensive vacuum-processing techniques.

1.5. Glass forming ability of Metallic Glasses

Understanding the glass forming ability (GFA) is equivalent to understand the crystallization process both from kinetic and of thermodynamic point of view. One approach to represent the competition between crystallization and glass formation is the time-temperature-transformation (TTT) diagrams. Fig.1.7 shows an example of a TTT diagram of $\text{Pd}_{40}\text{Cu}_{30}\text{Ni}_{10}\text{P}_{20}$ [41] where the onset times for isothermal crystallization are plotted as a function of temperature. This TTT diagram exhibits the typical “C” or “nose” shape due to the fact that the thermodynamic driving force for crystallization increases with increasing undercooling, while the atomic mobility in liquid reduces, and it can provide a good estimation of the processing time available for an amorphous solid to be formed.

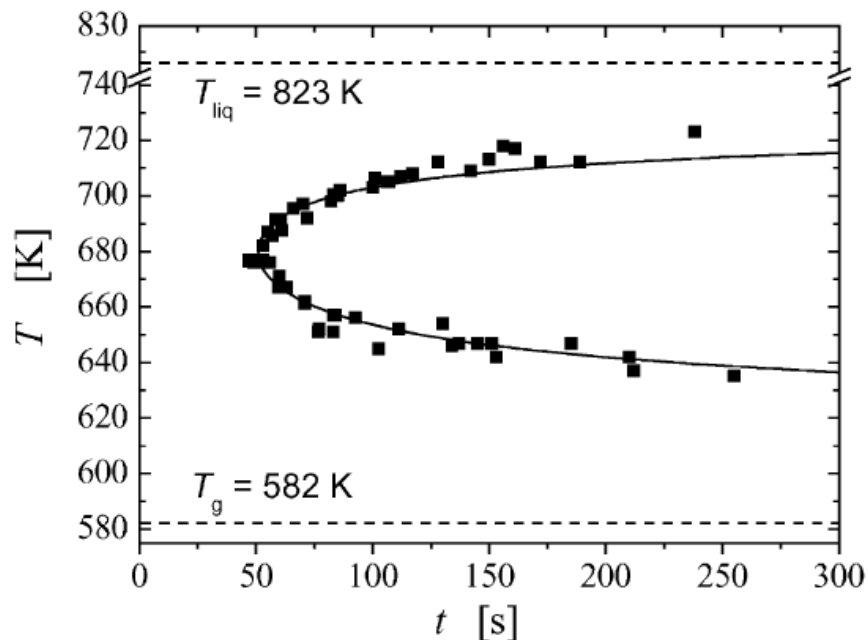


Fig.1.7. Typical TTT diagram of $\text{Pd}_{40}\text{Cu}_{30}\text{Ni}_{10}\text{P}_{20}$ [41]

Some of the most well known, from 1970, indicators of GFA, based on thermodynamic parameters as temperature, combine the three important temperatures such as T_g , T_x and T_l (the glass formation temperature, the onset of crystallization and the liquidus temperature, respectively) which can be easily measured from Differential Scanning Calorimetric curves (DSC) [42,43].

One of them is the reduced glass transition temperature T_{rg} ($T_{rg} = T_g/T_l$) which is defined as the ratio of T_g and T_l and it was shown that for metallic glasses with $T_{rg} > 2/3$ the homogeneous nucleation was suppressed [42] and thus a higher GFA was achieved. Besides T_{rg} another GFA indicator, proposed by Inoue [44], is the supercooled liquid region the temperature difference between T_g and T_x , $\Delta T_{xg} = T_x - T_g$. It pointed out that the GFA is higher when the ΔT_{xg} is higher because it shows that the supercooled liquid can exist in a wider temperature range without being crystallized and thus it is characterized by a higher resistance to nucleation and growth of crystalline phases and indirectly it exhibits a higher thermal stability. The γ parameter, $\gamma = T_x / (T_g + T_l)$ was also proposed by Lu and Liu [45,46] in order to predict GFA.

From an engineering point of view the GFA is strongly affected by the critical cooling rate and the critical casting thickness (the appropriate cooling rate to bypass crystallization and the maximum achievable thickness that an alloy can be cast to without being crystallized, respectively) [47]. More specifically the lower the cooling rate and the higher the casting thickness, the higher the GFA of a metallic glass will be.

In the same direction, Inoue proposed three empirical rules to achieve high GFA [48, 49]. The metallic glass should contain three or more components, 2) The atomic size mismatch between the constituent elements should be greater or equal to 12%; 3) The elements should have large negative of mixing.

An expansion of Inoue's criteria was the confusion principle suggested by A.L. Greer [50], which states that the GFA of an alloy is enhanced due to fact that the addition of large number of constituent elements in the alloy prevents the formation of possible crystalline phases upon cooling. Actually this is achieved because the addition of more elements "frustrates" the tendency of the alloy to become crystalline by making the melt more stable than the crystalline phases.

From thermodynamic and kinetic point of view, during the cooling of a liquid below its melting point, the free energy difference (ΔG) between the liquid and the crystal creates a driving force for the crystal nucleation, and at the same time the creation of a liquid-crystal interface creates also a positive interfacial energy that suppresses nucleation. So, there is an energy barrier that it has to be overcome in order a nucleus to be formed. To this purpose the atoms of the liquid need to be rearranged and the rate of such atomic transport is described by the atomic diffusivity, D , which is inversely proportional to the viscosity, η , according to the Stokes-Einstein equation $D = k_B T / 3\pi\eta l$ where k_B is Boltzmann's constant, l is the atomic diameter and η the viscosity.

The crystal nucleation rate I_v is given by:

$$I_v = \frac{A_n}{n(T)} e^{-\frac{\Delta G}{k_B T}} \quad (1.1)$$

where the kinetic part is the first term of the product and the thermodynamic part is the second one. A_n is a constant, k_B is Boltzmann constant, T is the temperature, $n(T)$ is the viscosity and ΔG is the energy barrier that has to be overcome in order for a stable nucleus to be formed; for the case of a spherical nucleus ΔG is given by:

$$\Delta G = \frac{16\pi\sigma^3}{3(\Delta G_{l-s})^2} \quad (1.2)$$

Where σ is the interfacial energy between liquid and nuclei and ΔG_{l-s} is the Gibbs energy difference between the liquid and crystal phase per unit volume. In equation (1) the term $n(T)$ is given by the Vogel–Fulcher–Tamman (VFT) relation [51].

$$n(T) = n_0 e^{\left(\frac{D^* T_0}{T - T_0}\right)} \quad (1.3)$$

where D^* is the fragility parameter and T_0 is the VFT temperature, and n_0 is a constant which is inversely proportional to the molar volume of the liquid. Actually, D^* represents how much the viscosity of a supercooled liquid deviates from the Arrhenius behavior and T_0 is the temperature where the viscosity $\eta \rightarrow \infty$. Obviously the fragility, the VFT temperature and the liquidus temperature influence the nucleation rate of a crystal, through their relation with viscosity, and thus the glass forming ability. More specifically higher reduced VFT temperatures (T_0/T_1) lead to smaller values of nucleation rate and consequently to enhanced GFA.

1.6. References

- [1] H. S. Chen, H. J. Leamy, and C. E. Miller *Ann. Rev. Mater. Sci.* 1980. 10. 363-9
- [2] J. Kramer, *Ann. Phys.* 19 (1934) 37.
- [3] W. Buckel, R. Hilsch, *Z. Phys.* 132 (1952) 420
- [4] Y.P. Deng, Y.F. Guan, J.D. Fowlkes, S.Q. Wen, F.X. Liu, G.M. Pharr, P.K. Liaw, C.T. Liu, P.D. Rack Vol 15, Issue 9, 2007, 1208–1216
- [5] Uhlmann, D.R. (1972). *J. Non-Cryst. Solids* 7: 337–348.
- [6] D. Turnbull, *Metall. Trans. A* 12 (1981) 695,
- [7] A.L. Greer, *Science* 267 (1995) 1947.
- [8] H. S. Chen, H. J. Leamy, and C. E. Miller, *Ann. Rev. Mater. Sci.* 1980, 10, 363-91
- [9] Klement, W., R.H. Willens, and P. Duwez (1960), *Nature* 187: 869–870.
- [10] Duwez, P. (1981). *Metallic glasses—Historical background*. In *Glassy Metals I* eds. H.-J. Güntherodt and H. Beck, pp. 19–23. Berlin, Germany: Springer-Verlag.
- [11] Inoue A, Zhang T, Masumoto T. *Mater Trans JIM* 1989;30 965–72.
- [12] Inoue A, Kato A, Zhang T, Kim SG, Masumoto T. *Mater Trans JIM* 1991;32:609
- [13] Zhang T, Inoue A, Masumoto T.. *Mater Trans JIM* 1991;32:1005–10.
- [14] Peker A, Johnson WL. *Appl Phys Lett* 1993;63:2342–4.]
- [15] A. Inoue, B.L. Shen, H. Koshiba, H. Kato, A.R. Yavari, *Nat. Mater.* 2 (2003) 661.
- [16] T. Gloriant, *J. Non-Cryst. Solids* 316 (2003) 96,
- [17] X.Y. Fu, D.A. Rigney, M.L. Falk, *J. Non-Cryst. Solids* 317 (2003) 206
- [18] M.F. Ashby, A.L. Greer *Scripta Mater*, 54 (2006), p. 321
- [19] M.F. Ashby, A.L. Greer *Scripta Mater*, 54 (2006), p. 321

- [20] Jiangbo Cheng, Xiubing Liang, Binshi Xu, Yixiong Wu, *J. Mater. Sci. Technol.*, 25, 5, (2009).
- [21] F. Otsubo and K. Kishitake: *Mater. Trans.*, 2005, 46, 80.
- [22] Y. Wu, P. Lin, C. Chu, Z. Wang, M. Cao and J. Hu: *Mater. Lett.*, 2007, 61, 1867.
- [23] L. Ajdelsztajn, B. Jodoin, P. Richer and E. Sanoucy: *J. Therm. Spray Technol.*, 2006, 15(4), 495.
- [24] A.I. Salimon, M.F. Ashby, Y. Bréchet, A.L. Greer *Mater. Sci. Eng. A*, 375–377 (2004), pp. 385–388
- [25] M. Long, H.J. Rack, *Biomaterials* 19 (1998) 1621–1639.
- [26] M. Niinomi, *Metals for Biomedical Devices*, CRC Press, 2010
- [27] K. Yokoyama, T. Ichikawa, H. Murakami, et al., *Biomaterials* 23 (2002) 2459–2465.
- [28] M.G.Manda, P.P. Psyllaki, D.N. Tsipas, P.T. Koidis, *J. Biomed. Mater. Res. B* 89B (2009) 264–273.
- [29] W.H. Wang, *Adv. Mater.* 2009,21,4524-4544
- [30] B. Zhang, W. H. Wang, *J. Non-Cryst. Solids* 2006, 352, 5687.
- [31] X. F. Liu, R. J. Wang, D. Q. Zhao, M. X. Pan, W. H. Wang, *Appl. Phys. Lett.* 2007, 91, 041901
- [32] J. Q. Wang, W. H. Wang, H. Y. Bai, *Appl. Phys. Lett.* 2009, 94, 041910.
- [33] C.C. Yuan X. K Xi *J. Appl. Phys.* 109 033515 (2011)
- [34] W. L. Johnson and K. Samwer *PRL* 95, 195501 (2005)
- [35] W.H. Wang/ *Progress in Materials Science* 57 (2012) 487–656
- [36] A. L. Greer, E. Ma, *MRS Bull.* 2007, 32, 611.
- [37] W. H. Wang, C. Dong, C. H. Shek, *Mater. Sci. Eng. R: Rep.* 2004, 44, 45.
- [38] W. H. Wang, *Prog. Mater. Sci.* 2007, 52, 540
- [41] Loffler JF, Schroers J, Johnson W L. *Appl Phys Lett* 2000, 77,681-3
- [42] Turnbull D. *Contemp Phys*, 1969, 10, 473-488.

- [43] Davies H. A, Lewis B G. *Scripta Met*, 1975, 9(10): 1107-1112.
- [44] A. Inoue, T. Zhang, T. Masumoto, J. *Non-Cryst. Solids* 156–158 (1993) 473
- [45] LU Z P, LIU C T. *Acta Mater*, 2002, 50: 3510-3512.
- [46] LU Z P, LIU C T. *Phys Rev Lett*, 2003, 91: 115505
- [47] E. Axinte et al. *Materials and Design* 35 (2012) 518–556
- [48] Inoue, A., *Materials science foundations*, 1998, Uetikon-Zurich, Switzerland
Enfield, N.H.:Trans Tech. 116 p.
- [49] Inoue, A. *Trans Tech Publication* 1998: Zurich
- [50] A.L.Greer A.L. Greer, *Nature* 366 (1999) 303
- [51] Angell CA. *Science* 1995;267:1924–35.

II. Chapter 2

2.1. Introduction. (Aim of the present work)

Contrary to monocrystalline and polycrystalline materials, MGs are not characterized by any of the typical features of the formers, like defects, slip lanes, stacking faults, grain boundaries e.t.c., which contribute in the accommodation of an imposed deformation. MGs can be safely seen on a macroscale as near ‘ideal’ isotropic and homogeneous materials. However, from the microscopic point of view it has repeatedly proven, both experimentally, namely by means of neutron and X-ray scattering techniques, and theoretically that they manifest short range order (SRO) and even medium range order (MRO).

This SRO and MRO order is mainly expressed in terms of icosahedral-like clusters and they are accepted as the prevailing motif of metallic liquids and glasses the last decades. The icosahedral clusters, due to their five-fold symmetry cannot fill the whole space in three dimensions (for geometrical reasons) without inducing distortion and open spaces and thus they prevent the crystallization of the material, resulting in the enhancement of their Glass Forming Ability (GFA).

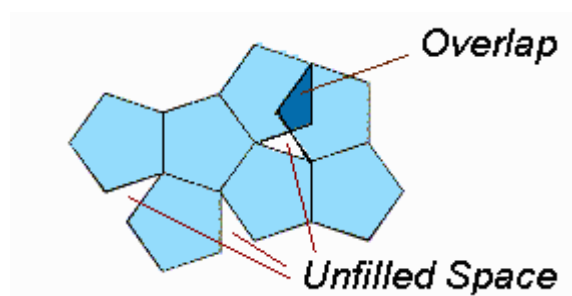


Fig. 2.1. Schematic representation of five-fold symmetry in 2D.

Since the discovery of MGs until now, a lot of efforts have been made, aiming in explaining this alternative type of structure arguably by focusing on the study of these clusters and namely how the presence of these clusters affects the physical, mechanical and their other properties. This is the main scope of this dissertation: to exhaustively study all the alterations in the microstructure of MGs in relation with temperature, concentration, geometry and mechanical behavior of the alloy, using as model system the binary CuZr alloy.

To this end we employed Molecular Dynamic simulations (MD) based on a potential model in analogy to the Tight Binding scheme in the Second Moment approximation (TBSMA). We analyzed a variety of stoichiometries of $\text{Cu}_x\text{Zr}_{100-x}$ in the range $20 < x < 80$. First of all, the microstructure was examined exhaustively in order to gain a deep insight on the possible alterations occurring when the temperature was changing or their stoichiometry was varied.

Moreover, we prepared two different categories of systems, namely, the first category was systems in bulk geometry ('infinite' systems) and the second one refer to systems with free surfaces in one or more directions. Consequently, we imposed tensile deformation with different strain rates and we analyzed how this deformation was accommodated in the two categories of systems, through their microstructure. In our efforts to understand whether there was any correlation between the stress of the systems and the evolution of the microstructure upon deformation, we calculated the cross correlation coefficient and we found out that the two quantities were highly correlated, resulting in the conclusion that possible changes in the microstructure of the systems are reflected in the stress induced in the system and vice-versa.

Regarding the second category, i.e systems with free surfaces in one or more directions, we studied their behavior upon tensile deformation and the corresponding evolution of the microstructure. More specifically, we prepared several systems in foil geometry (free surfaces in one axis, 2D material) and in ribbon geometry (free surfaces in two axes, 1D material) and for each of these geometries we studied their mechanical behavior, when the thickness was changed.

Concerning the catalytic behavior of Cu-Zr and due to the fact that non-uniform structure of a surface promotes catalytic reactions and selectivity, mainly because of the existence of steps or kinks, we made nanostructured surfaces by depositing Mackay clusters of different sizes (number of atoms) and stoichiometries on a substrate consisting of a system in foil geometry. We analyzed the characteristics of the deposited clusters from geometrical point of view, i.e. their structural characteristics eg. gyration radius, displacement of the center of mass etc. and how stable they were after their deposition.

Additionally, we calculated the surface energies of the surfaces aiming in ensuring their stability after the cluster deposition. The validity of our results was tested by trying different cooling rates during the preparation of our substrate and by using a different potential model, namely an Embedded Atom Method (EAM), in order to examine their influence to the phenomena that took place during and after the cluster deposition.

2.2. Selection of Cu-Zr as model system

The system selected in this dissertation is the binary alloy Cu-Zr. The Cu-Zr system exhibits good glass forming ability, against to one of Inoue's empirical rules, namely that multicomponent alloys are required for the enhancement of GFA, in a wide compositional range (35-70 at.% Cu). However, it satisfies the other two criteria for good glass formers, i.e. it has negative heat of mixing -23 kJ/mol and an atomic size mismatch that is greater than 12%. More specifically, the atomic radii of Zr is 1.58 Å and Cu, 1.27 Å and accordingly the ratio $R_{Zr}/R_{Cu}=1.244$ or 12.44%. Additionally, there is rich bibliography from both experimental and theoretical studies, it has a well-known phase diagram Fig, and due to the fact that it is binary it is more simple to model compared to other alloy systems with more than two constituent elements.

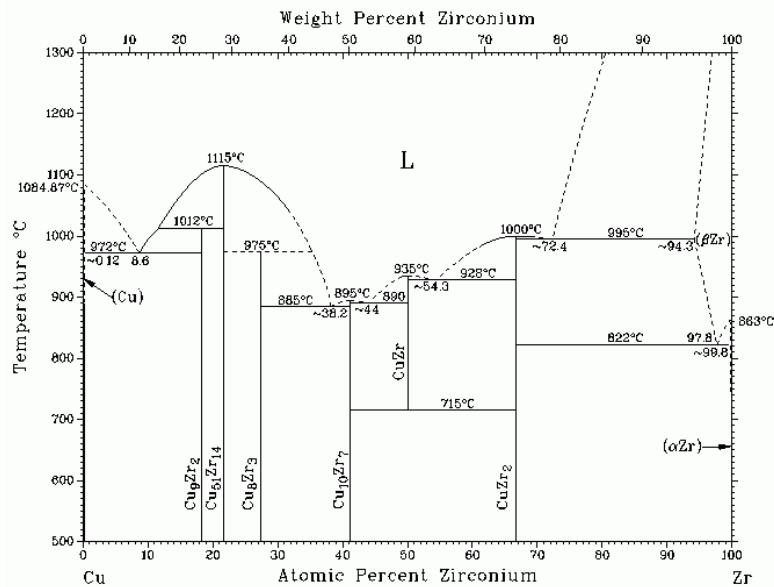


Fig.2.2. Phase diagram of CuZr alloy [21].

Moreover Cu-Zr alloy systems are good candidates for BMGs, e.g. the $\text{Cu}_{46}\text{Zr}_{54}$ alloy has been successfully casted into 2 mm fully amorphous strips by copper mold casting method [22] due to their structural and thermal stability that was proven through X-ray diffraction and pair distribution functions in a wide compositional range [23]. It is also well-known that Cu-based alloys are potential candidates for industrial fabrication as a result of their high strength and their relatively low price.

It is accepted that the presence of deep eutectic points in the phase diagram of an alloy correlates well with the ability of the alloy to form glass. This is due to the fact that the presence of deep eutectic points at temperatures much lower than the melting points of the constituent elements, reveals a relatively stable liquid phase in comparison with the competitive crystalline phases. Thus during the rapid quenching process of the alloy, the amorphous state can be achieved more easily due to the frustration of the crystallization process. Cu-Zr has five eutectic points as shown in the figure above, the deepest occurring at 885 C and around 35% at. in Zr.

2.2. Why Simulations- techniques

Computer simulations is a scientific tool widely used in the modeling of natural systems of many scientific fields, via a mathematical model, like in physics, chemistry, biology, economics, psychology, social science etc. in order to gain a deeper insight into the mechanisms that govern these systems. It is achieved through numerical solutions to problems, where analytical solutions are impossible, which permits the prediction of the system under a set of parameters and initial conditions.

A Simulation technique is also a useful tool to study scientific phenomena when experiment fails. Such cases are for example in the inside of stars or for the weather

forecast where the experiment is most of the time impossible or dangerous as in the case of flight or explosion simulation, or expensive and sometimes improper because the properties under study acquire short time scales and small space scales. In conclusion, simulation can sometimes replace, provoke, explain or confirm the observations of an experiment.

Over the years the number of simulation techniques has greatly expanded resulting to large variety of techniques not only classical, but even quantum simulations and very often mixed quantum - classical simulations (hybrid methods), when the quantum effects cannot be neglected. Regarding the classical ones the most well known in addition to MD, is the classical Langevin Dynamics (LD) and the Monte Carlo simulations (MC) [24] and concerning the mixed techniques is the quantum based techniques involving path-integral and Monte Carlo methods [25], the MD combined with electron density-function theory, as well as discrete approaches such as cellular automata and the lattice-Boltzmann method [26].

The main difference between quantum and classical techniques is that the formers produce more accurate results, but “expensive” in computational time, resulting to studies of small systems, while the latter are less accurate but they are faster and much larger systems can be studied.

2.3. Molecular Dynamic Simulations (MD).

The history of Molecular Dynamics (MD) method starts in the late 1950's when Alder and Wainwright [27,28] joined their efforts in studying the interactions of hard spheres. Their study contributed significantly in understanding the behavior of simple liquids. Another later study by MD took place in 1964 by Rahman who used a realistic potential for liquid

Argon [29] and after a decade in collaboration with Stillinger they used a realistic potential in order to simulate the liquid water [30].

Nowadays, MD is a fundamental tool in studying a wide variety of scientific subjects in almost all the scientific fields. Some of the most usual applications are in fundamental studies like equilibration, kinetic theory, diffusion, transport properties and in phase transitions (first- and second-order), and in collective behaviors like time correlation functions, coupling of translational and rotational motion, vibration, spectroscopic measurements etc. Additionally, Molecular Dynamics simulations permit the study of complex and dynamic processes and can provide detailed information about dynamics, thermodynamics and structure in biological systems, in complex fluids, polymers, solids, biomolecules and in fluid mechanics.

A simplified definition of Molecular dynamics (MD) simulation could describe it as a technique by which one can generate atomic trajectories of a system consisted by N interacting particles by numerical integration of Newton's equation of motion, for a given interatomic potential, and under specific initial conditions and boundary conditions. The design of a molecular dynamics simulation system is restricted by the available computational power.

The basic parameters of a simulation like the simulation size (n =number of particles), the timestep and the total duration of the simulation must be selected in such a way as that the calculation can be finished within a reasonable time interval. The validity of the conclusions, from a statistical point of view, is ensured if the simulation time matches with the kinetics of the natural process. The usual atomistic simulation time ranges from a few picoseconds to hundreds of nanoseconds. A simulation is reliable when the simulation time

lasts longer than the relaxation time of the quantities under study in order to attain stability or lowest energy state.

The main advantage of MD relies on the capability that provides to the estimation of macroscopic properties like temperature, pressure, heat capacity etc, through the statistical processing of the microscopic properties, like atomic positions and velocities. In conclusion, the key role to the connection between macroscopic world to the microscopic is the statistical mechanics.

2.4. Basic concepts of Molecular Dynamic Simulation

A model for Molecular Dynamic simulation (MD) contains basically two contributions: one that describes the interaction between the molecules of the system and a second contribution that refers to the interaction between the molecules and their ‘environment’. The first contribution is actually the function of the potential model. This means that this function describes (even indirectly) the shape of these molecules or in a better meaning, it describes their electronic structure. In fact, since we define the function of the potential model, we have determined the symmetry of the molecules, their elasticity etc. For simplicity, we assume isolated systems and consequently we refer to interactions that depend only on the inter-molecular potential model. For particles described as spheres, such a function of N particles is given by $U(r^N)$ where r^N is one pattern of the molecules-particles system. For an isolated system the quantity that is conserved is the total energy, namely the combination of the kinetic and potential energy. This quantity is, in fact, the Hamiltonian:

$$H(r^N, p^N) = \frac{1}{2m_i} \sum p_i^2 + u(r^N) = E \quad (2.1)$$

In order to find the equations of motion we find, firstly, the total time differential of the Hamiltonian:

$$\frac{dH}{dt} = \sum_i \frac{\partial H}{\partial p_i} \dot{p}_i + \sum_i \frac{\partial H}{\partial r_i} \dot{r}_i + \frac{\partial H}{\partial t} \quad (2.2)$$

But the Hamiltonian is time independent, thus:

$$\frac{dH}{dt} = \sum_i \frac{\partial H}{\partial p_i} \dot{p}_i + \sum_i \frac{\partial H}{\partial r_i} \dot{r}_i = 0 \quad (2.3)$$

For the case of an isolated system we take:

$$\frac{dH}{dt} = \frac{1}{m_i} \sum_i p_i \dot{p}_i + \sum_i \frac{\partial U}{\partial r_i} \dot{r}_i = 0 \quad (2.4)$$

If we compare the previous two equations we take:

$$\frac{\partial H}{\partial p_i} = \frac{p_i}{m} = \dot{r}_i \quad (2.5)$$

and

$$\frac{\partial H}{\partial r_i} = \frac{\partial U}{\partial r_i} \quad (2.6)$$

And by substitution we take

$$\sum_i \dot{r}_i \dot{p}_i + \sum_i \frac{\partial H}{\partial r_i} \dot{r}_i = 0 \quad (2.7)$$

$$\sum_i \left(\dot{p}_i + \frac{\partial H}{\partial r_i} \right) \dot{r}_i = 0 \quad (2.8)$$

Due to the fact that the velocities are independent from each other, the last equation is satisfied only when for each molecule i :

$$\frac{\partial H}{\partial r_i} = -\dot{p}_i \quad (2.9)$$

The equations (1) and (2) are the Hamiltonian equations of motion.

For a system of N spherical particles the above two equations correspond to a system of $6N$ first order differential equations which are equivalent to the $3N$ second order differential equations of Newton. This can be proved very easily if we take

$$p_i = m \dot{r}_i \quad (2.10)$$

And if we eliminate the momentum from Hamiltonian equations, we take

$$\frac{\partial H}{\partial r_i} = -m \ddot{r}_i \quad (2.11)$$

And by using the relation

$$\frac{\partial H}{\partial r_i} = \frac{\partial U}{\partial r_i} \tag{2.12}$$

We find in comparison with the Newton's law that

$$F_i = -\frac{\partial H}{\partial r_i} = -\frac{\partial U}{\partial r_i} \tag{2.13}$$

which is, in fact, the ordinary relation of a conservative force.

From the above discussion we can conclude that there is a difference between the Newtonian and the Hamiltonian dynamics. In the former, the motion is the result of an applied force, while in the latter, forces don't appear directly, and the motion takes place in such way that the Hamiltonian must be conserved. In the previous analysis we considered our system as isolated. In the case that the system interacts with its environment, the Hamiltonian would contain additional terms and it would not correspond to the total energy of the system, which is not conserved whereas the Hamiltonian itself is conserved. Concluding, the Hamiltonian description is more general than the Newtonian.

2.5. Verlet algorithm

Let's consider an isolated system of N particles that are placed in a box of volume V. In the classical limit one can study the motion of particles by using the Newtonian mechanics and more specifically by solving the differential equations of every particle i. Hence, once the force acting on every atom is known using the,

$$F_i = -\frac{\partial H}{\partial r_i} = m \frac{d^2 \vec{r}_i}{dt^2} \tag{2.14}$$

as mentioned above, the particle accelerations can be obtained and combined with velocities and positions at that t to compute the new positions and velocities at a later time, $t+dt$. Therefore, a numerical integration method is applied to the system. Common numerical integration techniques include Verlet algorithm, predictor-corrector scheme, Leap Frog algorithm and Beeman algorithm. The mathematical derivation of the Verlet algorithm is given to the following paragraphs.

The first time derivate of a function $u(t)$ can be written as:

$$\frac{du(t)}{dt} = h^{-1}[u(t+h) - u(t)] + O(h) = h^{-1}[u(t) - u(t-h)] + O(h) \quad (2.15)$$

In the above relation the error is in the order of h . By writing the Taylor expansions of the terms $u(t+h)$ and $u(t-h)$ we take:

$$u(t+h) = u(t) + h \frac{du(t)}{dt} + \frac{1}{2} h^2 \frac{d^2u(t)}{dt^2} + R_3 \quad (2.16)$$

$$u(t-h) = u(t) - h \frac{du(t)}{dt} + \frac{1}{2} h^2 \frac{d^2u(t)}{dt^2} + R_3^* \quad (2.17)$$

Where R_3 and R_3^* correspond to the error of the equations (2.16) and (2.17) respectively and it is of order h^3 .

By subtracting (2.16) from (2.17) one gets the relation:

$$u(t+h) = u(t-h) - 2h \frac{du(t)}{dt} + R_3 - R_3^* \quad (2.18)$$

$$\text{Or } \frac{du(t)}{dt} = \frac{1}{2h} [u(t+h) - u(t-h)] + O(h^2) \quad (2.19)$$

By adding the equations (2.16) and (2.17) we get an expression for the second derivative:

$$\frac{d^2u(t)}{dt^2} = h^{-2} [u(t+h) - 2u(t) + u(t-h)] + O(h^2) \quad (2.20)$$

Consequently the initial differential equation $F_i = m \frac{d^2\vec{r}_i}{dt^2}$, by using the equation (2.20)

becomes:

$$\frac{d^2r_i}{dt^2} = h^{-2} [r_i(t+h) - 2r_i(t) + r_i(t-h)] = \frac{1}{m} F_i(t) \quad (2.21)$$

$$\text{Or } r_i(t+h) = 2r_i(t) - r_i(t-h) + \frac{1}{m} F_i(t) h^2 \quad (2.22)$$

If we set $t_n = nh$, the time that have passed after n steps, the position and the force acting

on the particle i after n steps can be written as $r_i^n = r_i(t_n)$ and $F_i^n = F_i(t_n)$, respectively.

Finally, the Verlet algorithm can be written as:

$$r_i^{n+1} = 2r_i^n - r_i^{n-1} + \frac{F_i^n h^2}{m} \quad (2.23)$$

The velocity of every particle i, for each time step n, is the first time derivative of the particles position:

$$u_i^n = \frac{(r_i^{n+1} - r_i^{n-1})}{2h} \quad (2.24)$$

where h is the integration step of a molecular dynamic simulation. In conclusion, the Verlet algorithm connects the position/velocity of a particle with the position/velocity of the particle at a previous and a next time.

2.6. A short description of Statistical Mechanics-Ensembles

Since, it is in fact impossible to calculate the equation of motion and the trajectory of a system with an order of magnitude of 10^{23} atoms, we use ensemble averages in order to determine the thermodynamic properties. A thermodynamic ensemble is the collection of all microscopic states that correspond to an identical macroscopic state and a macroscopic state of the system is represented by a point (r, p) in the phase space of the system, where $r = (r_1, \dots, r_N)$ and $p = (p_1, \dots, p_N)$ are the positions and the momenta of the N atoms of the system respectively.

A macroscopic state can be fully described by the number of particles (N), by the chemical potential (μ), the volume (V), the pressure (P), the energy (E) and the temperature (T). Some of the most known ensembles are the micro-canonical ensemble NVE, the canonical isothermal NVT and the isothermal-isobaric ensemble NPT that are described in the following paragraphs.

Micro-canonical ensemble (NVE):

This ensemble is characterized by fixed values of moles (N), volume (V) and energy (E) of the system. It corresponds to an adiabatic process where with no heat exchange occurs. It may be considered as an exchange of potential and kinetic energy, with the total energy being conserved.

Canonical isothermal (NVT) ensemble:

In this ensemble, moles (N), volume (V) and temperature (T) are conserved. In NVT, the energy of endothermic and exothermic processes is exchanged with a thermostat. There is a wide variety of thermostat methods which are applied in order to add and remove energy from the boundaries of an MD system in a more or less realistic way, approximating the canonical ensemble.

Isothermal–Isobaric or NPT ensemble:

In this case of ensembles, moles (N), pressure (P) and temperature (T) are fixed. Additionally to a thermostat, a barostat is also needed to control the pressure, thus approximating more a realistic situation.

Grand-Canonical ensemble:

In Grand Canonical the values of the pressure (P), the temperature (T) and the chemical potential (μ) are fixed.

Boltzmann showed that the canonical probability of a microstate i , is given by: $P_i = \frac{1}{Z} e^{-\beta E_i}$

(2.25)

where Z is the partition function, $\beta = 1/(k_B T)$ and k_B is the Boltzmann constant. So

$$Z = \sum e^{-\beta E_i} \quad \text{such that} \quad \sum_i P_i = 1 \quad (2.26)$$

The partition function is a very complex function to compute, because it represents a measure of the whole space accessible to the system. Once the partition function is computed all the thermodynamic properties can be derived in such a way:

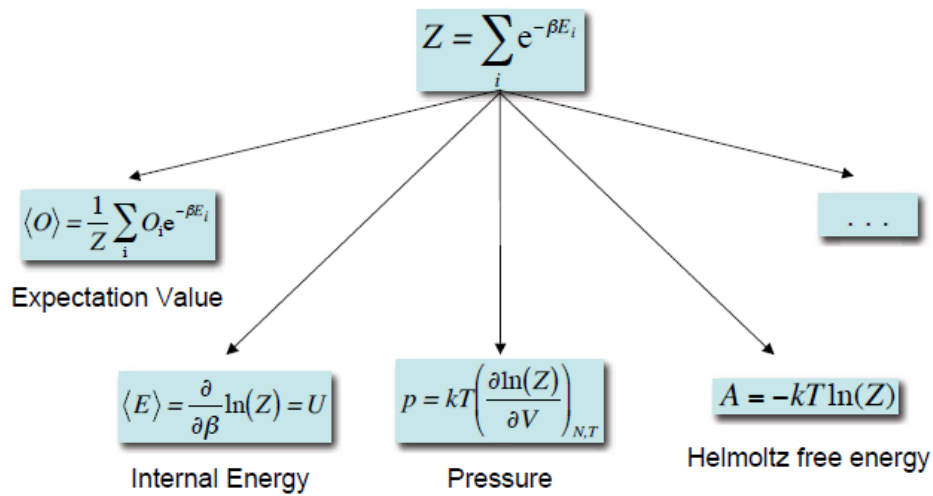


Fig.2.3. Basic thermodynamic properties and their relationships with the partition function [31].

The main reason why ensemble averaging is used in MD is that the time average of an evolving single system is equivalent to the ensemble averaging and it is called the ergodic hypothesis and it is one of the key axioms in statistical mechanics. The ergodic hypothesis is that the ensemble averages used to compute expectation values can be replaced by time averages over the simulation.

$$\langle O \rangle_{ensemble} \stackrel{ergodicity}{=} \langle O \rangle_{time} \tag{2.27}$$

$$\frac{1}{Z} \int O(r, p) e^{-\beta E(r, p)} dr dp = \frac{1}{\tau} \int_0^{\tau} O(t) dt \quad (2.28)$$

In fact the sum of the microstates sampled by molecular dynamics are usually a small subset of the entire thermodynamical ensemble. The validity of the ergodicity hypothesis depends on the quality of the sampling produced by the MD technique. The sampling should reach all important minima and explore them with the correct probability where for the most known ensembles it equals:

- NVE simulations -Microcanonic ensemble $\Leftrightarrow P = \text{cst.}$
- NVT simulations -Canonical ensemble $\Leftrightarrow P(E) = e^{-\beta E}$
- NPT simulations -Isothermic-isobaric ensemble $\Leftrightarrow P(E) = e^{-\beta(E+PV)}$

NVT

In order to expand MD simulation from the Microcanonical ensemble to the Canonical-

Isothermal it is necessary to introduce an hypothetical variable of time $r'_i = r_i$, $P'_i = \frac{P_i}{s}$ and

$t' = \int \frac{dt}{s}$ and then the Hamiltonian of the system in NVT ensemble can be written as:

$$H = \sum_{i=1}^N \frac{P_i^2}{2m_i s^2} + \varphi(r_{ij}) + \frac{P_s^2}{2Q} + g k_B T \ln s \quad (2.29)$$

In the Canonical Isobaric ensemble (NPH) (Andersen) we consider the reduced variables

$r_i' = r_i V^{\frac{1}{3}}$ and $P_i' = \frac{P_i}{V^{\frac{1}{3}}}$ and thus the resulting Hamiltonian equals to:

$$H = \sum_{i=1}^N \frac{P_i^2}{2m_i V^{\frac{1}{3}}} + \varphi(r_{ij}) + \frac{P_V^2}{2W} + P_{ext} V \quad (2.30)$$

In the Canonical-Isobaric-Isothermal (NPT) ensemble the reduced variables are $r_i' = r_i V^{\frac{1}{3}}$,

$$t' = \int \frac{dt}{s} \quad \text{and} \quad P_i' = \frac{P_i}{V^{\frac{1}{3}}}$$

and the Hamiltonian of the system in NPT equals to:

$$H = \sum_{i=1}^N \frac{P_i^2}{2m_i s^2 V^{\frac{1}{3}}} + \varphi(r_{ij}) + \frac{P_s^2}{2Q} + g k_B T \ln s + \frac{P_V^2}{2W} + P_{ext} V \quad (2.31)$$

In the above relations φ corresponds to the potential model, V is the volume of the system and P_i and r_i are the momenta and positions of atom i , respectively. The variables P_i' and r_i' are variables related with the constants Q and W , which play the role of pseudo-masses of the thermostat Nose and piston Andersen respectively. These pseudo-masses define the dynamics of the additional variables and their values must be selected properly in order some physical quantities to be reproduced correctly and thus their association with the system to be ensured. Finally, g corresponds to the degrees of freedom and k_B stands for Boltzmann constant.

In the general case of **NPT** ensemble the equations of motion are:

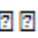
$$\frac{d^2 \bar{r}_i}{dt'^2} = -\frac{1}{mV^{\frac{1}{3}}} \frac{\partial \Phi}{\partial \bar{r}_{ij}} - \frac{1}{s} \frac{ds}{dt'} \frac{d\bar{r}_i}{dt'} - \frac{2}{3} V \frac{dV}{dt'} \frac{d\bar{r}_i}{dt'} \quad (2.32)$$

$$\frac{d^2 s}{dt'^2} = -\frac{s}{V} V^{\frac{2}{3}} \sum_{i=1}^N m_i \left(\frac{d\bar{r}_i}{dt'} \right)^2 - \frac{gk_B T s}{Q} + \frac{1}{s} \left(\frac{ds}{dt'} \right)^2 \quad (2.33)$$

$$\frac{d^2 V}{dt'^2} = -\frac{s^2}{3WV^{\frac{1}{3}}} \sum_{i=1}^N m_i \left(\frac{d\bar{r}_i}{dt'} \right)^2 - \frac{s^2}{3WV} + \frac{1}{s} \sum_{i=1}^N \bar{r}_i \left(\frac{\partial \Phi}{\partial \bar{r}_i} \right) + \frac{1}{s} \frac{ds}{dt'} \frac{dV}{dt'} - P_{ext} \frac{s^2}{W} \quad (2.34)$$

where P_{ext} and T stand for the external pressure and temperature, respectively.

For a given system of N particles we have to solve $3N$ second order differential equations (DEs). Thus $6N$ initial conditions are required. The $3N$ initial conditions could be the lattice positions corresponding to the Cartesian coordinates of the crystal lattice of the system. The other $3N$ initial conditions could be the velocities of the particles and they could be chosen randomly from the Maxwell-Boltzmann distribution, in such a way that the mean value of their momentum corresponds to the desirable temperature of the simulation. The expression of the distribution of velocities according to Maxwell-Boltzmann is given by the relation:

▮ EMBED Equation. DSMT4 

(2.35)

where $N(u)$ is the number of particles with velocity u , N is the total number of particles of the system, m is the mass of each particle, T is the temperature of the system and k_B is Maxwell-Boltzmann's constant. The integration step (dt) is usually chosen one hundred times smaller than the inverse of the maximum oscillation frequency of the particles meaning $dt < \frac{1}{100} \frac{1}{\omega_{\max}}$, where ω_{\max} is the maximum phonon frequency.

From the successive integrations of the equations of motion we obtain the trajectory of the system in the phase space, meaning the positions and momenta of the particles within the simulation time length. The determination of macroscopic quantities like temperature, pressure, elastic constants etc. from the time evolution of the system requires the use of the statistical mechanics.

2.7. TBSMA – Potential model

The potential used in this dissertation is a semi-empirical potential and it is in analogy to the theory of Tight Binding scheme in the Second Moment Approximation (TBSMA). This kind of potential is mainly used for simulating systems where their constituent elements are at the end of the transition metal series or noble metals. The general TBSMA [32] is given like the total energy of any atom at a site i can be written as the sum of two terms, a repulsive pair interaction and an attractive band energy:

$$E_i = E_i^r + E_i^b$$

$$\Phi = \sum_{\alpha} \sum_{l_{\alpha}=1}^{N_{\alpha}} \left\{ \sum_{\beta} \sum_{\substack{j\beta=1 \\ j\alpha=1}}^N A_{\alpha\beta} e^{-p_{\alpha\beta} \left(\frac{r_{ij}^{\alpha\beta}}{d_{\alpha\beta}} - 1 \right)} - \sqrt{\sum_{\beta} \sum_{\substack{j\beta=1 \\ j\beta \neq j\alpha}}^N \xi_{\alpha\beta}^2 e^{-2q_{\alpha\beta} \left(\frac{r_{ij}^{\alpha\beta}}{d_{\alpha\beta}} - 1 \right)}} \right\}$$

(2.36)

In the above expression, the first term is a short-range repulsive term which is described as a sum of Born-Mayer ion-ion repulsions [33] and denotes the pair-wise repulsive energy terms. The free parameter $p_{\alpha\beta}$ of this term is related with the bulk modulus.

The second term is attractive and denotes the many-body metallic bonding potential that is obtained by integrating the local density of states up to the Fermi level [34]. The parameter q_{ij} , represents the distance dependence of the hopping integrals between atoms at sites i and j , ξ_{ij} is an effective hopping integral, $d_{\alpha\beta} = (r_0^{ii} + r_0^{jj})/2$ where r_0^{ii} and r_0^{jj} stand for the first-neighbor distance in the metal i and j , respectively and r_0^{ij} is the distance between atoms i and j . The interactions of atoms taken into account beyond a cutoff radius r_{ij}^c are canceled

Some important physical properties of the system like elastic constants, cohesive energy, bulk moduli etc. were derived by density functional theory (DFT) quantum mechanics calculations on various phases namely from pure Cu, pure Zr, CuZr (B1 and B2), Cu₃Zr, CuZr₃. The results showed good agreement with experimental data and subsequently they were used as reference in order the four free parameters $A_{\alpha\beta}$, ξ , p and q of the potential to be obtained.

The obtained free parameters of the TBSMA potential used in this dissertation are shown in Table below for Zr-Zr, Cu-Cu, and Cu-Zr respectively.

	r_o (Å)	$A_{\alpha\beta}$ (eV)	ξ (eV)	q	p
Zr-Zr	4.5396	0.3688	2.3365	2.0250	7.9273
Cu-Cu	3.7273	0.2149	1.3483	2.7490	10.2215
Cu-Zr	4.1134	0.3615	2.0100	2.7960	8.6020

Table.2.1. Parameters of TBSMA potential model for CuZr alloy.

It came out that this potential describes well the Cu-Zr alloy and thus it is suitable in studying binary Cu-Zr metallic glasses by Molecular Dynamic simulations.

2.8. Boundary conditions.

With respect to the boundary conditions there are two common types: namely the isolated boundary condition (IBC) and the periodic boundary condition (PBC). The former type, IBC, is more suited for studying isolated clusters and molecules, while PBC is suited for studying bulk liquids and solids. In IBC, the N-particle system is surrounded by vacuum; these particles interact among themselves, but are presumed to be so far away from everything else and thus there are no interactions with the outside. In PBC, one explicitly keeps track of the motion of N particles in the so-called supercell, but the supercell is surrounded by infinitely replicated periodic images of itself. It should be noted that IBC can often be well mimicked by a large enough PBC supercell so that the images do not interact.

2.9. Basic thermodynamic properties extracted from trajectories of MD simulations.

From the time evolution of the positions and the momenta of system's particles, when the system is in thermodynamic equilibrium, we can calculate many physical quantities by means of statistical thermodynamics. Some of them are presented in the following paragraphs. Starting from the temperature of the system:

$$T = \frac{2}{3NK_B} \left\langle \sum_{i=1}^N \frac{P_i^2}{2m_i} \right\rangle \quad (2.37)$$

The pressure of the system is given by the Virial theorem:

$$P = \left\langle \frac{N}{\Omega} K_B T \right\rangle - \left\langle \frac{1}{3\Omega} \sum_{i=1}^N \sum_{j>i}^N \vec{r}_{ij} \frac{\partial \Phi(\vec{r}_{ij})}{\partial \vec{r}_{ij}} \right\rangle \quad (2.38)$$

where r_{ij} corresponds to the distance between particles i and j .

Another useful quantity is the local density profile, which equals to: $\rho(\vec{r}) = \sum_{i=1}^N \delta(\vec{r} - \vec{r}_i)$

(2.39)

By using this function we are able to calculate various quantities which are used very often to the specification of the structure factor of the materials and their surfaces.

The averaged position of the atoms in a atomic plane along X-direction and between x_1 and x_2 is given by:

$$\langle x \rangle = \int_{x_1}^{x_2} x \rho(x) dx \quad (2.40)$$

While the mean squared displacement, a quantity which is highly related with X-ray and neutrons diffraction experiments, can be calculated as follows:

$$\langle u^2 \rangle = \frac{\int_{x_1}^{x_2} (x - \langle x \rangle)^2 \rho(x) dx}{\int_{x_1}^{x_2} \rho(x) dx} \quad (2.41)$$

Also, from the local density profile some other structure factors can be estimated by:

$$\rho(\vec{k}) = \int e^{-i\vec{k} \cdot \vec{r}} \delta(\vec{r} - \vec{r}_i) d\vec{r} = \sum_{i=1}^N e^{-i\vec{k} \cdot \vec{r}_i} \quad (2.42)$$

$$\text{and } S(\vec{k}) = \frac{1}{N^2} \langle \rho(\vec{k}) \bullet \rho(-\vec{k}) \rangle \quad (2.43)$$

Moreover, the fluctuations of the potential and kinetic energy are also associated with some very useful thermodynamic quantities. For example the specific heat capacity, where in the case of the Micro-Canonical ensemble corresponds to the specific heat capacity at constant volume, is given by the following equation:

$$C_v = \frac{3}{2} \frac{1}{1 - \frac{2N \langle \delta E^2 \rangle}{3K_B^2 \langle T \rangle^2}} = \frac{3}{2} \frac{1}{1 - \frac{2N \langle \delta K^2 \rangle}{3K_B^2 \langle T \rangle^2}} \quad (2.44)$$

Additionally, some other dynamical and not only static quantities can be exported from MD trajectories, like the diffusion coefficient, the dynamical structure factors, the ionic and thermal conductivity, by using the Fourier transform of specific correlation functions.

For example, the diffusion coefficient can be calculated from the autocorrelation of velocities like this:

$$D = \lim_{T_{\max} \rightarrow \infty} \frac{1}{N} \int_0^{T_{\max}} \sum_{i=1}^N \langle \vec{v}_i(0) \cdot \vec{v}_i(t) \rangle \left(1 - \frac{t}{T_{\max}}\right) dt \quad (2.45)$$

2.10. Computational Tools for structural analysis

2.10.1. Radial Distribution Function

The radial distribution function, RDF or $g(r)$, is a useful and widely used computational tool to reveal the structure features of a system, especially for liquids and amorphous systems, through the calculation of the variations in atomic density as a function of distance from a chosen atom (origin). It is in analogy with X-ray crystallography that uses a function that describes how light scatters by a crystal. More specifically, the Fourier transform of the scattering function from X-ray crystallography is the radial distribution function, plus one.

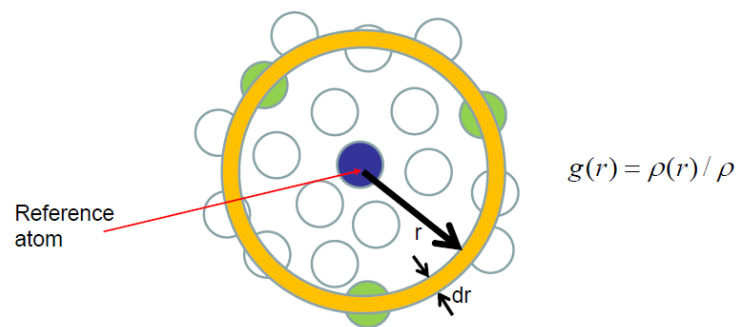


Fig.2.4. Schematic representation of the calculation of radial distribution function in 2D [35].

RDF can be defined as the ratio of the local density of atoms at a distance from r to $r+dr$ over the whole area. Such calculation results to a relative density of atoms as function of radius. Thus:

$$g(r) = \frac{p(r)}{p} \quad (2.46)$$

where $p(r)$ and p correspond to the local density (r to $r+dr$) and the overall density of the system respectively. If we substitute the local density $p(r)$ with

$$p(r) = \frac{n(r)}{d^3r} \quad (2.47)$$

And due to the fact that $d^3r = 4\pi r^2 dr$ and $n(r)$ is the number of particles which can be found in the shell from r to $r+dr$. Accordingly, the $g_i(r)$ for a specific atom i is given by:

$$g_i(r) = \frac{n(r)}{4\pi r^2 dr} \frac{1}{p} = \frac{n(r)}{4\pi r^2 dr} \frac{V}{N} \quad (2.48)$$

where N is the total number of atoms in the system and V is the total volume of the system. For a monoatomic system, if we perform the same calculation at a given r , for all the atoms of the system, and then by taking the mean value (thus dividing by N) we end up to:

$$g(r) = \frac{V}{N^2} \left\langle \sum_{i=1}^N \frac{n(r)}{4\pi r^2 \Delta r} \right\rangle \quad (2.49)$$

And especially for a binary alloy system, the partial radial distribution function (PRDF) for atom α and atom β is given by:

$$g_{\alpha\beta}(r) = \frac{V}{N_{\alpha}N_{\beta}} \left\langle \sum_{i=1}^{N_{\alpha}} \frac{n_{i\beta}(r)}{4\pi r^2 \Delta r} \right\rangle \quad (2.50)$$

It comes out that $g(r)$ is a dimensionless quantity that provides structural information namely the structural changes of the system but it cannot provide any information about how fast the atoms move for example.

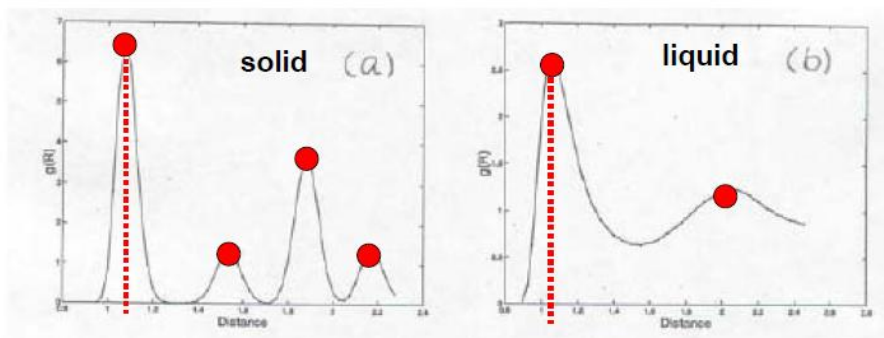


Fig.2.5. RDFs of a crystalline solid material (left) and of a liquid (right).

The left picture corresponds to the RDF of a crystalline solid material. In order to estimate the number of the first second, third neighbors etc., one can integrate this graph till the first, second, third minimum respectively. For a perfect lattice at $T=0K$ this graph would be a delta-function, but for $T > 0$ the peaks are broadened due to thermal vibrations. The right picture corresponds to the RDF of a liquid and as we can see the peaks are clearly more broadened and only the first two neighborhoods are boldly distinguished. This phenomenon would be highlighted in the case of a gas where only the first neighborhood is clearly distinguished.

2.10.2. Common Neighbor Analysis (CNA)

Common-neighbor analysis (CNA) [36, 37] is a very common technique in simulation studies for the exhaustive analysis of structure. It systematically classifies the whole structure in bonded pairs in the following way:

it considers that there is a bond (geometrical bond, not chemical) between two atoms if their distance is less or equal to a certain distance, which is call r_c , where c comes from the word cut-off. This distance corresponds to the first peak of the RDF and it represents the first neighbors distance. Consequently, it attributes to each of these "bonded" pairs a set of three indices jkl that specifies their local environment.

More specifically the first index j refers to the bond itself and it is equal to the number of neighbors common to both atoms. The second and third indices refer to neighbors of this bond, namely the second index k is the number of bonds between the common neighbors, while the third index l is the number of bonds in the longest continuous chain formed by the k bonds between common neighbors. In the figure below an example of two bonds that have fcc and hcp local environment is provided.

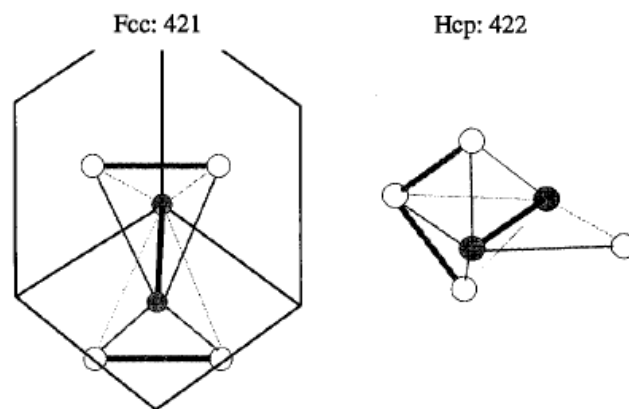


Fig.2.6. Illustration of the classification of pairs of atoms corresponding to an fcc and an hcp environment. The atoms of the "pair" are colored black, while the common neighbors are white [38].

CNA is a powerful method to distinguish between various local structures, for example fcc, hcp, and icosahedral environments. Different types of pairs are associated with different types of local order. For example, bonded pairs of type 555 are characteristic of icosahedral order, whereas 421 and 422 pairs are characteristic of fcc and hcp order. The only bonded pairs in the fcc crystal are 421, while the hcp crystal has equal numbers of 421 and 422. The difference between the two pairs is the arrangement of the two bonds between the four neighbors. In 421 each of the neighbors forms one of those bonds, in 422 one of the neighbors forms two, two neighbors form one, and the fourth neighbor does not participate in either of the two bonds.

2.11.References

- [1]. T. Schenk, D. Holland-Moritz, V. Simonet, R. Bellissent, D. M. Herlach, *Phys. Rev. Lett.* 89, 075507 (2002).
- [2] K. Saks et al., *Appl. Phys. Lett.* 83, 3924 (2003).
- [3] K. F. Kelton et al., *Phys. Rev. Lett.* 90, 195504 (2003).
- [4] A. Hirata, L. J. Kang, T. Fujita, B. Klumov, K. Matsue, M. Kotani, A. R. Yavari, M. W. Chen, *Science* 341(2013)
- [5] Lagogianni A. E. et al. *Journal of Alloys and Compounds*, 483, 658-661
- [6] G.B. Bokas, A.E. Lagogianni, G.A. Almyras, Ch.E. Lekka, D.G. Papageorgiou, G.A. Evangelakis. *Intermetallics*, 43(0):138, 2013.
- [7] Ch E. Lekka, G. B. Bokas, G. A. Almyras, D. G. Papageorgiou, and G. A. Evangelakis. *Journal of Alloys and Compounds*, 536(1):S65–S69, 2012.
- [8] 4) A. Hirata et al., *Nat. Mater.* 10, 28–33 (2011).50.
- [9] J. L. Finney, *Nature* 266, 309–314 (1977).
- [10] P. J. Steinhardt, D. R. Nelson, M. Ronchetti, *Phys. Rev. Lett.* 47, 1297–1300 (1981).
- [11] T. Tomida, T. Egami, *Phys. Rev. B* 52, 3290–3308 (1995).
- [12] M. W. Chen, T. Zhang, A. Inoue, A. Sakai, T. Sakurai, *Appl. Phys. Lett.* 75, 1697 (1999).
- [13] D. B. Miracle, *Nat. Mater.* 3, 697–702 (2004).
- [14] H. W. Sheng, W. K. Luo, F. M. Alamgir, J. M. Bai, E. Ma, *Nature* 439, 419–425 (2006).
- [15] P. F. Guan, T. Fujita, A. Hirata, Y. H. Liu, M. W. Chen, *Phys. Rev. Lett.* 108, 175501 (2012).
- [16] D. Ma, A. D. Stoica, X.-L. Wang, *Nat. Mater.* 8, 30–34(2009).
- [17] T. Takagi et al., *Appl. Phys. Lett.* 79, 485 (2001).]

- [18] J. F. Sadoc, R. Mosseri, Geometrical Frustration (Cambridge Univ. Press, Cambridge, 1999).
- [19] D. R. Nelson, Defects and Geometry in Condensed Matter (Cambridge Univ. Press, Cambridge, 2002)
- [20] D. R. Nelson, Phys. Rev. Lett. 50, 982–985 (1983)
- [21] R. Arroyave et al./Journal of alloys and compounds 351 (2003) 158-170
- [22] Duan et al. Phys. Review B 71, 224208, 2005
- [23] M. Imrana, F. Hussaina M. Rashida, Y. Caib, S. A. Ahmada, Chin. Phys. B Vol. 22, No. 9 (2013) 096101
- [24] Landau, D. P. and Binder, K., A Guide to Monte Carlo Simulations in Statistical Physics, Cambridge University Press, Cambridge, 2000
- [25] Schmidt, K. E. and Ceperley, D., Monte Carlo techniques for quantum fluids, solids and droplets p. 205.
- [26] Doolen, G. D., ed., Lattice Gas Methods for PDEs, North-Holland, Amsterdam, 1991
- [27] Alder and Wainwright, 1957, 1959) Alder, B. J. and Wainwright, T. E. J. Chem. Phys. 27, 1208 (1957)
- [28] Alder, B. J. and Wainwright, T. E. J. Chem. Phys. 31, 459 (1959)
- [29] Rahman, A. Phys. Rev. A 136, 405 (1964)
- [30] Stillinger, F. H. and Rahman, A. J. Chem. Phys. 60, 1545 (1974)
- [31] Molecular Dynamic Simulations. Michel Cuendet EMBL 2008
- [32] J. Friedel: The Physics of Metals, (Cambridge University Press, 1969), p. 340.
- [33] F. Ducastelle, J. Phys. (Paris) 31, 1055 (1970)
- [34] J. Friedel: The Physics of Metals, ed. J. M. Ziman (Cambridge University Press, 1969), p. 340
- [35] Markus J. Buehler. Laboratory for Atomistic and Molecular Mechanics (MIT)
- [36] J. D. Honeycutt and H. C. Andersen, J. Phys. Chem. 91, 4950 (1987)
- [37] H. Jonsson and H. C. Andersen, Phys. Rev. Lett. 60, 2295 (1988)
- [38] D. Faken, H. Jonsson, Computational Materials Science 2 (1994) 279-286.

III. Chapter 3

Relationship between microstructure, temperature and stoichiometry

• **Stoichiometry**

• **Temperature**

		Bulk-Surfaces
Microstructure	Deformation	Influence of strain-rates
		Cross-Correlation
		Mechanical behaviour of 1D and 2D nanosized systems
		Clusters as building blocks of MGs

3.1. RESULTS -Introduction

The Cu-Zr metallic glasses (MGs), despite the relatively weak elemental interactions [1], pass into the glassy state over a broad compositional range and they are, thus, used as a basis for a large number of bulk amorphous materials [2,3]. Another important feature is their casting ability into 2mm fully amorphous strips by copper mold casting method [4]. Amorphous alloys consist of various types of short range ordered (SRO) atomic clusters [5]. Sheng et al. [6] reported that these SRO influence the properties of every alloy. It is demonstrated that the $\text{Cu}_{46}\text{Zr}_{54}$ glass consists mainly by very tiny clusters, basically of icosahedral shape, whose number evolves under tensile sollicitation, thus establishing the prevailing role of the SRO not only at the equilibrium micro-structure of the MG, but also in the mechanisms responsible for the accommodation of the deformation [7]. In addition, in the Cu-Zr case, Wakeda et al. [8] attributed the SRO to icosahedral clusters and they showed that their number was increased upon enrichment in Cu content and when the temperature was decreased. Moreover, they also reported that despite the fact that the size of Zr atoms is about twice that of Cu atoms, Cu-rich glasses appeared to have lower free volume than the Zr-rich counterparts. Our intention is to further study this correlation and to reveal whether this finding can be related to the formation and the cluster composition. To this end we studied six different stoichiometries of the $\text{Cu}_x\text{Zr}_{100-x}$ glasses that were analyzed in order to reveal the morphology of the micro-structure as well as the composition of the constituent nanoclusters.

3.2. Preparation of the systems

Initially, aiming in investigating the influence of stoichiometry and temperature on the microstructure we prepared six different stoichiometries $\text{Cu}_x\text{Zr}_{100-x}$ for compositions in the range $20 \leq x \leq 80$. The simulations were based on a potential model in analogy to the tight-binding scheme in the second moment approximation (TBSMA) [4]. The equations of motion were integrated using the Verlet algorithm and a time step of 5fs.

The amorphous alloy models were prepared starting from a cubic cell box with periodic boundary conditions containing 128,000 atoms in the B2 structure of the appropriate composition. At each case, the positions of all atoms were redistributed randomly within the simulation cell and the resulting systems were subsequently heated to 2000K for melting.

After sufficient equilibration at the liquid state we removed the boundary condition in one direction, thus introducing free surfaces; afterwards, the systems were cooled down to 300K imposing a cooling rate of 10K/ps. Finally all systems were equilibrated at room temperature for 100 ps. In all simulations the temperature was controlled by means of the Nose's demon.

3.3. Results

In order to assess the structure of the systems at 300K we calculated the radial distribution functions (RDF), depicted in (Fig.3.1)

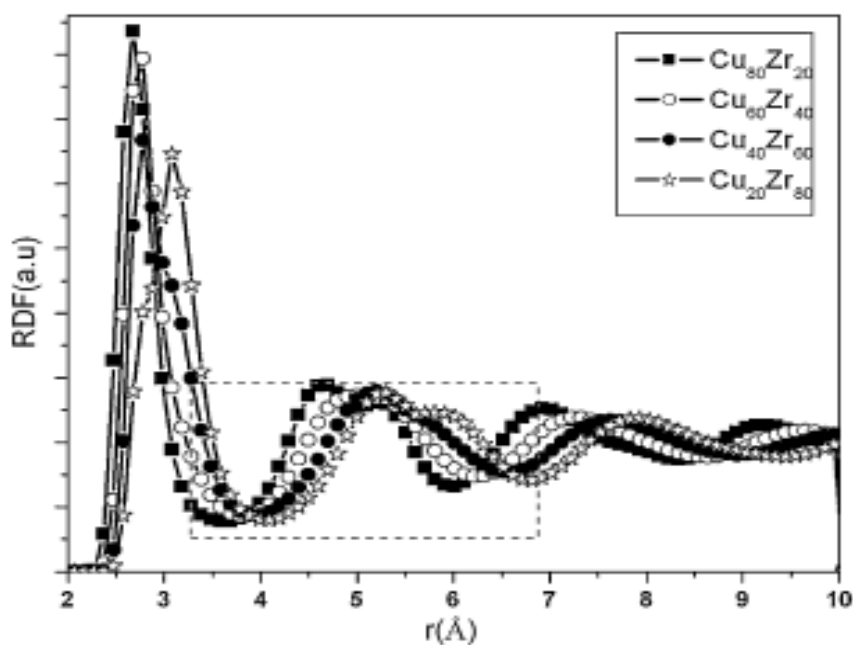


Fig.3.1. Radial distribution functions for various stoichiometries $\text{Cu}_x\text{Zr}_{1-x}$.

It came out that all systems exhibit typical amorphous characteristics and that there is a clear shift of the positions of all peaks to larger distances upon increasing the Zr content. It turns out therefore, that the elemental ratio in the glass influences significantly the resulting system's micro-structure.

In order to gain further insight we performed detailed Common Neighbor Analysis (CNA) [9, 10]. From our analysis it came out that 555 was the prevailing index in all

stoichiometries. Detailed inspection of the results revealed the presence of icosahedral (ICO) 13-atom clusters, in line with previous results [8]. It also came out that in all compositions studied approximately 25% of the atoms belong into these ICO clusters. In addition, for the different stoichiometries studied, we calculated the evolution of the number of ICO clusters as a function of temperature (during the cooling process) (Fig. 3.2).

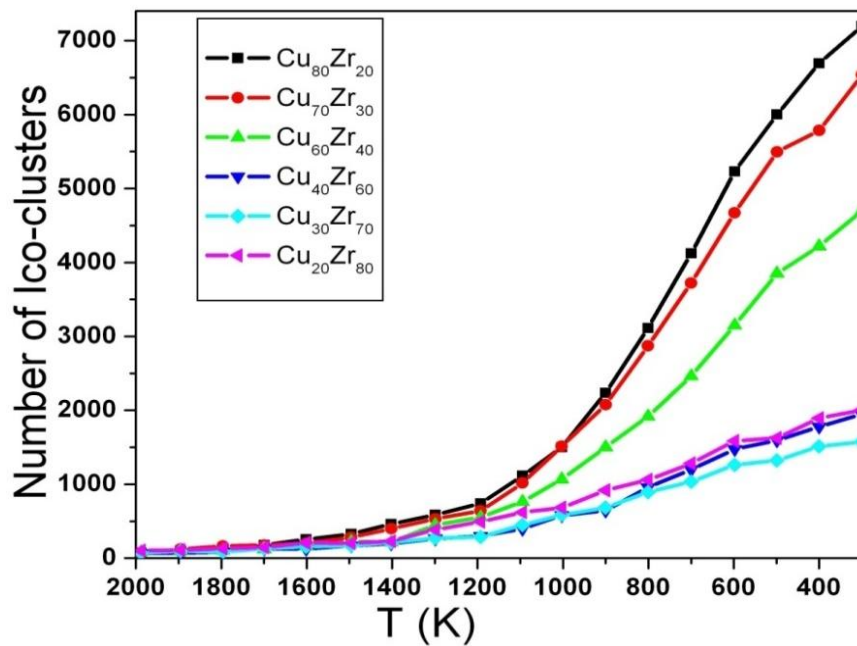


Fig.3.2. Temperature evolution of the number of icosahedral clusters (N_{ico}) upon cooling.

It turns out that at every composition the number of ICO clusters increases as the temperature drops. Again, this result is in agreement with recent findings according to which the number of pentagons as counted by a Voronoi analysis [8] increases upon cooling resulting in micro-structural changes of the glass.

Moreover, we evaluated the correlation between the Cu content of the examined systems and their corresponding number of icosahedral clusters for various temperatures around T_g and for the room temperature respectively (Fig. 3.3). We can conclude that the Cu-rich systems contain more ICO clusters for each of the examined temperatures.

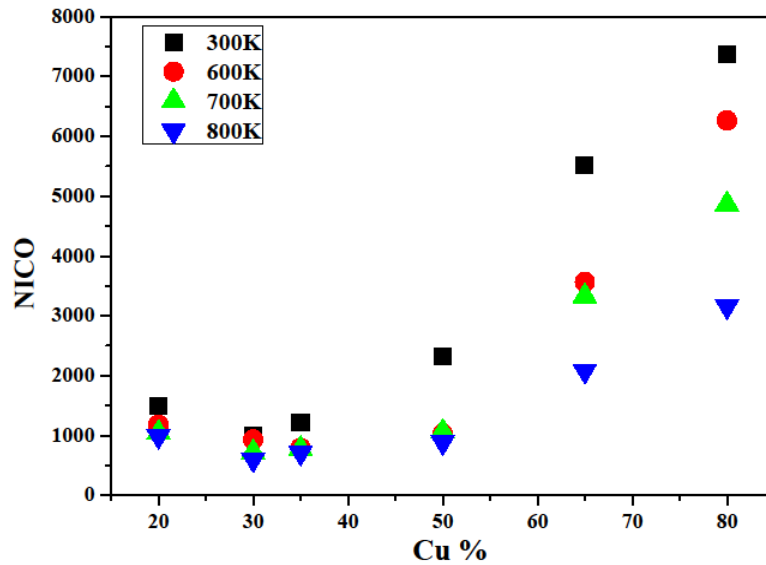


Fig.3.3. Number of icosahedral clusters contained in systems with different stoichiometries $\text{Cu}_x\text{Zr}_{1-x}$ versus 100% Cu content at various temperatures.

Last but not least, we calculated for all compositions the average numbers of Zr and Cu-based 13-atom ICO clusters along with their compositions. The results are gathered in Table 3.1.

It comes out that with the exception of the $\text{Cu}_{20}\text{Zr}_{80}$ system which is Zr-centered, all other cases are Cu-centered clusters, while the cluster's Cu content increases when the glass is enriched in Cu. Interestingly, the later conclusion holds even for the Zr-centered clusters, a fact that albeit their small number in the Zr-based clusters, it is nevertheless indicative for

the ICO cluster forming ability of this element. Moreover, considering the high packing capability of the ICO clusters in conjunction with their tendency in Cu enrichment, this finding explains also the finding that Cu-rich compositions exhibit lower free volume than Zr-rich counterparts [8].

Composition	Cu-ICO			Zr-ICO		
	Abundance (%)	Average cluster stoichiometry		Abundance (%)	Average Cluster Stoichiometry	
		Number of Cu atoms	Number of Zr atoms		Number of Cu atoms	Number of Zr atoms
Cu₈₀Zr₂₀	99,6	9,9	3,1	0,4	11,6	1,4
Cu₇₀Zr₃₀	99,3	8,4	4,6	0,7	10,0	3,0
Cu₆₀Zr₄₀	98,7	7,1	5,9	1,3	8,3	4,7
Cu₄₀Zr₆₀	89,1	4,6	8,4	10,9	4,7	8,3
Cu₃₀Zr₇₀	65,9	3,3	9,7	34,1	3,0	10,0
Cu₂₀Zr₈₀	30,2	2,2	10,8	69,8	1,7	11,3

Table 3.1. Number of Cu and Zr-centered ICO clusters, along with the average cluster atomic compositions.

3.4. Concluding remarks

We analyzed the microstructural characteristics of the $\text{Cu}_x\text{Zr}_{100-x}$ ($20 \leq x \leq 80$) metallic glasses. With the exception of the Zr-rich system, we found that the Cu-centered small icosahedral clusters (ICO) are the basic structural unit of the systems, while their number and their Cu content increases with Cu concentration. In addition, we found that upon cooling the solidification process proceeds via the formation of these ICO clusters.

3.5. References

- [1] V.T.Witusiewicz, F. Sommer, J. Alloys Compd. 289 (1999) 152.
- [2] A. Inoue, D. Kawase, A.P. Tsai, T. Zhang, T. Masumoto, Mater. Sci. Eng. A 178 (1994) 255.
- [3] E. Kneller, Y. Khan, U. Gorres, Metallkd. 77 (1986) 152.
- [4] G. Duan, D. Xu, Q. Zhang, G. Zhang, T. Cagin, W.L. Johnson, W.A. Goddard, Phys. Rev. B 71 (2005) 224208.
- [5] D.B. Miracle, Nat. Mater. 3 (2004) 697.
- [6] H.W. Sheng, W.K. Luo, F.M. Alamgir, J.M. Bai, E. Ma, Nature 439 (2006) 419.
- [7] Ch.E. Lekka, A. Ibenskas, A.R. Yavari, G.A. Evangelakis, Appl. Phys. Lett. 91 (2007) 214103.
- [8] M. Wakeda, Y. Shibutani, S. Ogata, J. Park, Intermetallics 15 (2007) 139.
- [9] J.D. Honeycutt, H.C. Andersen, J. Phys. Chem. 91 (1987) 4950.
- [10] A.S. Clarke, H. Jonsson, Phys. Rev. E 47 (1993) 3975.

IV.Chapter 4

Correlation between microstructure and tensile deformation

Stoichiometry

Temperature

- **Bulk-Surfaces**
- Microstructure** ◦ **Deformation** ◦ **Influence of strain-rates**
- **Cross-Correlation**

Mechanical behaviour of 1D and 2D nanosized systems

Clusters as building blocks of MGs

4.1. Introduction

It is well known that the microstructure of a material plays a key role to the way that it accommodates each imposed deformation and also affects strongly its mechanical properties. The same phenomenon occurs in MGs and there are several studies, both experimental and theoretical [1-7], focusing on the mechanisms that take place upon deformation and how these mechanisms are related with the possible alterations in microstructure. Some of these studies relate even the shear bands (SBs) [8-13] with the microstructure, claiming that the SBs (the cause of the MGs failure) are in fact networks of interconnecting clusters [14-18]. Nevertheless there is no generic theory about how the microstructure evolves upon mechanical deformation. Aiming in investigating the evolution of the microstructure and its relation with the deformation, we studied several systems with different stoichiometries, in bulk geometry and also systems with free surfaces. We imposed tensile deformation under a constant strain rate, aiming in finding the possible alterations in their mechanical behavior and in their properties during solicitation. Regarding the microstructure of the systems, we performed CNA analysis, in order to extract the clusters contained in every system and we analyzed the evolution of their number and their inner characteristics upon tension. In order to nominate the correlation between the stress that these system exhibit upon tension and the evolution of the number of the dominant type of clusters we calculated the cross correlation coefficient. Additionally we investigated the influence of the strain rate to the same systems and their microstructure.

4.2. Computational details

We examined six systems with different stoichiometries of $\text{Cu}_x\text{Zr}_{1-x}$ where x stands for $x=20, 30, 35, 50, 65, 80$ with equal number of total atoms $N=128000$. The systems had cubic geometry with dimensions of approximately $13 \times 13 \times 13$ nm (size depends on the stoichiometry) and periodic boundary conditions in all directions. At first we equilibrated our systems at 300K in the NPT ensemble where the temperature and the pressure were controlled by means of the Nose's thermostat and Andersen's barostat, respectively. In the cases of the systems with free surfaces we imposed an empty space of 10nm in the X-direction, thus introducing two free surfaces and we further re-equilibrated the systems at room temperature for additional 200ps. The equilibrated subsystems in bulk geometry and those with free surfaces were then subjected to tensile loads with various strain rates in the Z-direction and a Poisson ratio of 0.34 in the directions with periodic boundary conditions. The equilibrium configurations were analyzed by means of detailed Common Neighbor Analysis (CNA) [19, 20]. Based on our previous work [21] we focused on ICOs, which were found to be the majority in the present systems and we followed their evolution upon tensile deformation for different strain rates.

4.3. Results

4.3.1. Bulk systems

Firstly, we focused on the systems in bulk geometry and we examined their behavior under tensile deformation when imposing a constant strain rate of $10^9(\text{sec})^{-1}$ up to strain of 40 % at RT. In Fig.4.1 the stress strain curves of the systems are depicted and as we can see, all the systems fail before the strain value of 40 % except the poorest stoichiometry in Cu (%), i.e. in $\text{Cu}_{20}\text{Zr}_{80}$.

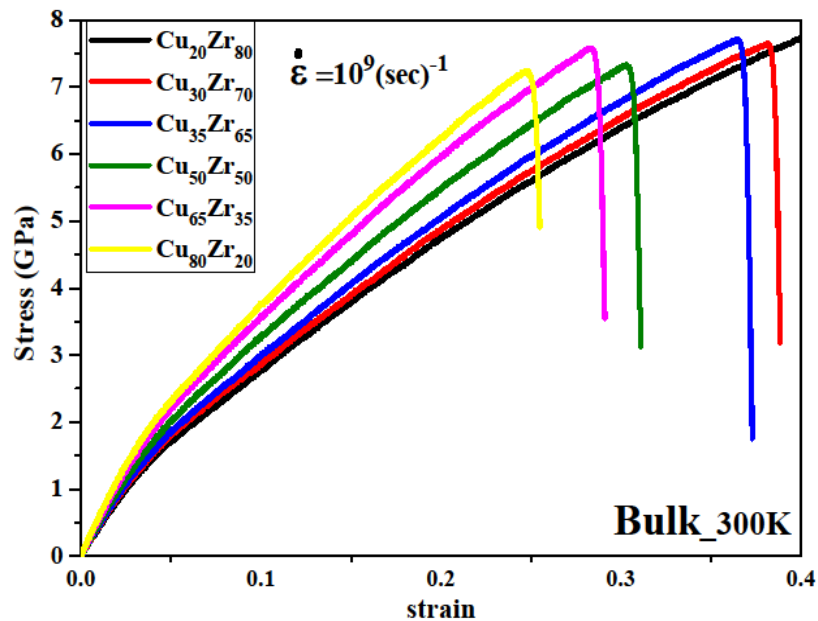


Fig. 4.1. Stress strain curves for all the systems $\text{Cu}_x\text{Zr}_{1-x}$ in bulk geometry at RT under constant strain rate.

Additionally, it is clearly shown that, as Cu (%) content increases, the systems appear to be less ductile, and thus they fail sooner. In addition, they appear to have higher Young modulus (larger slope in the elastic regime). Aiming to find out how the elastic constants are altering as the Cu content changes, we calculated the Young modulus and the yield

strength (0.2% offset) of the systems versus the Cu (%) content which are shown in the Fig.4.2.

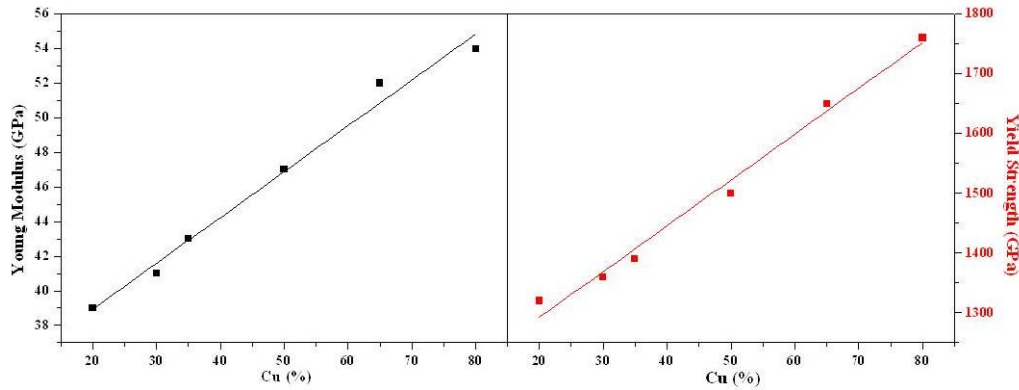


Fig.4.2. Young modulus and yield strength of the bulk systems versus Cu (%) content.

We found out that there is a linear dependence between these two elastic properties, namely the Young modulus and the yield strength versus Cu content, which lead us to the conclusion that the richer systems in Cu are stronger and they exhibit larger elastic regime (higher yield strength). Up to this point the only parameter that changes in our study is the Cu content, which has a direct consequence in the microstructure as we saw, even at equilibrium. More specifically the number of icosahedral clusters, which are the majority in our systems, increases with the increase of Cu content not only at RT but even at 600K, 700K and 800K.

The question that arises from this finding is how the microstructure changes upon deformation, as the stoichiometry changes. To this end we performed CNA analysis in all the systems at every 100 simulation steps which corresponds to a strain step of 0.0005. Fig.4.3 displays the evolution of the dominant type of clusters upon tension. As we can see from this figure the number of icosahedral clusters decreases continuously till failure.

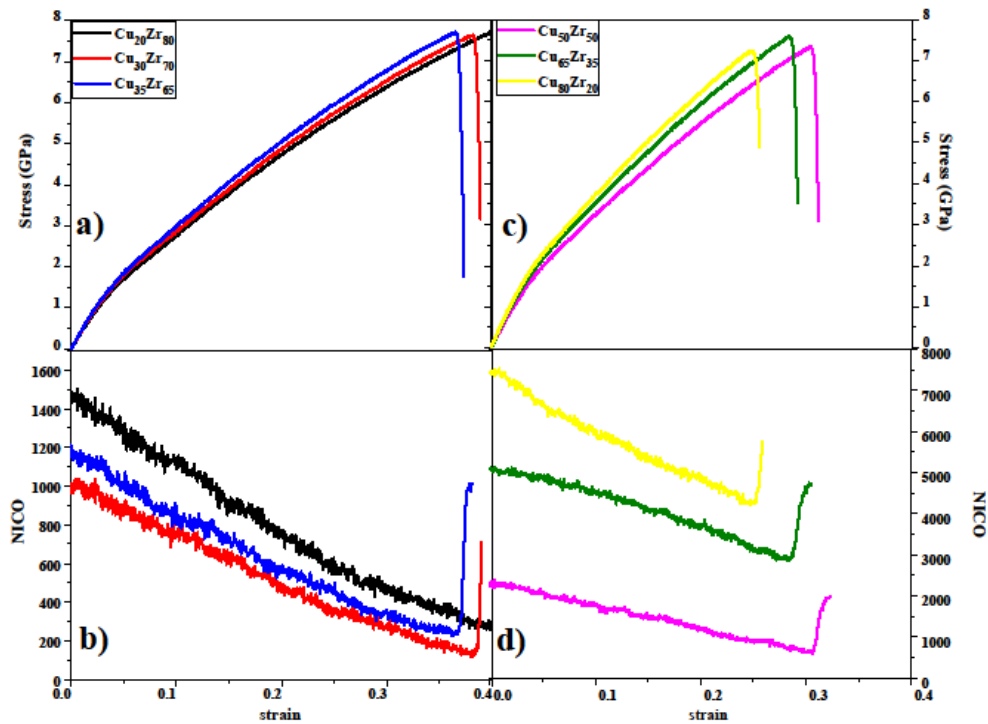


Fig.4.3. Stress strain curves and the corresponding evolution of the number of icosahedral clusters (NICO) of the low Cu (%) content [a) and b)] and of the rich Cu content [c) and d)].

From the above figure it is obvious that the continuous increase in the stress of all systems is accompanied with a continuous decrease in the number of icos. This result is a clear proof that the changes in the microstructure are simultaneously reflected at the mechanical behavior of the systems. Additionally, it is well known that the as the number of clusters increases in a metallic glass, the free volume decreases because the alloy becomes more denser-packed. Consequently, stoichiometries with high percentage of clusters appear to be more denser-packed, and taking into account that icosahedral clusters are one of the most denser-packed types of clusters, these stoichiometries display greater resistance to deformation, namely greater structural stability than those stoichiometries with low

percentage of clusters. Arguably it is expected that systems with poor stoichiometries in ICOS (less Cu %) can be more ductile than the rich in ICOS stoichiometries.

Looking closer in Fig.4.3 we can see that richer in Cu stoichiometries (left column) display greater resistance to deformation (higher stresses) than the poor ones. They can be deformed as long as the number of ICOS decreases, meaning that their free volume increases and thus further deformation is allowed (larger ductility).

Another interesting observation about the correlation between the changes of the microstructure and the mechanical behavior under tension is that even the way that slope changes in the stress strain curves is identical with the slope changes of the evolution of ICOS number. This is illustrated in the Fig.4.4 showing a superposition of the strain-stress and the evolution of the percentage of system atoms participating in ICOS of $\text{Cu}_{50}\text{Zr}_{50}$.

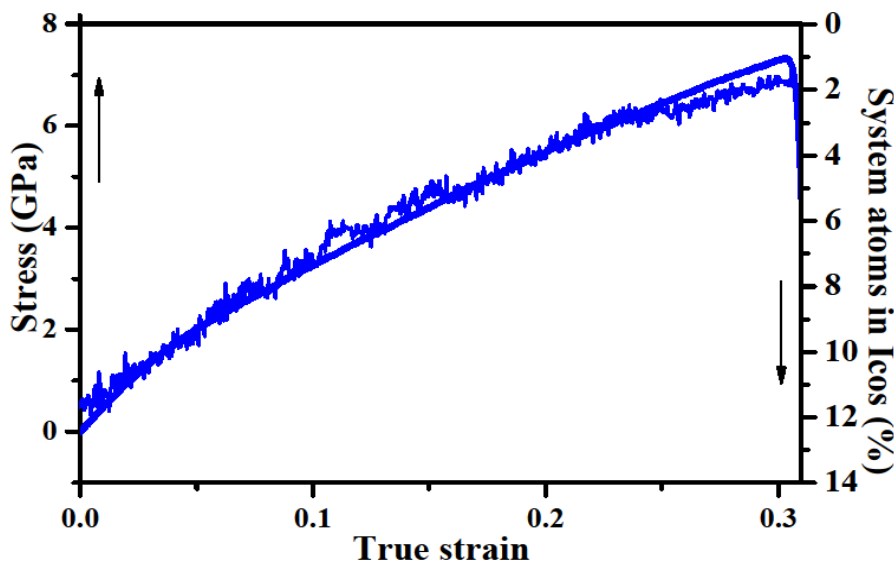


Fig.4.4.Stress-

strain curve and the evolution of ICOS versus strain for strain rate= 10^9sec^{-1} .

From the SSC (with strain rate of 10^9 (sec)^{-1}) we estimated that the elastic region lasts till 3% strain, which is in agreement with another theoretical work by Zhang Y. et al. [22]

where a potential based on the Embedded Atom Method was used. In addition, we deduced a bulk modulus around 50 GPa, which is lower from the experimental value estimated by electromechanical device [23] by 16%, and 21% from the one obtained by XRD [23], while it deviates by approximately 30% from the value estimated by Wang et al. [24]. The yield strength, using 0.2% offset strain, was found to be around 1500 MPa. Interestingly, this agreement is confirmed by considering another approach for the estimation of these numbers, related with the evolution of the microstructure. Given that in the plastic region the SSC follows a power law relation, a log-log representation would provide linear dependence within this region and therefore would result in a more convincing criterion for the estimation of the yielding point. In addition, if this effect is correlated with the NICO evolution we could conclude on the origin of the phenomenon. Fig. 4.5 depicts these plots for both SSC and NICO.

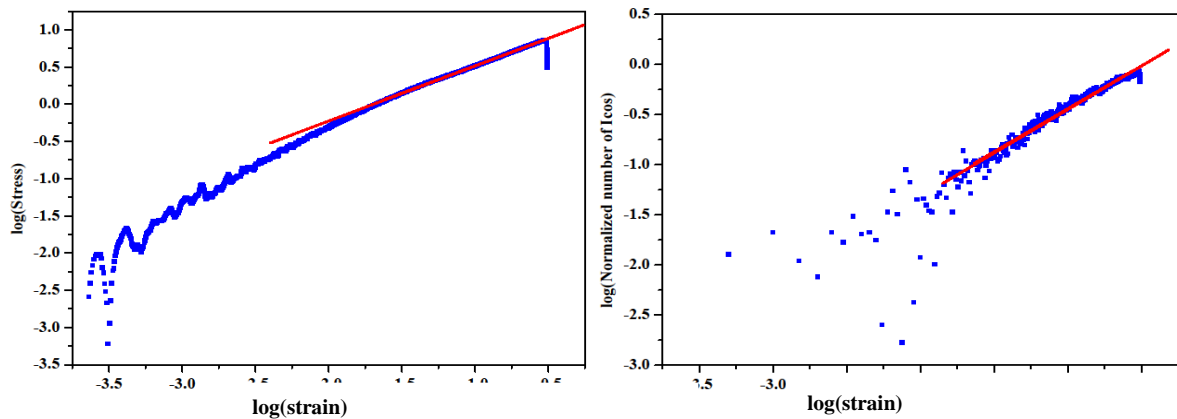


Fig.4.5. Log-Log diagrams for the relations of stress-strain and normalized number of Icos-strain

We can see that both quantities deviate from linearity for $\log(\text{strain})$ values that are lower than -1.5, suggesting this value as the end of the elastic region (or the onset of the plastic region). Therefore, the yield strength is estimated again around 1500 MPa, in agreement with the experimental value of 1500GPa [24]. Moreover the onset of necking is now predicted from both Figs. 4.4 and 4.5 at strain of 32%.

Moreover, we found that this reduction in the ICO number is accompanied by important alterations in the ICOs' stoichiometries. Indeed, careful analysis of these ICO clusters (that are basically by more than 90% Cu centered) revealed that upon deformation the mean number of the participating Cu atoms increases at expense of the Zr atoms, Fig. 4.6 as calculated in three stoichiometries $\text{Cu}_{35}\text{Zr}_{65}$, $\text{Cu}_{50}\text{Zr}_{50}$ and $\text{Cu}_{65}\text{Zr}_{35}$.

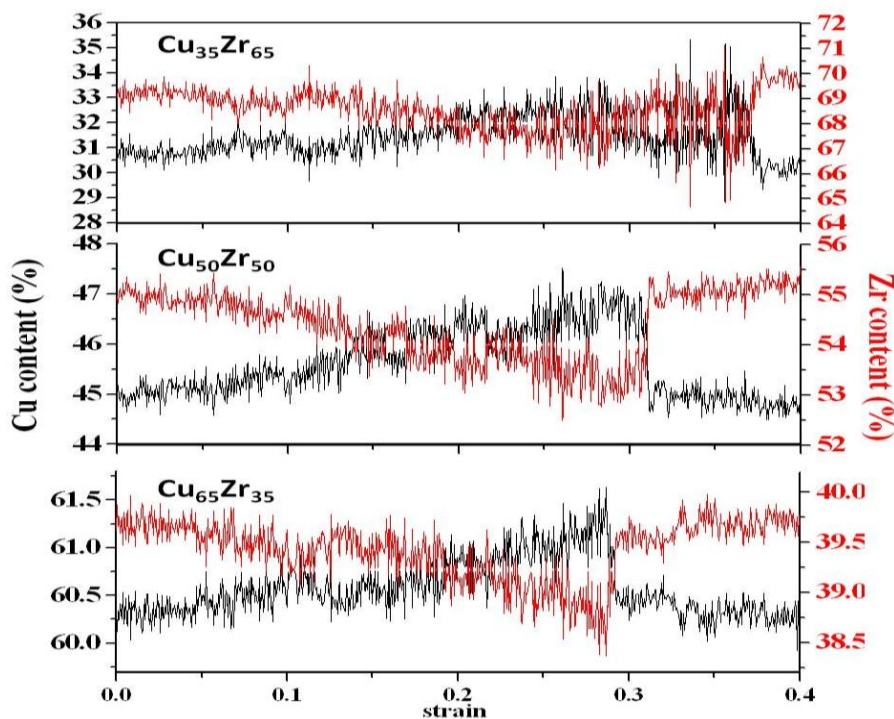


Fig.4.6. The evolution of Cu and Zr atoms participating in ICO clusters versus strain for three stoichiometries $\text{Cu}_{35}\text{Zr}_{65}$, $\text{Cu}_{50}\text{Zr}_{50}$ and $\text{Cu}_{65}\text{Zr}_{35}$ (strain rate 10^9 sec^{-1}).

Taking into account that there is a kind of substitution of Zr atoms by Cu atoms in the ICO's stoichiometry, during sollicitation, and that the size of Zr atoms is almost twice the size of Cu atoms, the calculated mean radius of the ICOS clusters was expected to decrease. However, the mean radius of ICOS displays an increase, for three of the stoichiometries $\text{Cu}_{35}\text{Zr}_{65}$, $\text{Cu}_{50}\text{Zr}_{50}$ and $\text{Cu}_{65}\text{Zr}_{35}$ as depicted in Fig.4.7. This fact leads to the conclusion that even the most densed-packed structures in MGS, become less dense resulting to the enhancement of the free volume in systems which in turn allows for further deformation.

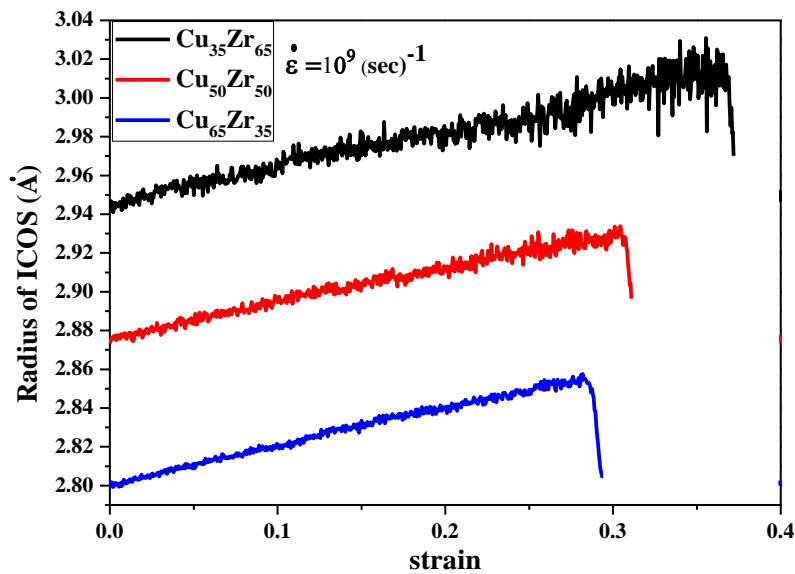


Fig.4.7. The evolution of the mean radius of ICOS upon tension at RT and under a constant strain rate (10^9 sec^{-1}).

Another structural characteristic of ICOS, eg. the mean radius follows the same motif as their number and stoichiometry, which means that it displays a clear drop at the exact strain value where the system fails proving once more that all the inner characteristics of ICOS are changing in a synchronized way with the imposed deformation.

4.3.1.1. Influence of the strain rate on bulk systems

In order to examine the influence of the strain rate on the bulky systems we examined the mechanical behavior of three different stoichiometries $\text{Cu}_{35}\text{Zr}_{65}$, $\text{Cu}_{50}\text{Zr}_{50}$ and $\text{Cu}_{65}\text{Zr}_{35}$ under three different strain rates, namely $10^8, 10^9$ and $10^{10} \text{ (sec)}^{-1}$ upon solicitation at RT and till the strain of 40%.

The SSCs of each stoichiometry are illustrated in Fig.4.8 and as we can see are almost identical except from the strain value that corresponds to the failure of systems. More specifically, the systems imposed to the faster strain rate namely the $10^{10} \text{ (sec)}^{-1}$ fail later in all stoichiometries, and expect the case of $\text{Cu}_{50}\text{Zr}_{50}$, we could say that as the strain rate increases, the systems display higher ductility and thus they fail later than that systems that were subjected to the slower strain rates.

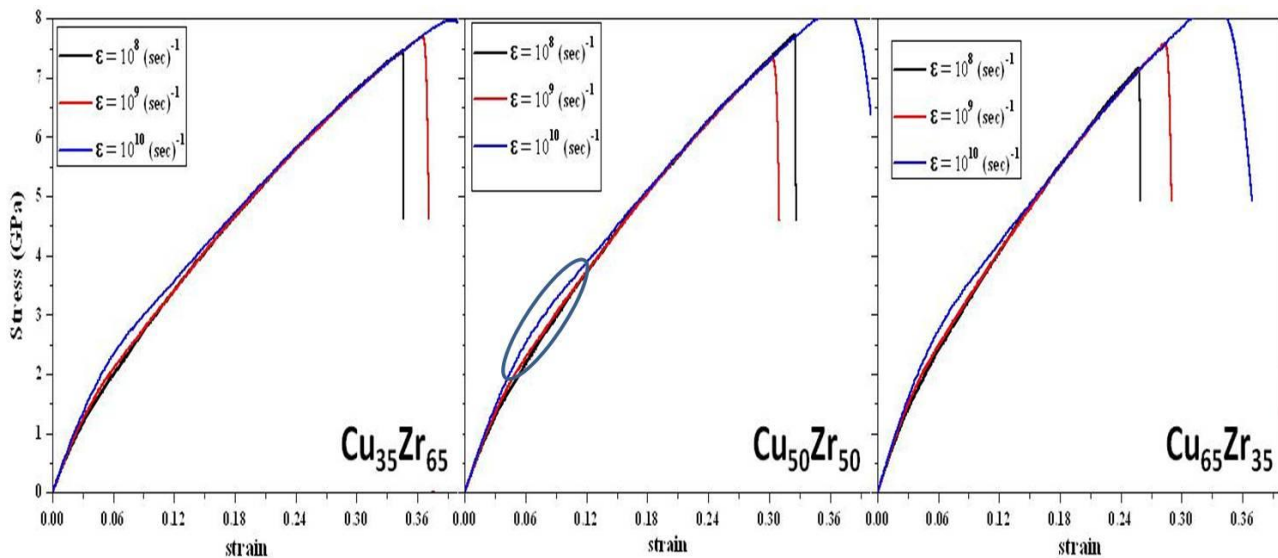


Fig.4.8. Stress strain curves under three different strain rates of $\text{Cu}_{35}\text{Zr}_{65}$, $\text{Cu}_{50}\text{Zr}_{50}$ and $\text{Cu}_{65}\text{Zr}_{35}$ bulk systems at RT.

However, except from the obvious difference in the strain value at failure the bulk systems exhibit almost zero strain rate sensitivity at RT. The strain rate sensitivity (SRS), (m) demonstrates how sensitive is a system to the imposed strain rate and thus a system with zero SRS is strain rate insensitive, meaning that the stress strain curves of different strain rates are identical. It is also related to the resistance of a system towards necking (higher SRS denotes higher resistance to necking) and it is given by the relation:

$$m = (\partial \ln \sigma / \partial \ln \dot{\epsilon})_{\epsilon} \quad (4.1)$$

Where σ and $\dot{\epsilon}$ denote the stress and the strain rate, respectively.

In the case of $\text{Cu}_{50}\text{Zr}_{50}$ where the stress strain curve corresponding to the strain rate of 10^9 $(\text{sec})^{-1}$ fails sooner than the one with the rate of 10^8 $(\text{sec})^{-1}$, we present in Fig.4.9 the corresponding evolution of ICOS. We can see that the microstructure follows the behavior of the stress strain curves, and more specifically, the evolution of ICOS corresponding to rate 10^9 exhibit sooner a clear increase of their number compared with the one corresponding to the rate of 10^8 $(\text{sec})^{-1}$. Additionally, even the slight difference that appears between the stress strain curve of strain rate of 10^{10} $(\text{sec})^{-1}$ and 10^9 $(\text{sec})^{-1}$ in the strain range of 0.06 till 0.12 it is clearly reflected in the evolution of ICOS at the very same strain range.

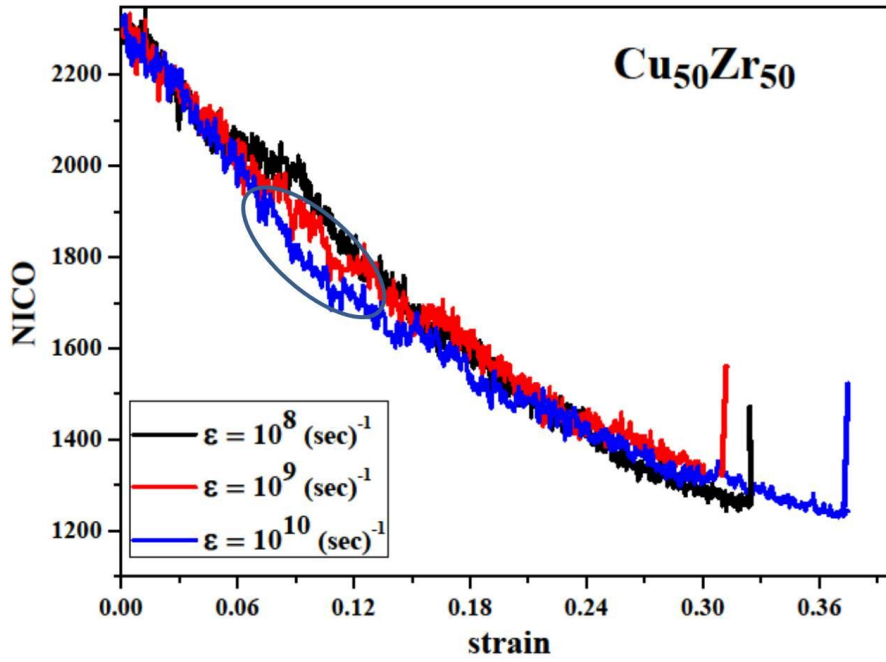


Fig.4.9. The evolution of ICOS of the $\text{Cu}_{50}\text{Zr}_{50}$ bulk system for three different strain rates upon tension at RT.

Furthermore in order to investigate the influence of the strain rate when the stoichiometry is the only parameter that changes and the strain rate is kept constant, we present in the Fig. 4.10 the stress strain curves for the three stoichiometries mentioned above.

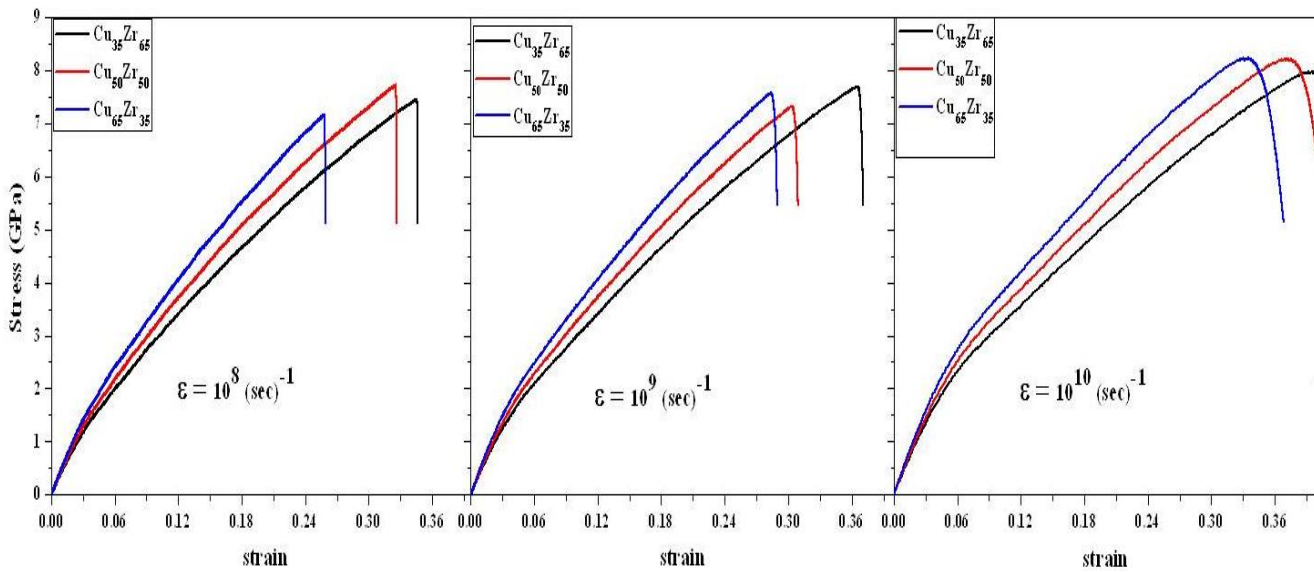


Fig.4.10. Influence of the strain rate for different stoichiometries of bulk systems at RT.

As we can see the same motive as in case of $\text{Cu}_{50}\text{Zr}_{50}$ is followed by the other two stoichiometries, meaning that for all the examined strain rates the Cu rich stoichiometries fail sooner than the Cu poor, while the former exhibits higher Young modulus and yield strength.

4.3.1.2. Concluding remarks

Summarizing we could say that the bulk systems exhibit higher Young moduli and yield strengths as the Cu content (%) in $\text{Cu}_x\text{Zr}_{1-x}$ increases and they fail earlier upon tensile deformation, under a constant strain rate. This fact is highly correlated with the number of ICOS that these systems contain and its evolution. The richer stoichiometries in Cu (%) contain greater number of ICOS, at equilibrium, but in all stoichiometries their number decreases and the evolution of their number matches with the corresponding stress strain curves. This high correlation between the two quantities, i.e. the stress and the evolution of the number of ICOS originates from the fact that as their number decreases, the free volume of the systems increases, leading to less dense systems, and thus more ductile systems. Regarding the influence of the strain rate on the mechanical behavior of a system the bulk systems don't exhibit strain rate sensitivity, which means that for such high rates the produced strain rates are almost identical and the same phenomenon is reflected to the evolution of ICOS.

4.3.2. Results

4.3.2.1. Systems with surfaces

Aiming in the study of the influence of free surfaces in the mechanical deformation, we performed similar analysis for the same systems with surfaces and a constant strain rate of 10^9 (sec)^{-1} , Fig.4.11.

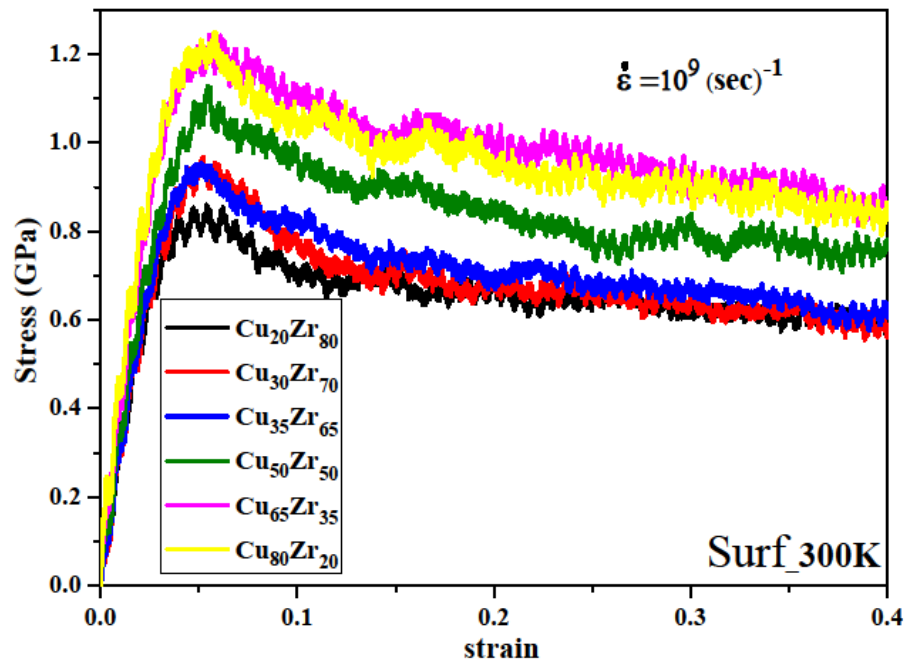


Fig. 4.11. Stress strain curves for all the systems $\text{Cu}_x\text{Zr}_{1-x}$ with free surfaces.

We see that none of the systems fail till the strain of 40%, contrary to the bulk systems, probably due to the existence of free surfaces. This phenomenon is attributed to the presence of free surfaces that give to the systems more freedom to relax and thus to accommodate the imposed deformation, avoiding the drastic changes in the microstructure, as in the bulk case. In this sense we would expect extended plasticity for these systems.

In addition, the SSCs of all systems are marked by significant serrations. We recall that this effect was not visible in the corresponding curves of bulk systems, but it was present

in the corresponding evolution of the number of ICOs with strain. It turns out therefore, that the presence of surfaces enable the observation of these effects, suggesting that the accommodation of the strain is closely related to distinct events occurring in the clusters through atomic rearrangements that are enforced from the applied strain.

Moreover, the richer in Cu stoichiometries appear higher ultimate strength and higher Young moduli (although less than that of the bulk systems) and yield strengths, Fig.4.12.

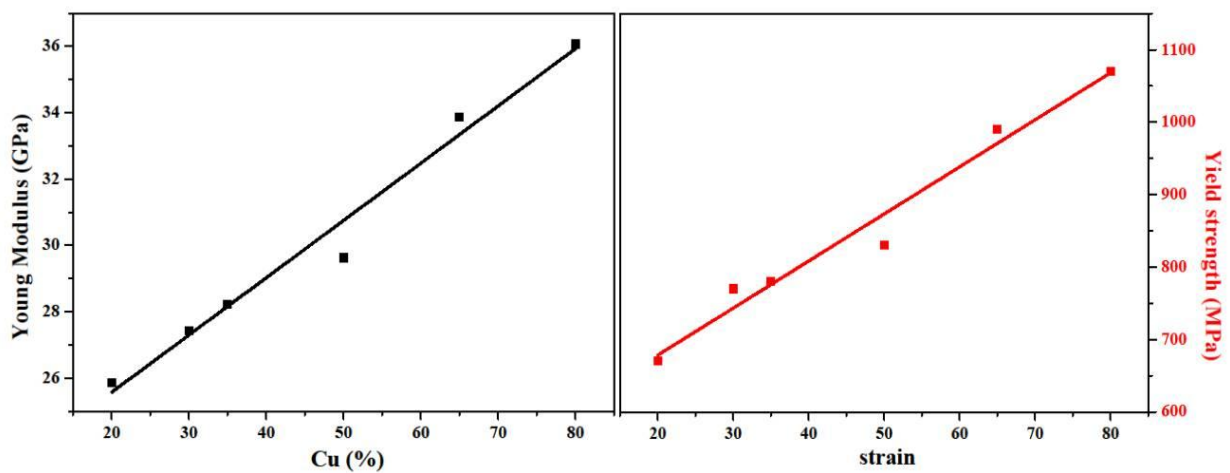


Fig.4.12. Young moduli and yield strengths of the systems with surfaces versus Cu (%) content.

Regarding the study of the microstructure upon tension, we extracted the clusters contained in every system and their evolution upon deformation by performing CNA analysis. In the next Fig.4.13 we present both the stress strain curves and the evolution of the number of the icosahedral clusters

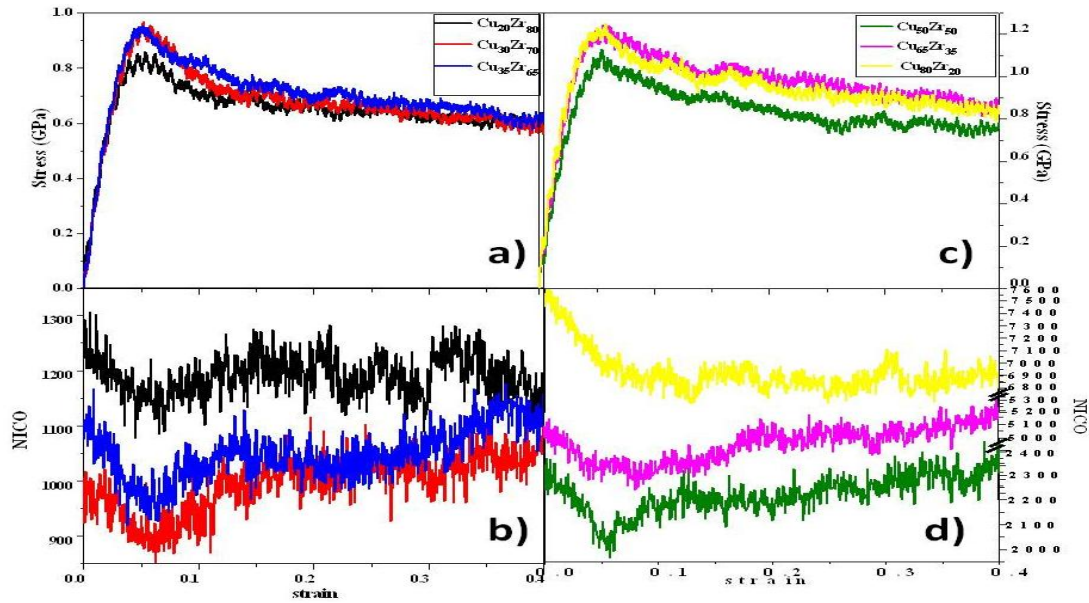


Fig.4.13. Stress strain curves and the corresponding evolution of the number of icosahedral clusters (NICO) of the poor stoichiometries in Cu (%) systems [a) and b)] and of the rich [c) and d)].

As we can see the phenomenon of the serrations now is highlighted even in the case of the evolution of the number of ICOS. Moreover, if we focus on the down half pictures b and d we can see that for all stoichiometries the number of ICOS remains approximately constant till the elastic limit, (the upper point where the linearity of the stress strain ends), which is estimated in a narrow region till 0.025 and it is in agreement with another work [25]. This is due to the fact that in this small strain region the ICOS conserve their number through creations of news and construction of old ICOS and thus enhancing the ability of the system to deform reversibly.

Beyond the elastic limit, the number of ICOS decreases continuously (as the stress increases) up to a minimum that matches with the maximum value of the stress (ultimate tensile strength). Again, as in the case of bulk systems, the decrease in the number of ICOS leads to the increase of the free volume and the systems are able for further deformation.

Beyond the ultimate strength the stress decreases and this is accompanied by an increase in the number of ICOS and when the stress starts to fluctuate around a mean value, the number of ICOS follows the same trend. In order to highlight the correlation between the microstructure of the systems with surfaces and the accommodation of the tensile deformation, we performed, as in the bulk case of $\text{Cu}_{50}\text{Zr}_{50}$, a mirror operator to the graph of the number of ICOS along the x-axis, illustrated in the Fig.4.14.

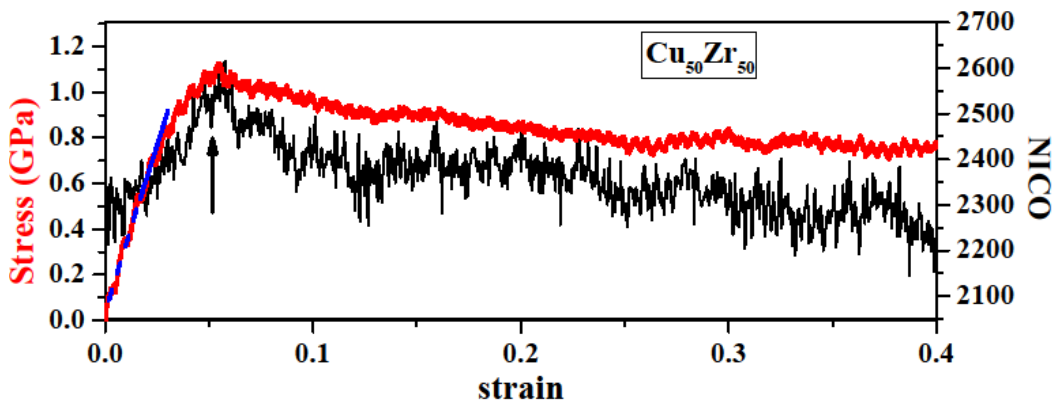


Fig.4.14. Stress strain curve of $\text{Cu}_{50}\text{Zr}_{50}$ along with the number of ICOS.

In the same direction as previously we investigated the evolution of the ICOS stoichiometry upon tension for the three stoichiometries studied in the bulk case, $\text{Cu}_{35}\text{Zr}_{65}$, $\text{Cu}_{50}\text{Zr}_{50}$ and $\text{Cu}_{65}\text{Zr}_{35}$ and under the same strain rate of 10^9 sec^{-1} and the results are presented in the following Fig.4.15.

As we can see from all stoichiometries, in contrast with the bulk case, where the Cu content continuously increases and the Zr content decreases, the contents in the two elements vary in a more complicated way as their corresponding stress strain curves of the same strain rate. More specifically, their content in both elements remains constant till the elastic limit, and beyond this, the trend of Cu is to increase (and thus the Zr content to

decrease) in line with the bulk case, but with greater oscillations in their values and changes in their slopes exactly as their stress strain curves.

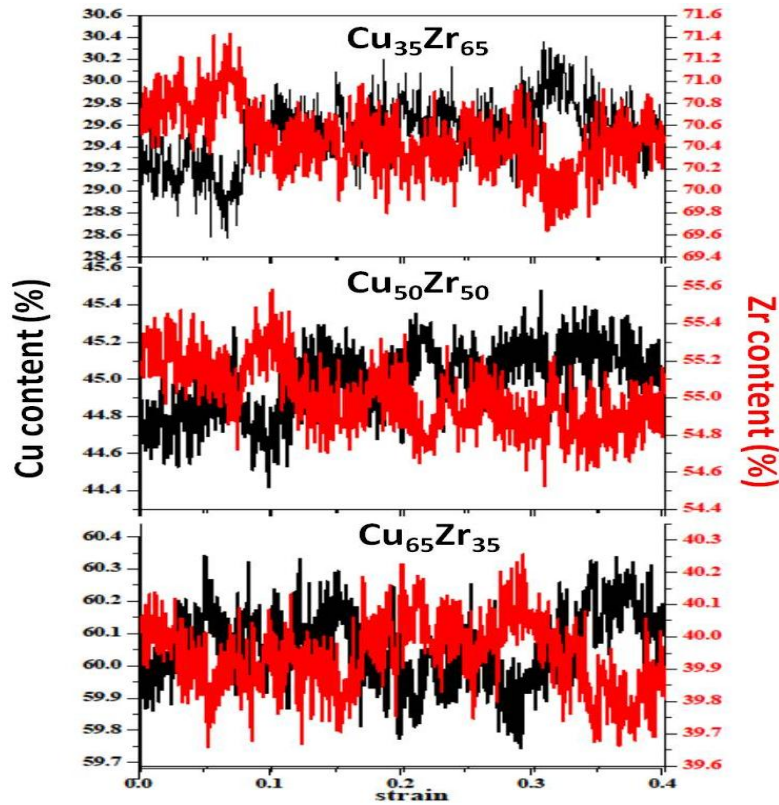


Fig.4.15. Evolution of ICOS stoichiometry under tension (strain rate of 10^9 (sec)⁻¹) of the system (with free surfaces) $\text{Cu}_{50}\text{Zr}_{50}$.

Moreover, the mean radius of the ICOS doesn't continuously increases, as in the bulk case, but at first it increases till a maximum value and then it fluctuates around a mean value. This fact leads to the conclusion that, due the presence of free surfaces allows the system to be deformed in a less forced way than the bulk systems with no drastic changes in the inner characteristics of ICOS.

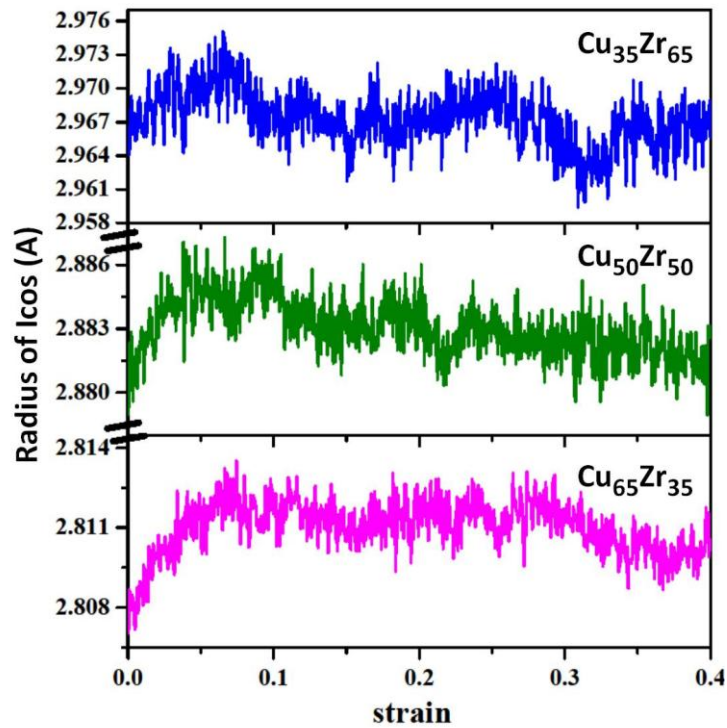


Fig.4.16. The evolution of the mean radius of ICOS upon tension at RT and under a constant strain rate (10^9 sec^{-1}) of systems with surfaces.

4.3.2.2. Influence of the strain rate on systems with surfaces

As in the case of bulk systems we examined our systems with free surfaces under two strain rates in order to study the possible alterations, as illustrated in Fig.4.17. It came out that even for the slowest of one order of magnitude strain rate, the motif was the same as in the bulk systems, namely as the Cu (%) increases the systems exhibit slightly higher Young Moduli, clearly higher ultimate tensile stresses and yielding points.

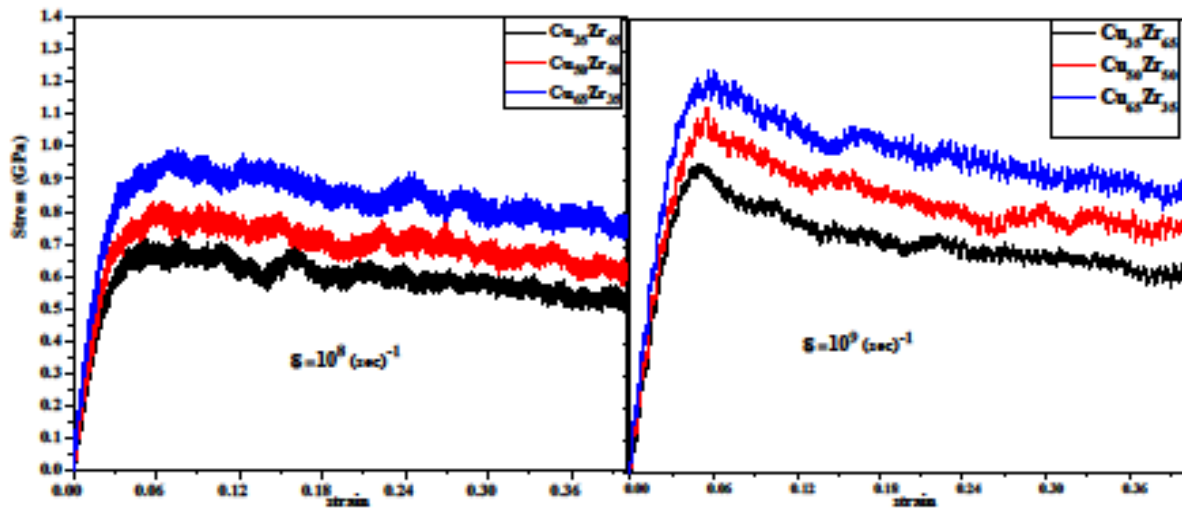


Fig.4.17. The influence of the strain rate on different stoichiometries of systems with free surfaces at RT.

Regarding the changes in the stress strain curves for a given stoichiometry, when the strain rate increases there is no changes in the Young moduli, Fig.4.18, but there is a clear increase in the ultimate tensile strengths. The fact that in systems with free surfaces the stress increases when the strain rate increases too, reveals a positive strain rate sensitivity, which in turn indicates greater resistance to necking and thus more ductility, the systems fail at strain value of 40%, contrary to the bulk cases.

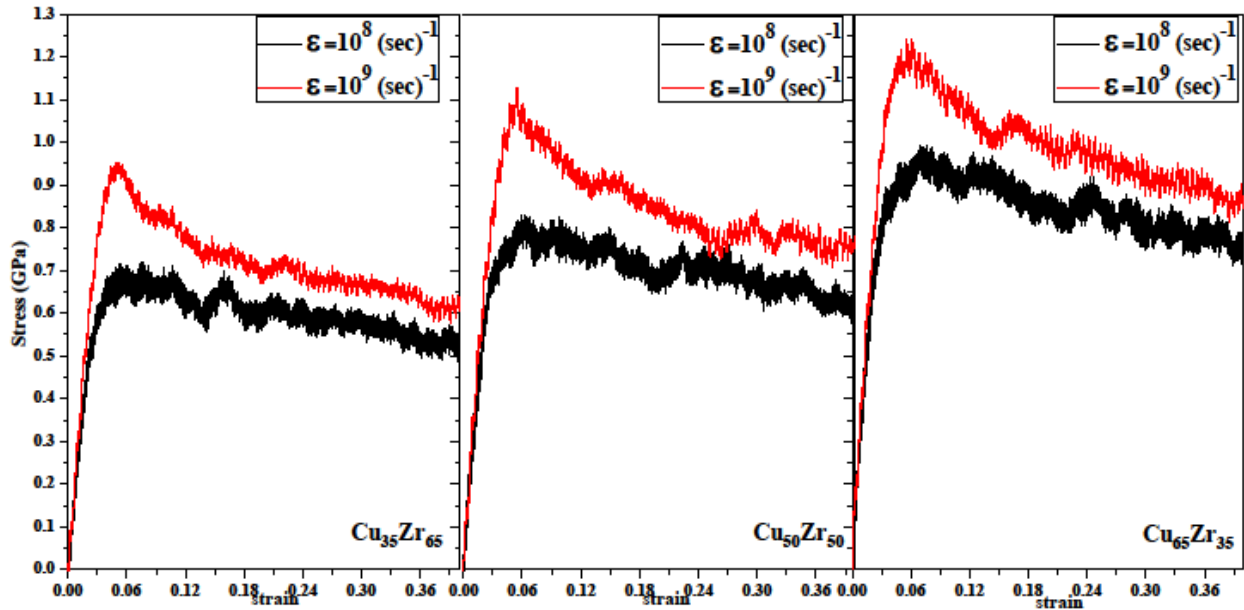


Fig.4.18. The influence of the strain rate on different stoichiometries of systems with free surfaces at RT.

4.3.3. Conclusions

Concluding, systems with free surfaces appear to have slightly higher Young moduli and yield strengths when Cu (%) content increases and higher ultimate tensile strengths. None of the stoichiometries fail till the strain value of 40%, however it starts decreasing after the strain value that corresponds to the ultimate stress. Focusing on the evolution of the icosahedral clusters they evolve in a different way than in the bulk systems. More specifically, they remain almost constant in number till the elastic limit, permitting in that way the reversibility of the deformation because no changes take place in the free volume of the system. Beyond the elastic limit they decrease continuously, leading in increase of the free volume of the system, and thus higher stresses can be achieved, while after a certain strain value they saturate around a mean value, similarly with the evolution of the stress. In the stoichiometries in which higher rate of decrease was observed the ICOS exhibit a slight increase of their value (decrease of free volume).

Moreover, systems with free surfaces exhibit positive strain rate sensitivity which means greater resistance to necking, contrary to their bulk counterparts that display zero strain rate sensitivity.

4.3.4. Cross-Correlation

Taking into account these results on bulk systems and systems with surfaces referring to the fact that the changes in the microstructure of MGs are closely related with the deformation accommodation of the systems, an arguable question is raised: are the stress of a system under tension and the evolution of the number of clusters correlated somehow? In order to investigate the existence of any correlation between the two signals (or time series) we calculated the cross correlation coefficient of these two quantities. The term ‘signal’ is used because every quantity that evolves with time can be characterized and faced as a signal.

We focused on the systems with free surfaces because the presence of the serrated flow [26-29] is more highlighted in both signals (stress and number of clusters). Despite the fact that these serrations have been observed even experimentally and nowadays it is a well known phenomenon in the metallic glasses, there is not any systematic study concerning their relationship with the microstructure of MGs.

Generally speaking, “correlation” is in fact a process that establishes whether or not a relationship exist between two signals. More specifically, correlation does not equal causation. If two signals are correlated it only means that two signals are related. Consequently, saying that one of them “causes” the other is completely wrong. Correlation tells you that when the one signal changes, the other seems to change in a predictable way.

Concluding, cross correlation is a well-known and accurate method of detecting the degree to which two signals are correlated. It is estimated through the following coefficient which is called cross correlation coefficient [30] and is given by:

$$CC(k) = \frac{C_{xy}(k)}{\sqrt{C_{xx}(0)C_{yy}(0)}} \quad (4.2)$$

Where x and y are two signals, each with N data points.

$C_{xy}(k) = \sum_i (x(i) - \bar{x})(y(i-k) - \bar{y})$ is the covariance of x and y and C_{xx} , C_{yy} are the standard deviations of x and y respectively. Also k is a number indicating the time shift of one signal with respect to the other. The values of k can be $k=0,1,2,\dots,N-1$. The time shift k (or time delay) between the two signals is this k that corresponds to the maximum or minimum value of $C_{xy}(k)$. When $k=0$ for the two signals it means that they are absolutely synchronized in time.

The $C_{xy}(k)$ lies between $-1 \leq C_{xy}(k) \leq 1$ and the higher the absolute value of $CC(k)$ the higher the correlation of the two signals. Moreover when the $CC(K)$ has a positive value, it means that the two signals vary in the same fashion e.g they both decrease or increase, whereas when it has a negative value it means that the two signals vary in an opposite way and finally when it equals to zero it means that two signals are not correlated. These cases are summarized below:

- $CC(k) > 0$, *positive correlated* $x \uparrow y \uparrow$, $x \downarrow y \downarrow$
- $CC(k) < 0$, *negative correlated* $x \uparrow y \downarrow$, $x \downarrow y \uparrow$
- $CC(k) = 0$, *not correlated*

In order to verify the obvious correlation between the microstructure and stress from a statistical point of view, we calculated the cross correlation coefficient between the evolution of the number of the clusters and the stress of a system $\text{Cu}_{50}\text{Zr}_{50}$ with free surfaces on x-axis upon tensile deformation and under a constant strain rate of 10^9 (sec)^{-1} . The system contained 70271 atoms and its dimensions were 55-250-90 (Å), respectively. We analyzed three representative areas of equal total strain $\Delta\varepsilon=0.025$ (5000 simulation steps) in the elastic region, in the plastic region and around yielding point as shown in the Fig.4.19.

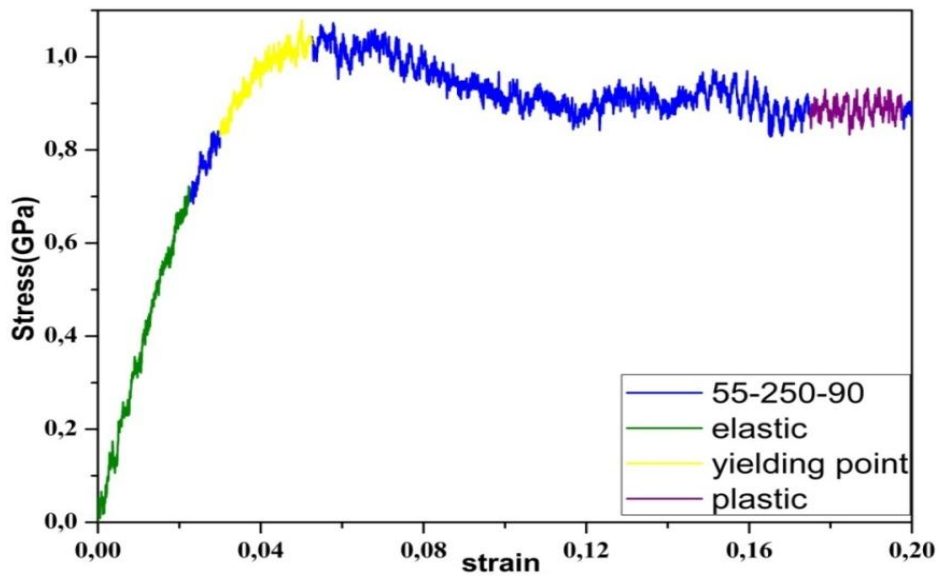


Fig.4.19. The three representative regions of the SSC of the system $\text{Cu}_{50}\text{Zr}_{50}$ with free surfaces.

At each one of these regions we performed exhaustive CNA analysis, which means that we analyzed our trajectory at every simulation step in order to extract the existent clusters and

their sequence evolution upon deformation. It came that the majority of the clusters were icosahedral clusters and the second dominant kind of clusters were the rhombic dodecahedra clusters. The sum of them is what we denote as total number of clusters (Ntot).

As we can see from the Fig.4.20 a) and b) their number decreases in the elastic region and around yielding point, while in the plastic region they display a small increase in their number, resulting in an expected decrease in their volume in two first regions and a small decrease in the plastic region.

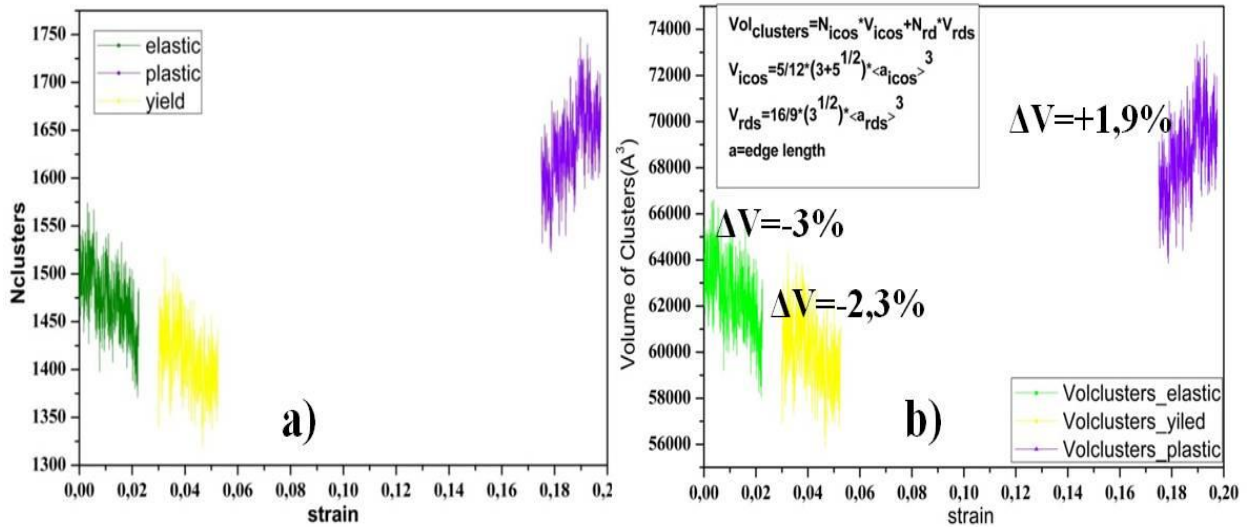


Fig.4.20. The evolution of the total number of clusters of the three regions of the SSC and their corresponding changes in their volumes.

Starting from the fact that both signals (stress and total number of clusters) oscillate with strain as shown in the Fig.4.21 where an example from a small part of the elastic region of the SSC is merged in the same graph with the evolution of clusters, we calculated the windowed cross correlation coefficient. With the term ‘window’ we are referring to each segment (window) of strain, in which the cross correlation coefficient was calculated in order to capture even the smallest changes in the dynamic evolution of the two signals. We

avoided to calculate the coefficient in the whole range of strain since it would be risky because we would have a high possibility to lose the possible random and slight changes of the signals even in the same region due to the evolution of the microstructure upon the deformation.

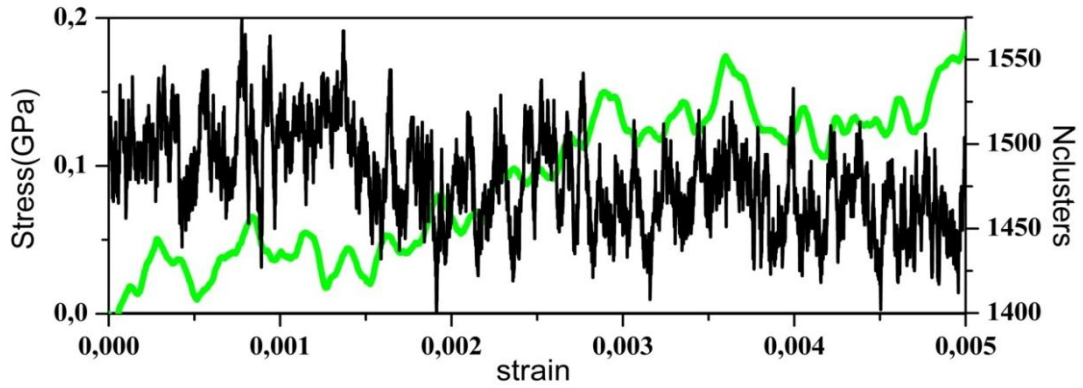


Fig.4.21. Both signals of stress (green line) and the total number of clusters upon tension in the same plot.

The size of the system was kept constant and equal to 100 steps or strain= $5 \cdot 10^{-4}$ in order to ensure the reliability of the results because the standard error of the cross correlation coefficient is given by:

$$SE_{CC(k)} = \sqrt{\frac{1 - cc^2(k)}{N - 1}} \quad (4.3)$$

where N is the number of strain point under study. Consequently, even for the minimum acceptable coefficient of 0.5 the standard error equals to 0.09. In our calculations we accepted only these values of CC(K) where $|CC(k)| > 0.5$.

In the next Fig.4.21 it is illustrated an example of segment again in the elastic region with two signals along with the values of the $CC(k)$ of every window depicted with bars red color. Each of these bars have the real height that corresponds to the absolute value of $CC(k)$ calculated at each window.

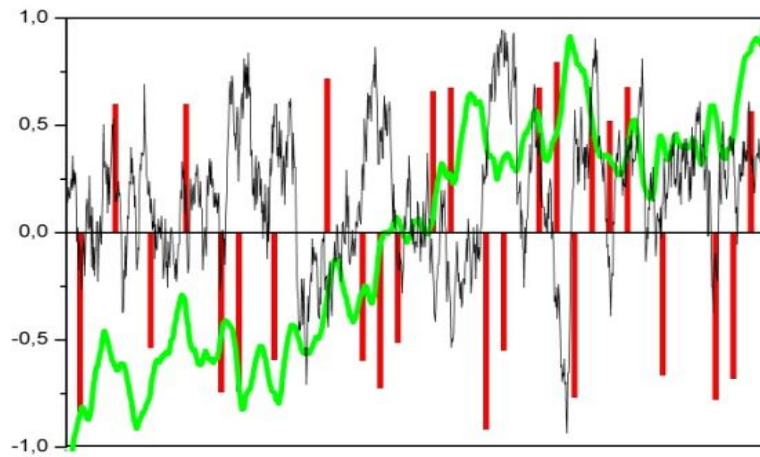


Fig.4.21. Both signals of stress (green line) and the total number of clusters upon tension in the same graphic along with the corresponding $CC(K)$ of every window.

Furthermore, we calculated the percentage of the windows with acceptable values of $CC(k)$ ($CC(k) > 0.5$) at each region independently from the sign of the coefficient. The percentages are gathered in the table below Table.4.1, and as we can see the lowest percentage of windows corresponds to the elastic region (59 %), which is expected, due to the fact in the elastic region the number of clusters remains almost constant resulting in a decrease of correlation between them, while the highest percentage corresponds to the plastic region.

Regions of SSCs	Regions with acceptable value of CC(k) (%)
Elastic	59 %
Yielding point	67%
Plastic	74%

Table.4.1. Percentages of the windows with $CC(k) > 0.5$.

The other interesting observation of this study is that more than the 90% of windows appear a lag or $k=0$, which means that the two signals are absolutely synchronized. A window with an acceptable $CC(k)$ of about -0.9 and zero lag is shown in the next Fig. 4.22.

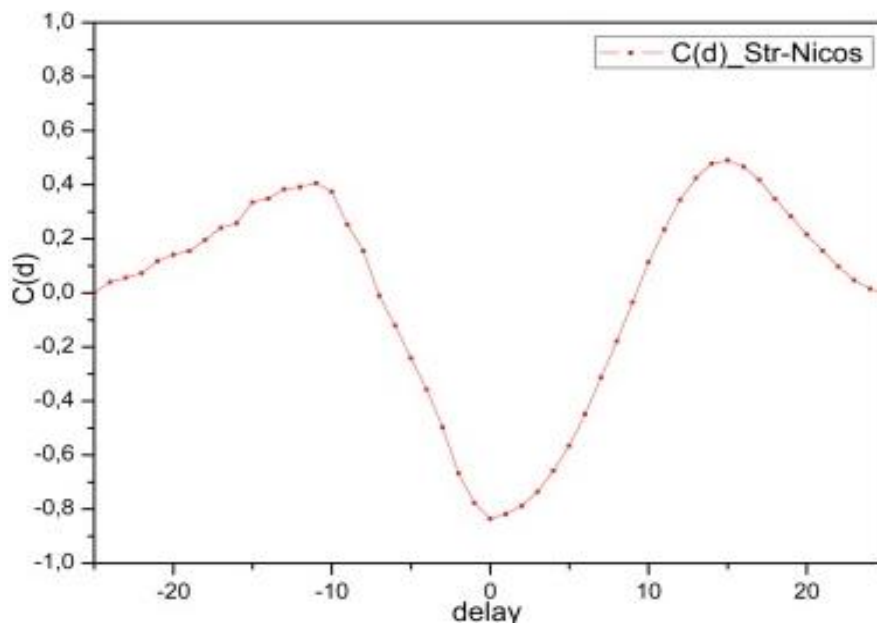


Fig.4.22. A window with $CC(k)$ of -0.9 and zero lag ($k=0$).

Finally, we evaluated the mechanical energy absorbed from the system in the areas of the stress strain curves related with negative, positive and zero $CC(k)$ in order to find the energetic cost for the system when the two signal decrease or increase together, when they vary in an opposite manner and when their behavior is uncorrelated. This was achieved by

integrating the corresponding areas of each window of the regions under study and finally summing them. The idea is depicted in the following Fig.4.23, where three windows with different signs of $CC(k)$ and their corresponding areas of their windows are depicted.

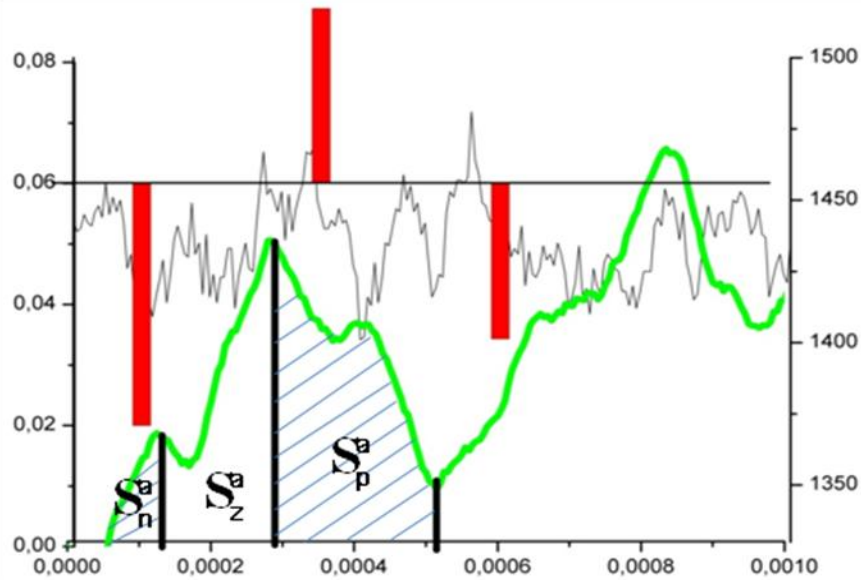


Fig.4.23. An example of the stored energy in the areas of the windows that display positive, negative and zero $CC(k)$.

The following Table.4.2. presents the sum of the stored energy for each of the three different cases.

Segments of $\Delta\varepsilon=0,025$ at (a), (b) and (c) regions	Energy stored in a window with $CC(k) > 0$ (MJ/m^3)	Energy stored in a window with $CC(k) < 0$ (MJ/m^3)
a) elastic	1,6	1,3
b) yielding point	2,9	2,5
c) plastic	2,3	3,2

Table.4.2 . Total energy stored in windows with positive (S_p), negative (S_n) and zero (S_0) in the elastic, plastic region and around yielding point.

Conclusions

The majority of the clusters founded are icosahedra and rhombic dodecahedra. The total volume of clusters decreases in the elastic and around yielding and increases in plastic region. The evolution of total number of clusters is directly correlated with the evolution of stress. Most of the changes in stress are accompanied by simultaneous changes in the number of clusters upon deformation.

4.3.5.References

- [1] Ramsey FP. Econ J 1928;38:543.
- [2] Miracle DB. Acta Mater 2006;54:4317.
- [3] Sheng HW, Cheng YQ, Lee PL, Shastri SD, Ma E. Acta Mater 2008;56:6264.
- [4] Yang L, Jiang JZ, Liu T, Hu TD, Uruga T. Appl Phys Lett 2005;87:061918.
- [5] Shi Y, Falk ML. Phys Rev B 2006;73:214201.
- [6]Ch.E. Lekka, A. Ibenskas, A.R. Yavari, G.A. Evangelakis, Appl. Phys. Lett., **91** (2007) 214103
- [7] M. Lee et al. / Acta Materialia 59 (2011) 159–170
- [8] Spaepen F. Acta Metallurgica 1977;25:407.
- [9] Argon AS. Acta Metallurgica 1979;27:47.
- [10] Steif PS, Spaepen F, Hutchinson JW. Acta Metallurgica 1982;30:447.
- [11] Wright WJ, Hufnagel TC, Nix WD. Journal of Applied Physics 2003;93: 1432.
- [12] Kanungo BP, Glade SC, Asoka-Kumar P, Flores KM. Intermetallics 2004;12:1073.
- [13] Schuh CA, Hufnagel TC, Ramamurty U. Acta Materialia 2007;55:4067.
- [14]L. O. Eastgate, J. S. Langer, and L. Pechenik, Phys. Rev. Lett. 90, 045506, 2003.
- [15]M. L. Falk, J. S. Langer, and L. Pechenik, Phys. Rev. E 70, 011507, 2004.

- [16] J. S. Langer, Phys. Rev. E 64, 011504, 2001.
- [17] M. L. Falk and J. S. Langer, Phys. Rev. E 57, 7192, 1998.
- [18] W. L. Johnson and K. Samwer, Phys. Rev. Lett. 95, 195501, 2005
- [19] J.D. Honeycutt, H.C. Andersen, J. Phys. Chem. 91 (1987) 4950.
- [20] D.Faken, H. Jonsson, Comp. Mater. Sci. 2 (1994) 279-286
- [21] A.E. Lagogianni, G.A. Almyras, Ch.E. Lekka, D.G. Papageorgiou, and G.A. Evangelakis, J. Alloys and Compds, 483, (2009), 658
- [22] Y. Zhang et al. / Acta Materialia 59 (2011) 4303–4313
- [23] J. Das, M. B. Tang, K. B. Kim, R. Theissmann, F. Baier, W. H. Wang, J. Eckert, PRL **94**, (2005) 205501
- [24] Wang G, Mattern N, Pauly S, Bednarcik J, Eckert J. Appl Phys Lett (2009) 95:251906
- [25] Ch.E. Lekka, A. Ibenskas, A.R. Yavari, G.A. Evangelakis, Appl. Phys. Lett., **91** (2007) 214103
- [26] W. J. Wright, R. Saha, and W. D. Nix, Mater. Trans. 42, 642 (2001).
- [27] F. H. D. Torre et al., Appl. Phys. Lett. 89, 091918 (2006).
- [28] C. A. Schuh and T. G. Nieh, Acta Mater. 51, 87 (2003).
- [29] A. L. Greer et al., Mater. Sci. Eng. A 375–377, 1182 (2004).
- [30] Chatfield C. The analysis of time series. New York: Chapman and Hall, 1984

V. Chapter 5

Mechanical behaviour of 1D and 2D nanosized systems

Stoichiometry

Temperature

Microstructure

Deformation

Bulk-Surfaces

Influence of strain-rates

Cross-Correlation

• Mechanical behaviour of 1D and 2D nanosized systems

Clusters as building blocks of MGs

5.1. Introduction

This chapter focuses on the microstructural alterations occurring upon tensile deformation of 2D (foils) and 1D (ribbons) nanosized [1-4] systems of $\text{Cu}_{50}\text{Zr}_{50}$ Metallic Glasses (MG). It came out that for 2D systems (foils, free surfaces only in x- axis) the thickness [1,5-7] may influence the mechanical response (basically yielding point and plastic region), while for thicknesses larger than 2.8nm no significant difference was observable in the SSCs. The microstructure is again marked by the presence of ICOs whose number evolves similarly with the bulk case in the elastic region, reaching a plateau value after yielding.

5.2. Computational details

The preparation of the amorphous alloy started from a cubic box with dimensions (32x32x32 nm) and periodic boundary conditions containing two million atoms in the B2 structure in the composition of $\text{Cu}_{50}\text{Zr}_{50}$. The atoms were redistributed randomly within the simulation cell and the resulting system was subsequently heated to 2000K for melting. After sufficient equilibration in the liquid state the system was cooled down to 300K with a cooling rate of 10K/ps. In all simulations the temperature was controlled by means of the Nose's thermostat. Subsequently, the system was relaxed for 100ps at room temperature. From this configuration we extracted several subsystems with dimensions of 1.8x25x9nm containing 22432 atoms, a system of 5.5x25x9nm containing 70271 atoms and a system of 18x25x9nm containing 224349 atoms respectively. The subsystems with foil geometries were created imposing an empty space of 10nm in the X-direction, thus introducing two free surfaces and were further re-equilibrated at room temperature for additional 200ps. The equilibrated subsystems in bulk and foil geometries were then subjected to tensile

loads with various strain rates in the Z-direction and a Poisson ratio of 0.34 to the directions with periodic boundary conditions. The equilibrium configurations were analyzed by means of detailed Common Neighbor Analysis (CNA) [8,9].

5.3. Results

5.3.1. 1D nanosized systems (ribbons)

We started our study with 1D systems, meaning that free surfaces were imposed on two (x and y) of the three axes and periodic boundaries on the z-axis. The systems were subjected to tensile deformation with a constant rate of 10^9 (sec)^{-1} . First we studied systems with different dimension on x-axis ranging from 55-180 Å, while keeping the other two dimensions constant and the SSCs are depicted in Fig.5.1.

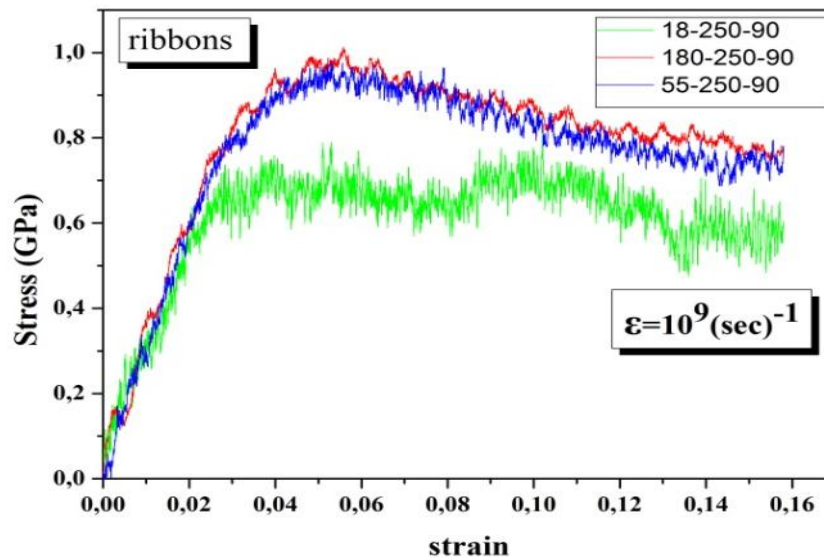


Fig. 5.1. SSCs of ribbon with different dimension on x-axis under constant strain rate.

It came out that beyond the dimension of 55Å the produced stress-strain curves were almost identical. We checked how the change in the dimensions on y-axis influences the

mechanical behavior of the systems, while the other two dimensions were kept constant. We found that the changes in the size of y-axis didn't cause any difference in deformation accommodation of the systems, as shown in Fig.5.2.

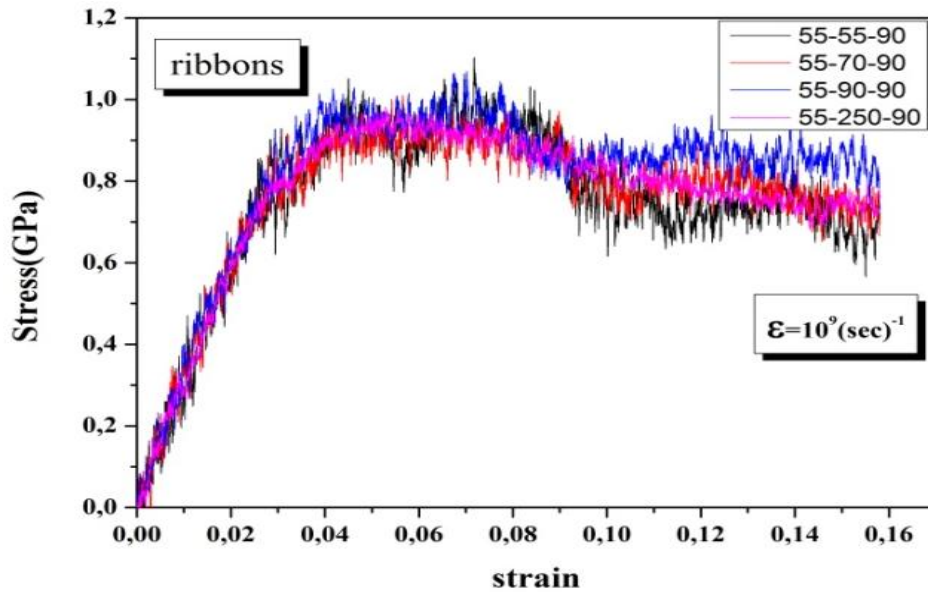


Fig. 5.2. SSCs of ribbons with different dimension on y-axis under constant strain rate.

5.3.2. 2D nanosized systems (foils)

Turning on the nanoscaled systems with foil geometries we studied three systems with equal dimensions in y and z axes but with different thicknesses (referring to x-axis where the free surfaces were imposed). In Fig. 5.3 we present the SSCs for these systems, along with one referring in a system having the dimensions of the bulk case but in foil geometry. It came out that the thickness may influence the mechanical response (basically yielding point and plastic region), while for thicknesses larger than 2.8nm no significant difference was found in the SSCs. In addition, the SSCs of all systems are marked by significant

serrations. We recall that this effect was not visible in the corresponding curves of bulk systems, but it was present in the corresponding evolution of the number of ICOs with strain. It turns out therefore, that the presence of surfaces and the small sizes of the systems enable the observation of these effects, suggesting that the accommodation of the strain is closely related to distinct events occurring in the clusters through atomic rearrangements that are enforced from the applied strain.

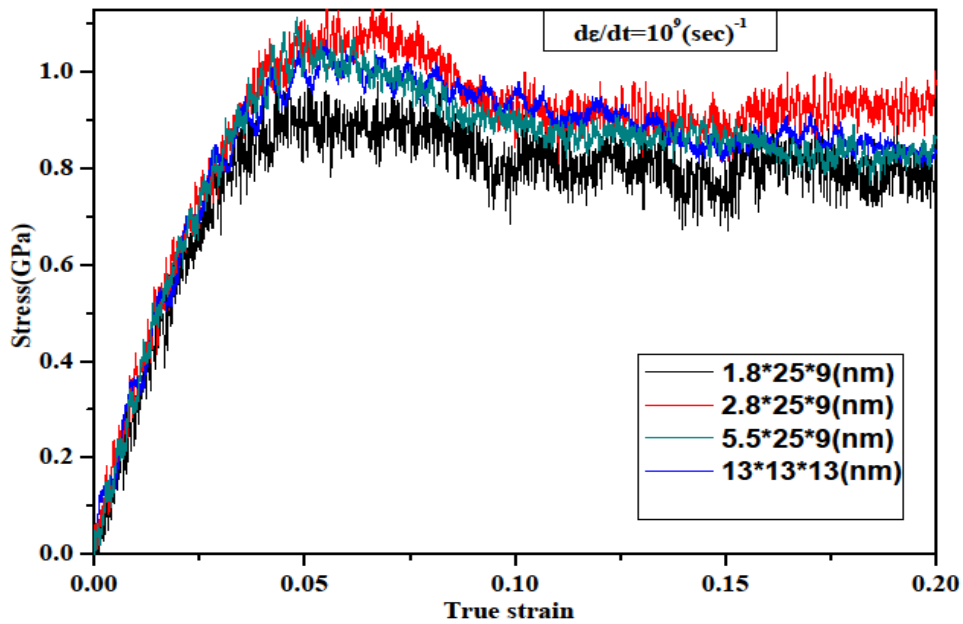


Fig. 5.3. Stress strain curves of systems with free surfaces on x-axis and different dimensions under tension with constant strain rate $d\varepsilon/dt=10^9(\text{sec})^{-1}$.

Furthermore we studied the effect of changes in the dimension of y-axis, where periodic boundaries conditions were imposed, Fig.5.4, in the SSCs. It came out that the resulting SSCs were almost the same.

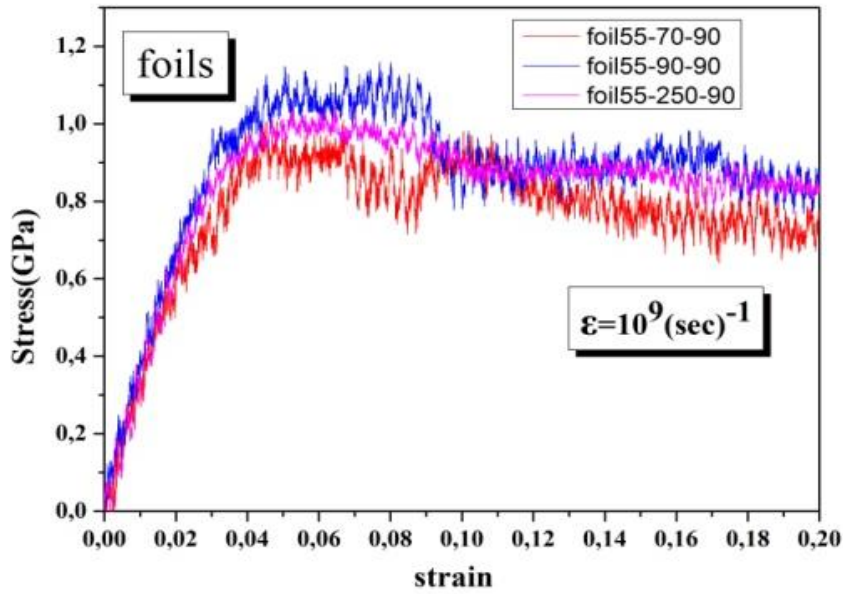


Fig. 5.4. Stress strain curves of systems with free surfaces on y-axis and different dimensions under tension with constant strain rate $d\varepsilon/dt=10^9(\text{sec})^{-1}$.

5.4. Comparison of the microstructural alterations between foils and ribbons.

In order to study the possible alterations of two systems with same dimensions but in different geometry we plot the corresponding SSCs in the same Fig. 5.4.

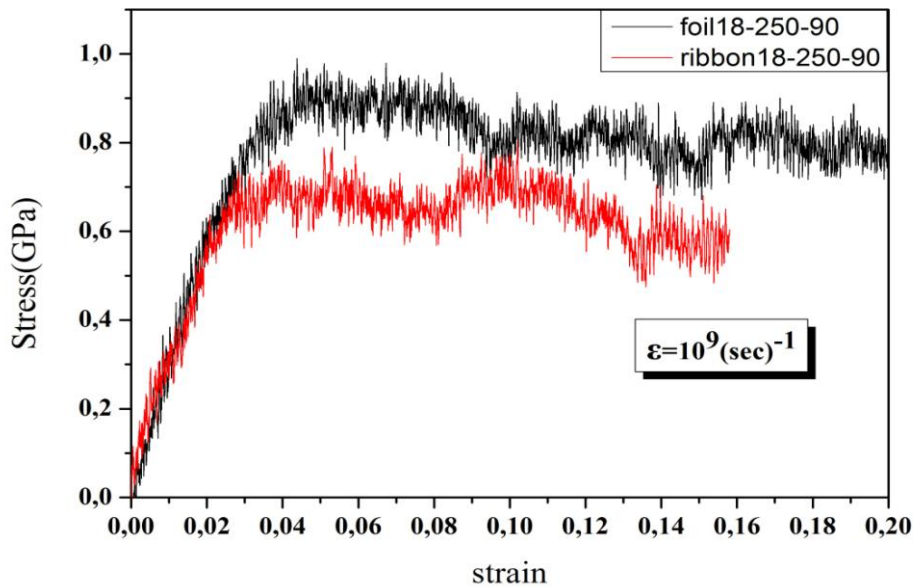


Fig. 5.5. Two systems with same dimension and different geometry upon tension.

We found that the ribbon system fails earlier than the foil exhibiting lower stress. In order to investigate what was happening in their microstructure upon tension we performed CNA analysis and the evolution of their ICOS is depicted in Fig.5.6

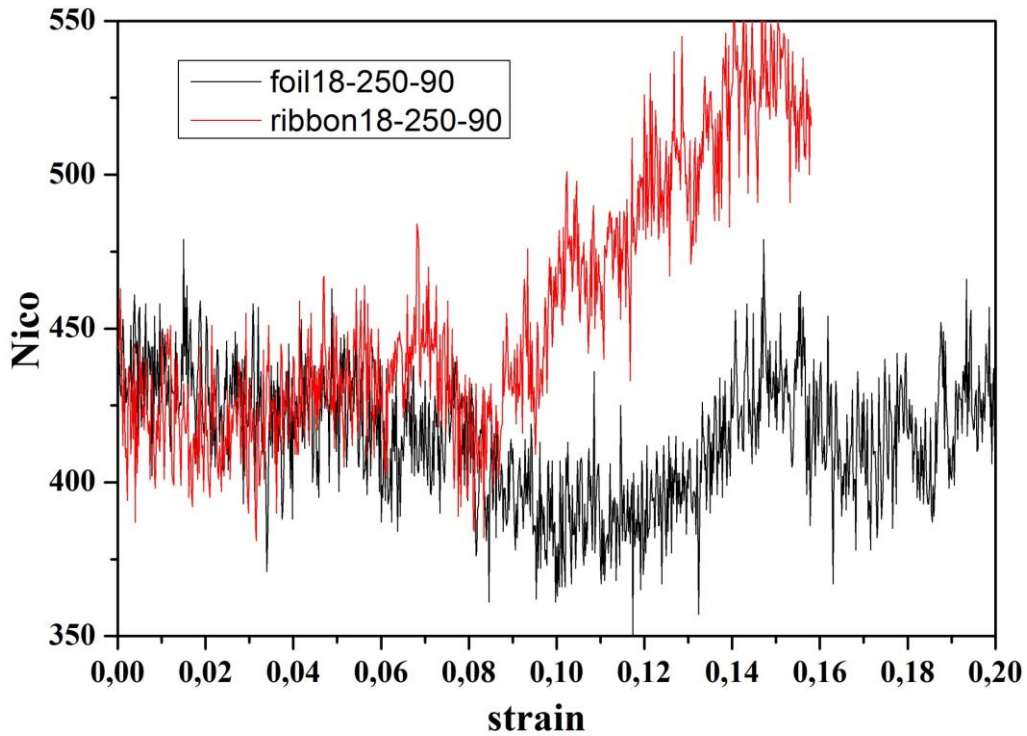


Fig. 5.6. The ICO evolution of the foil and ribbon system upon tension.

5.5. Influence of the strain rate on the foils

In order to investigate whether the strain rate affects the mechanical response of the foils, we focused on the largest system (dimensions 5.5-25-9 nm) and we applied tensile deformation using three different strain rates, ranging from $2 \cdot 10^8 (\text{sec})^{-1}$ to $2 \cdot 10^9 (\text{sec})^{-1}$, Fig.6. In the same figure we also give the evolution of the number of ICOS versus strain. It came out that the elastic region is not affected by the strain rate, while yielding points and the plastic regions depend on the strain rate, with high strain rates resulting in higher yielding points and retarded plastic regions.

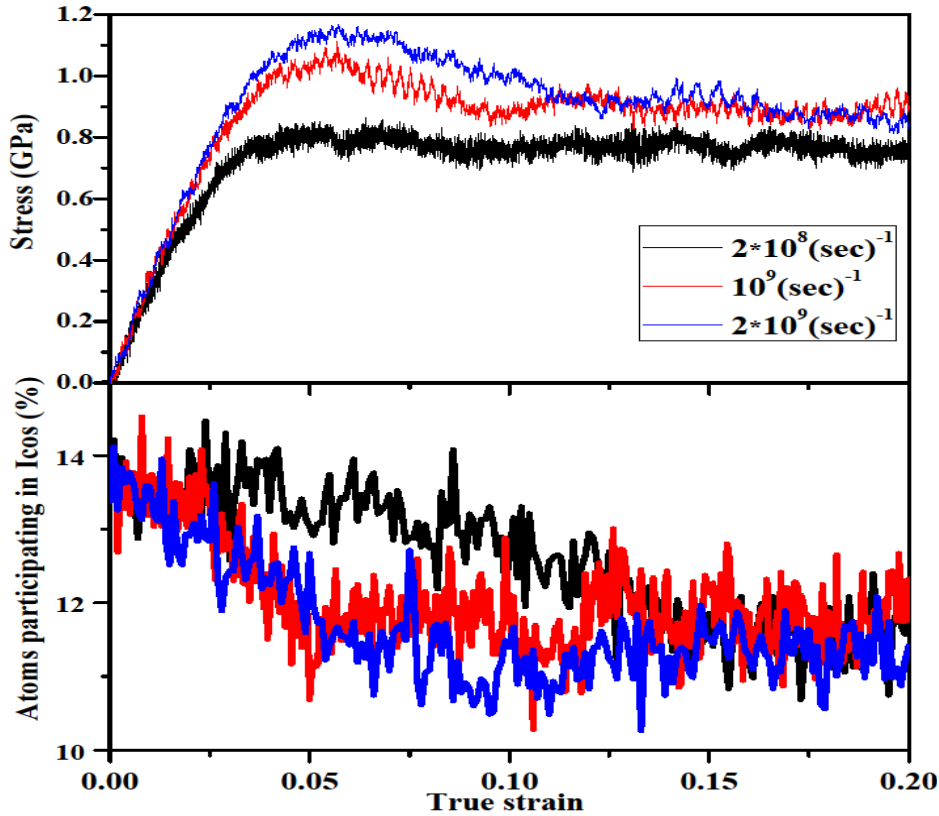


Fig. 5.7. SSCs of foil system 5.5-25-9 (nm) under different strain rates and the corresponding ICOs evolution versus strain.

In addition, in all SSCs depicted in Fig.6 we can see that the phenomenon of serrated flow is obvious not only in plastic region [10,11] but also in the elastic region, suggesting that the presence of the free surfaces and the small sizes of the systems facilitate atomic rearrangements leading to significant structural modifications that are manifested by the reduction of the ICO clusters. Moreover, we note that the magnitude of stresses drops follows the same motif as in bulk systems under compression [12,13] and indentation tests [14,15]. From the SSCs we evaluate a Young modulus around 30GPa and a yield strength of 850MPa for the two highest strain rates and about 600MPa for the slow one. Regarding the evolution of the number of ICOS with strain,

we found that within the elastic region (up to strain 0.025) their number remains almost constant. Beyond this region it decreases until the yielding point is reached, to saturate at the value of about 12% in the plastic region. Interestingly, we notice that the high rate of decrease of the ICO number corresponds to high stress in the systems and vice-versa, suggesting that the differences in the mechanical responses for different strain rates is closely related to the clusters' ability to deform-distort.

We note also that the decrease of NICOs is much smaller here, e.g. at strain of 20% it is ~3%, contrary to the bulk cases where the NICOs reached almost half value of their initial number at the same strain. This phenomenon is attributed to the presence of free surfaces that give to the systems more freedom to relax and thus to accommodate the imposed deformation, avoiding the drastic changes in the microstructure, as in the bulk case. In this sense we would expect extended plasticity for these systems.

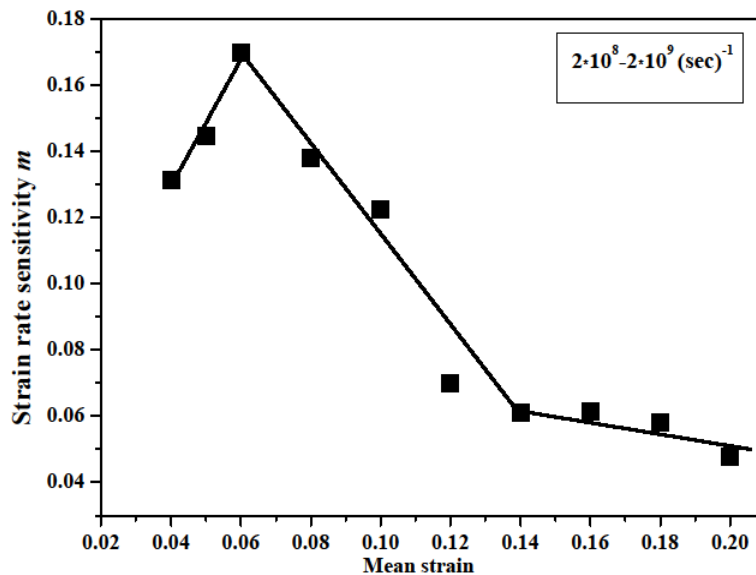


Fig.5.8.Strain rate sensitivity as a function of mean strain at 300K.

Given that the strain rate sensitivity (SRS), (m) is related to the resistance of a system towards necking [16-18], we evaluated m for the strain rates of $2 \cdot 10^8$ and $2 \cdot 10^9 (\text{sec})^{-1}$ and for strains from 4-20% by means of the relation [19,20]:

$$m = (\partial \ln \sigma / \partial \ln \dot{\epsilon})_{\epsilon} \quad (1)$$

Where σ and $\dot{\epsilon}$ denote the stress and the strain rate, respectively. Because of the presence of serrated flow, we evaluated (for both strain rates) the mean flow stress obtained as averaged values of the instantaneous stress within a plastic deformation interval of 0.1% and ensuring from the calculated corresponding confidence intervals expectation values with probabilities of 95%, Fig.5.8. We found that the SRS is positive, contrary to the bulky millimeter sized cylindrical $\text{Cu}_{50}\text{Zr}_{50}$ rods for which a slightly negative value was found [21]. As it can be seen in Fig.5.8, m increases up to 0.17, for a mean strain of 7%, beyond which it decreases and saturates after a strain of 14% at a strain rate sensitivity plateau value of 0.06. Although MGs differ substantially from their crystalline counterparts, in which plastic behavior and strain rate sensitivity correlate and determine their mechanical response, this result suggests enhanced resistance to necking and therefore large plastic region for these systems [22].

In order to validate this prediction we deformed a representative foil till fracture imposing a strain rate of $10^9 (\text{sec})^{-1}$. Fig.5.9a depicts the SSC of the foil from which we can see its high resistance to necking and eventually fracture that occurs at the strain of 140%. We have to note that this large elongation has to be primarily correlated with the presence of free surfaces and to the fact that the foil's dimensions are comparable with the size of shear bands, typically $\sim 10\text{-}20\text{nm}$ [21, 23]. Therefore, it has to be expected that this system would exhibit different behavior from the bulk system examined above.

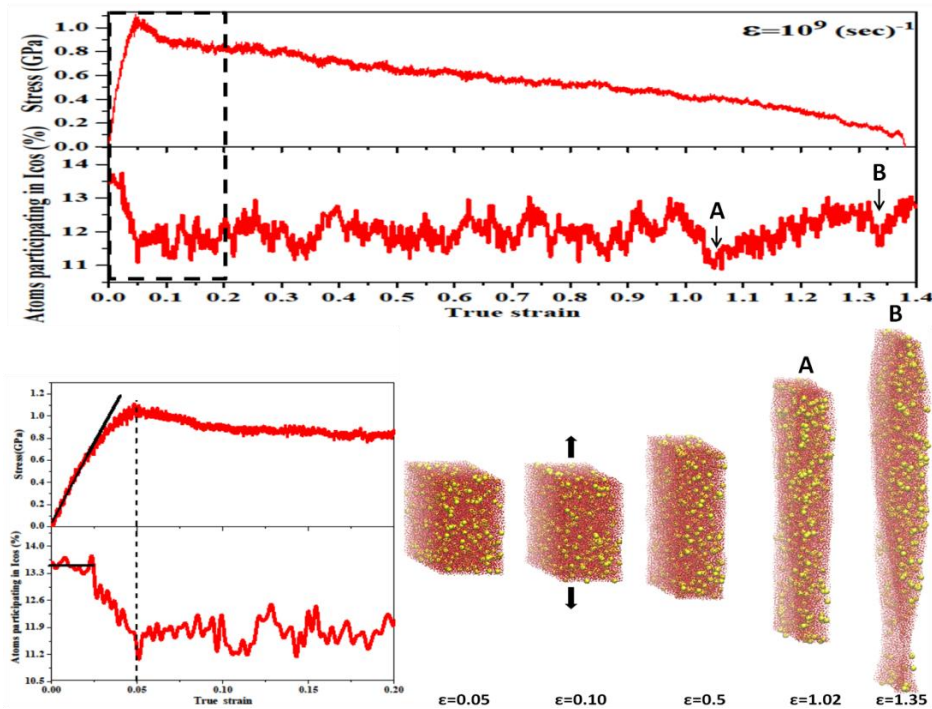


Fig.5.9. a) Exhaustive tension of foil till fracture b) focused area till 20% strain. c) Representative snapshots of the system for various strains.

Indeed, the inhomogeneous deformation of the MGs and stress localization into narrow regions (Shear Bands) does not take place in nanosized systems [24]. Instead, our system behaves like the usual trend of MGs at elevated temperatures (near or just above T_g) where the deformation accommodation appears to be homogeneous with absence of Shear Bands [25,26] and more specifically in our case it was accompanied by a extensive necking. It seems that the small volume of the system and the presence of the free surfaces suppress the creation and propagation of SBs.

Regarding the ICOs identification under tension we followed the same analysis as in the bulk case and their evolution with strain is illustrated in Fig.5.9b. It comes out that their number is constant up to a strain value of 2.5%, followed by a continuous decrease till the strain of 5%. Beyond this strain it oscillates around a mean value of about 12% and exhibits two significant steps marked by the arrows A and B, indicating possibly

remarkable changes, not visible in the SSC. In Fig. 5.9c we give a sequence of snapshots of the system for successive strains including A and B in which we can see the onset of necking at A, while at strain B the system is just before failure. These results underline that besides the fact that ICO and SSC are strongly correlated, monitoring of the ICO evolution with strain captures better than the SSC the microstructural alterations that are responsible for the accommodation of deformation. Consequently, a proper design of the clusters' composition and/or structure could be a pathway for tailoring the mechanical responses of new MGs.

Conclusions

Nanosized glassy foils exhibit large plastic region than the glassy ribbons and positive SRS. ICO clusters characterize again their microstructures and their number evolves similarly with the bulk case in the elastic region, reaching a plateau value after yielding. These results suggest that the ICOs play a decisive role in the deformation accommodation and that new MGs could be designed, e.g. by controlling their compositions

5.6. References

- [1] C. A. Schuh, A. C. Lund, and T. G. Nieh, *Acta Mater.* 52, 5879, 2004
- [2] B. E. Schuster, Q. Wei, M. H. Ervin, S. O. Hruszkewycz, M. K. Miller, T. C. Hufnagel, and K. T. Ramesh, *Scr. Mater.* 57, 517, 2007
- [3] H. Guo, P. F. Yan, Y. B. Wang, J. Tan, Z. F. Zhang, M. L. Sui, and E. Ma, *Nat. Mater.* 6, 735, 2007
- [4] Volkert, Donohue, and Spaepen *J. Appl. Phys.* 103, 083539, 2008
- [5] F. Shimizu, S. Ogata, and J. Li, *Acta Mater.* 54, 4293, 2006
- [6] M. D. Uchic, D. M. Dimiduk, J. N. Florando, and W. D. Nix, *Science* 305, 986, 2004
- [7] M. D. Uchic and D. M. Dimiduk, *Mater. Sci. Eng., A* 400–401, 268, 2005
- [8] J. D. Honeycutt, H. C. Andersen, *J. Phys. Chem.* 91 (1987) 4950.
- [9] D. Faken, H. Jonsson, *Comp. Mater. Sci.* 2 (1994) 279-286
- [10] Kimura H, Masumoto T. *Acta Metall* 1983;31:231.
- [11] Dalla Torre FH, Dubach A, Siegrist ME, Loffler JF. *Appl Phys Lett* 2006;89, 091918
- [12] Zhang J, Park JM, Kim DH, Kim HS. *Mater Sci Eng A* 2006;449–451:290.
- [13] Mukai T, Nieh TG, Kawamura Y, Inoue A, Higashi K. *Intermetallics* 2002;10:1071.
- [14] Nieh TG, Schuh C, Wadsworth J, Li Y. *Intermetallics* 2002;10:1177.
- [15] Schuh CA, Nieh TG. *Acta Mater* 2003;51:87.

- [16] Handbook of Workability and Process Design George E. Dieter, Howard A. Kuhn, S. Lee Semiatin, George Ellwood Dieter ASM International, 2003
- [17] HILL R. *Journal of the Mechanics and Physics of Solids*, 2001, 49: 2 055–2 070.
- [18] KEELER S . *Sheet Metal Industries*, 1965, 42(461): 683–691.
- [19] Zaiser M, Hañhner P. *Phys Stat Sol B* 1997;199:267.
- [20] McCormick PG. *Acta Metall* 1988;36:3061
- [21] Florian H. Dalla Torre *et al.*, *Materials Transactions* 48, 1774 (2007)
- [22] DING Lei, et al:- *Chinese Journal of Mechanical Engineering*, 26, 3, 2013
- [23] H. Chen, Y. He, G. J. Shiflet, and S. J. Poon, *Nature(London)* 367, 541 (1994).
- [24] Guo H. *et al* *Nature materials* 6, 735–9 (2007).
- [25] A. Dubach et al. / *Acta Materialia* 57 (2009) 881–892
- [26] Zhang Y, Greer AL. *Appl Phys Lett* 2006;89:071907

VI. Chapter 6

Clusters as *building blocks* of MGs

Stoichiometry

Temperature

Microstructure

Deformation

Bulk-Surfaces

Influence of strain-rates

Cross-Correlation

Geometry

• **Clusters as *building blocks* of MGs**

6.1. Introduction

From the very beginning of the discovery of MGs until now, numerous studies have been published concerning the structure of the MGs, but unfortunately there is not any generic model description of their structural characteristics until now. The only wide acceptable fact is that MGs are mainly consisting by tiny icosahedral clusters [1-4], proven by both theoretical [5-7] and experimental studies [8-9]. Based on this idea that the basic structural unit of MGs is the icosahedral clusters, very recently some models proposed that metallic glasses can be produced by their own building blocks eg. icosahedral metal clusters [10-14] and these models have been implemented with success in many theoretical and experimental studies [15-20].

In this direction, there are many works where nanoglasses were generated by sputtering [21-24], via atom by atom deposition [25,26] or by direct cluster deposition [27]. In terms of cluster's landing energy, cluster deposition may be classified into the three categories: soft-landing, low-energy cluster beam deposition [28], and energetic cluster impact. Cluster deposition with low initial kinetic energy is referred to, in the relevant literature, as soft-landing. More specifically by soft landing it is defined a collision outcome allowing for plastic deformation of the cluster, but not for fragmentation and implantation [29].

In this chapter Molecular Dynamics simulations [30,31] indicated that cluster implantation occurs at about 1eV/atom kinetic energy of the cluster, independently of the cluster-substrate system. Accordingly, this value can be regarded as the upper limit for soft landing deposition. In the present work we focus on the modifications of surface properties of the $\text{Cu}_{50}\text{Zr}_{50}$ MG induced by the deposition of softly landed $\text{Cu}_x\text{Zr}_{100-x}$ ($0 < x < 100$) icosahedral clusters.

The choice of this material was dictated from the fact that Cu-Zr based MGs exhibit a series of attractive properties among which large glass forming ability in a wide compositional range, property that makes them suitable for the formation of a large number of MGs [32, 33].

6.2. Computational details

The simulations were based on a potential model in analogy to the tight-binding scheme in the second moment approximation (TBSMA) [34]. The equations of motion were integrated by means of the Verlet algorithm with a time step of 5fs. The amorphous alloy model was prepared starting from a cubic cell box with periodic boundary conditions containing 128000 atoms in the B2 structure in the composition of $\text{Cu}_{50}\text{Zr}_{50}$. The atoms were redistributed randomly within the simulation cell and the resulting systems were subsequently heated to 2000K for melting. After sufficient equilibration at the liquid state the system was cooled down to 300K imposing a cooling rate of 10K/ps. In all simulations the temperature was controlled by means of the Nose's thermostat (Nose mass used 7×10^{-43} Joules sec^2). We have to note that although the model was tested and found to successfully reproduce several equilibrium bulk properties of the MG, like Radial Distribution Function, melting point and glass transition temperature, its application for the study of surfaces and interfaces has to be considered with precaution, while the obtained results have to be taken as indicative before experimental verifications. All cases were equilibrated for 100ps at room temperature, time length that was found to be sufficient for obtaining a plateau value of the heat content of the systems with a normalized fluctuation less than 10^{-4} . Subsequently, an empty space of 8nm was imposed in the X-direction, thus introducing two free surfaces. The equilibrated substrate had slab geometry with dimensions of 4x12x12nm and 38651 atoms. The $\text{Cu}_{50}\text{Zr}_{50}$ composition was selected in

order to have a substrate with no preferential concentration gradient caused from the relative abundance of one metal with respect to the other. In addition, we note that any possible compositional changes that may occur in the surface, due to ageing and/or preferential elemental segregation effects, are not considered in the present study.

The choice of Mackay icosahedral nanoclusters is due to the fact that these amorphous alloys consist of various types of short-range ordered atomic clusters [35], basically of icosahedral shape [36,37], whose number evolves under tensile sollicitation [38]. Moreover, these Mackay [39] icosahedral clusters exhibit the lowest cohesive energy against other types [40] (confirmed in several cases (Au [41, 42], Ag [43, 44], Cu [45], and Ni [46, 47])).

In order to quantify the structural and topological changes brought about in the deposited clusters we calculated several relevant quantities like the gyration radius, the location of their center of mass, the percentage of cluster's atoms above the substrate and their final stoichiometry. We also computed the alterations of the decorated with ICOs $\text{Cu}_{50}\text{Zr}_{50}$ surface energies. The initial geometries of $\text{Cu}_x\text{Zr}_{100-x}$ ($0 < x < 100$) clusters correspond to the more stable isomers for free closed-shell clusters of these materials. The clusters were shaped as Mackay icosahedra consisting of 147, 309, 561 and 923 atoms, resulting in diameters ranging from 1.16 to 2.72nm. For each cluster size, four different stoichiometries were tested: the two Cu and Zr pure cases ($x=100$ and $x=0$, respectively) and $x=86.4$, 93.5, 89 and 92.4, in the mixed Cu-rich elemental content cases, corresponding to ICO clusters having 147, 309, 561 and 923 atoms, respectively. The same concentrations were also used in the Zr-rich ($100-x$) cases. We have to note at this point that these concentration values do not represent any particular compositional preference; they were obtained as a result from the maximum number of substitutional atoms we could replace in each case of clusters and succeed in obtaining an energetically stable mixed cluster. It worth's also to be mentioned that the stability of the mixed ICOs seems to be closely related to the internal

stresses that are present even in pure ICO clusters [48]. Upon substitution of one element with another (Cu or Zr that have rather large atomic size difference) these stresses, the origin of which is basically electronic, become important, thus leading to amorphization of the resulting cluster.

The deposition procedure consisted of a) initially energy minimization of the cluster's structure at 0K b) equilibration for 50ps of the clusters and substrate separately at 300K and c) soft deposition of the ICO on the MG's surface (initial kinetic energy of about 25meV) and subsequent further equilibration of the resulting system for additional 50ps.

6.3. Results and discussion

6.3.1. Characterization of the microstructure

Representative snapshots of the initial and equilibrated configurations of a 147 Cu, 309 Cu-rich, 309 Zr-rich and 923 Zr atoms ICOs, are depicted in Figs.(6.1a-6.1d), respectively.

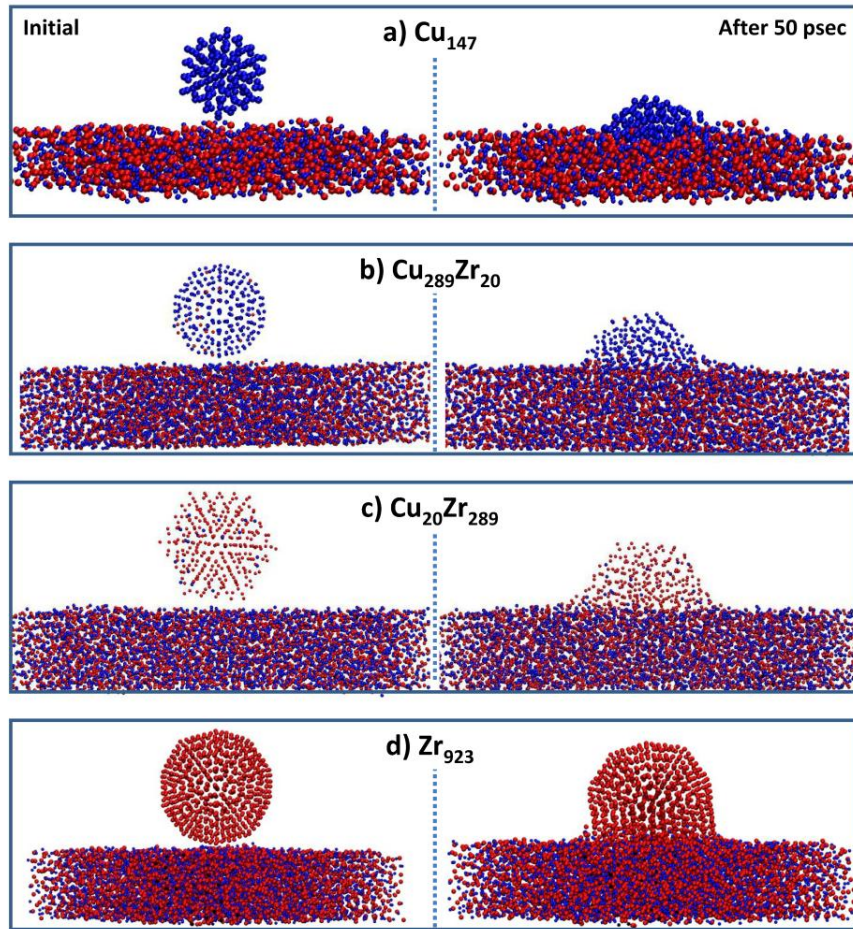


Fig.6.1. Representative snapshots of the deposition of ICO clusters before and after equilibration on the $\text{Cu}_{50}\text{Zr}_{50}$ surface (a) 147 atoms Cu ICO (b) 309 atoms Cu-rich ICO, (c) 309 atoms Zr-rich ICO and (d) 923 atoms Zr ICO.

As it can be seen, the deposited ICOs exhibit markedly different behavior, with the Cu cluster being heavily deformed, while the Zr ICO is anchored to the substrate preserving very well its geometrical characteristics.

Aiming in quantifying the geometrical features of the deposited nanoclusters, we investigated a) the compactness of the deposited clusters, b) their depth penetration into the substrate, as well as c) the final number of atoms remained in the ICOs. Taking into account that among all Platonic solids the ICO clusters are the most compact and closer to

the spherical shape, the former quantity can be evaluated by calculating the changes in gyroscopic radii, defined by:

$$R_g = \frac{1}{N} \sum_i (R_i - R_{cm})^2 \quad (6.1)$$

where R_{CM} and R_i are the position vectors of the cluster's centre of mass and the particle i respectively. The variation of this quantity normalized with respect to their zero temperature values for all cluster sizes, is depicted in Fig. (6.2).

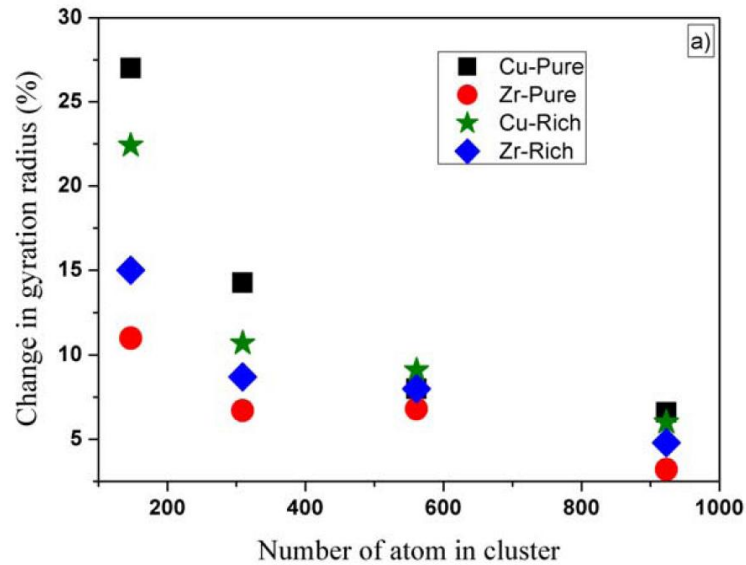


Fig.6.2. Change in gyration radius (%) with respect to the number of clusters atoms.

It comes out that R_g changes are inversely proportional to the ICO's size with the Zr-rich clusters being more compact than the Cu-rich, this difference becoming negligible for the large clusters.

Given the high symmetry of the ICOs, the penetration depth of the deposited clusters can be appraised from the calculation of the relative position of the cluster's centre of mass with respect to the substrate's surface, i.e the difference of its initial and final (equilibrated) position, Fig (6.3).

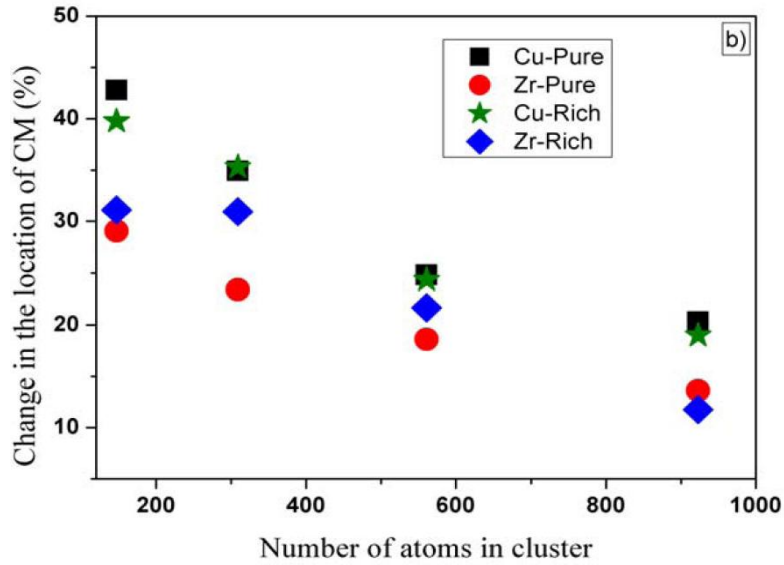


Fig. 6.3. Change in the location of clusters center of mass versus clusters atoms.

In line with the conclusions of the previous quantity (R_g) we found that the larger the cluster's size is, the smaller its penetration into the surface, the Cu-rich clusters being incorporated more easily. These results were further confirmed from the calculation of the number of the cluster atoms after the deposition, i.e. the atoms remaining above the surface (%), Fig. (6.4).

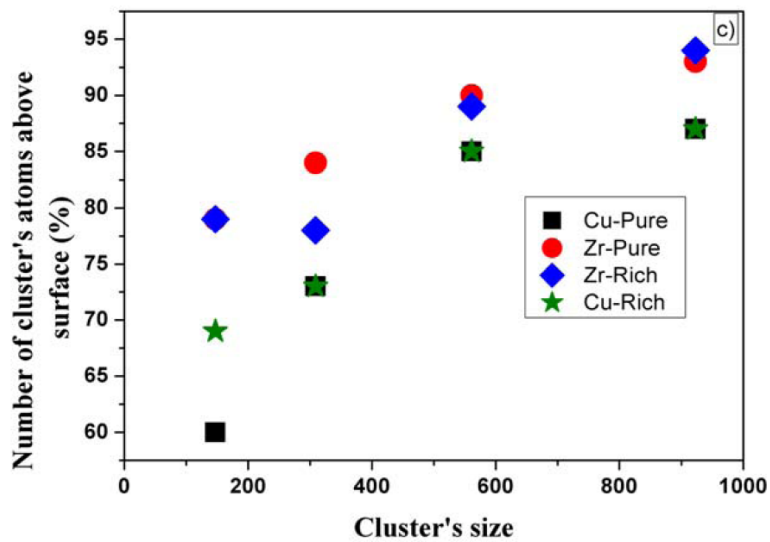


Fig. 6.4. The remained number of clusters atoms above surface versus cluster's size.

These findings highlight the importance of the cluster's properties that are related to their intrinsic stability and chemistry with the substrate; for instance, while both pure Cu or Zr ICOs impose at the interface with the substrate similar concentration gradients, they result in significantly different equilibrated systems. Moreover, we have to point out that these findings cannot be attributed only to the selective enhanced diffusivity of Cu, compared to that of Zr in the Cu-Zr MGs [49]. Indeed, trajectory investigation of the very early stages of the deposition processes revealed that although during the equilibration substrate's atoms diffused into the deposited clusters and vice-versa, the final clusters' stoichiometries remained practically unaltered, even for the ICOs' sections that penetrated the surface. This is an unanticipated finding revealing significant local compositional alteration of the substrate's surface. It is worth to be noted here that previous studies [50] on the deposition of energetic clusters showed that small Cu clusters impinging on a Cu substrate are completely embedded in the surface, while larger form defect-free epilayers and some penetration. The comparison with our soft landing case implies that the initial cluster's kinetic energy is decisive for the stability and the relaxation of the clusters on top of the surface.

6.3.2. Energetic considerations

Focusing on the consequences that may derive from the cluster deposition we calculated the changes induced in the surface energies. The surface energy at zero temperature is given from the potential energy difference between the system with free surfaces and a reference bulk system, normalized with respect to the free surface area A:

$$E_s = \frac{1}{2A} \left(U_s - N_{Cu} U_b^{Cu} - N_{Zr} U_b^{Zr} \right) \quad (6.2)$$

where, U_s and N_i are, respectively, the internal energy and the number of atoms of species i ($i = \text{Cu, Zr}$), in the system with free surfaces, and U_b^i is the internal energy of species i in the perfect bulk system. In the calculation of the surface area in the case a deposited cluster we included the additional area of the cluster's spherical shell above the surface, given by:

$$S=4\pi R_g^2-2\pi R_g d \quad (6.3)$$

where d stands for the penetration depth of the deposited cluster.

In Fig. (6.5) we give the calculated surface energies of all systems studied as a function of the clusters' sizes.

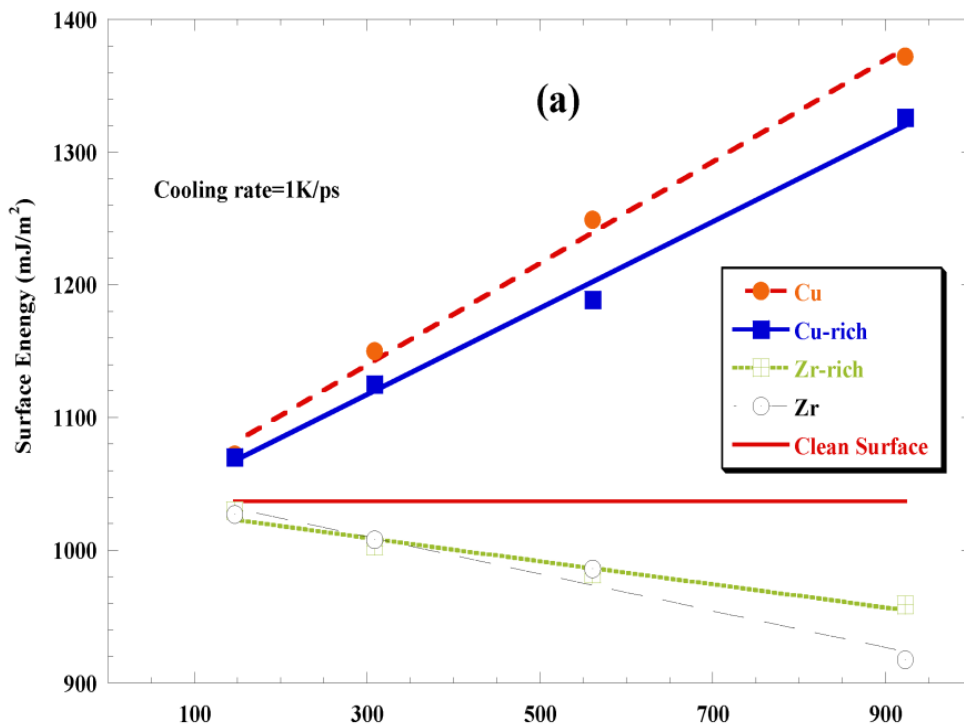


Fig.6.5. Calculated surface energy of the substrate and the deposited clusters versus cluster's size along with the surface energy of the "clean" surface (red line) .(Systems were prepared with a cooling rate of 1K/ps)

It turns out that in all cases the deposition of Zr-rich clusters lowers the surface energy, yielding more stable surfaces. On the contrary the deposition of Cu ICOs results in increase of the surface energy that may exceed 30% for the 923 Cu cluster. Taking into account that the Zr-rich ICOs exhibit the higher compactness and the smaller penetration depths, this result underlines the significance of the local topological order in conjunction with the intrinsic cluster stability. In addition, taking into account the semiempirical character of the potential model used and aiming in validating its transferability to the study of surface properties, we performed additional calculations for the surface energies in some representative cases using another potential model that is based on the Embedded Atom Method (EAM) [51]. We addressed the following cases: (1) Cu(111) and Zr(100), (2) clean $\text{Cu}_{50}\text{Zr}_{50}$ surface and (3) deposition of (3a) a Cu and (3b) a Zr 923 cluster on the glassy surface. It came out that both models underestimate the surface energies of the pure metals yielding, nevertheless, similar trends. More specifically the TBSMA potential resulted in 1.21J/m^2 and 1.4J/m^2 , while the EAM model yielded 0.9J/m^2 and 1.28J/m^2 for the Cu(111) and Zr(100) surfaces, to be compared with the experimental values of 1.83J/m^2 [52] and 1.91J/m^2 [53], respectively. In the (b) case we obtained the values of 0.96J/m^2 and 1.17J/m^2 , while in the case of (3a) we found 1.31J/m^2 and 1.28J/m^2 and the (3b) 0.90J/m^2 and 0.91J/m^2 for the TBSMA and EAM potentials, respectively. It turns out therefore, that despite the differences in the absolute values, both potential models yield the same trends for the surface energies.

In addition, in order to ensure that the effect of the high cooling rate imposed by the MD simulations restrictions does not influence qualitatively the obtained results, we performed two additional simulations depositing the larger Zr ICO on two different substrates prepared with faster and slower by an order of magnitude cooling rates. It came out that while in the former case no significant difference was found, in the latter case (slower

cooling rate) the value of the surface energy of the clean substrate was increased by 7%, in line with a previous study [54].

Moreover, in order to ensure that our findings are not affected by the surface preparation, we repeated all deposition simulations using as substrate the one obtained with this slower cooling rate (1K/ps). The obtained results are depicted in Fig.(6.6), in which we can see no significant alteration in the behaviour of the surface energy as function of the deposited cluster size. In addition, the stability of the deposited clusters was checked selectively in the case of the 923 Zr ICO in a simulation that lasted 10ns.

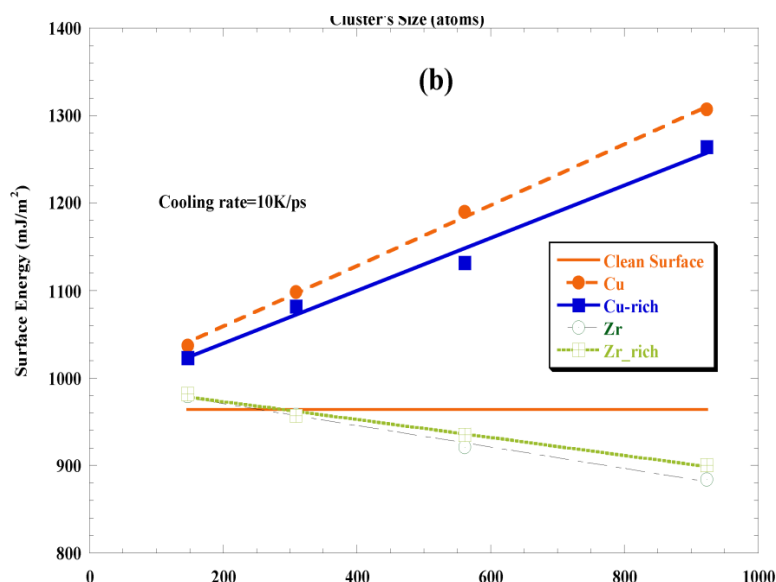


Fig.6.6. Calculated surface energy of the substrate and the deposited clusters versus cluster's size along with the surface energy of the "clean" surface (red line). (Systems were prepared with a cooling rate of 10K/ps).

These changes are correlated with the total surface area, a quantity closely related with the efficiency in catalysis. The increase of the active surface area due to the deposited nanoclusters and the associated change in the surface energy, normalized by the corresponding quantity of the clean surface, is depicted in Fig.(6.7).

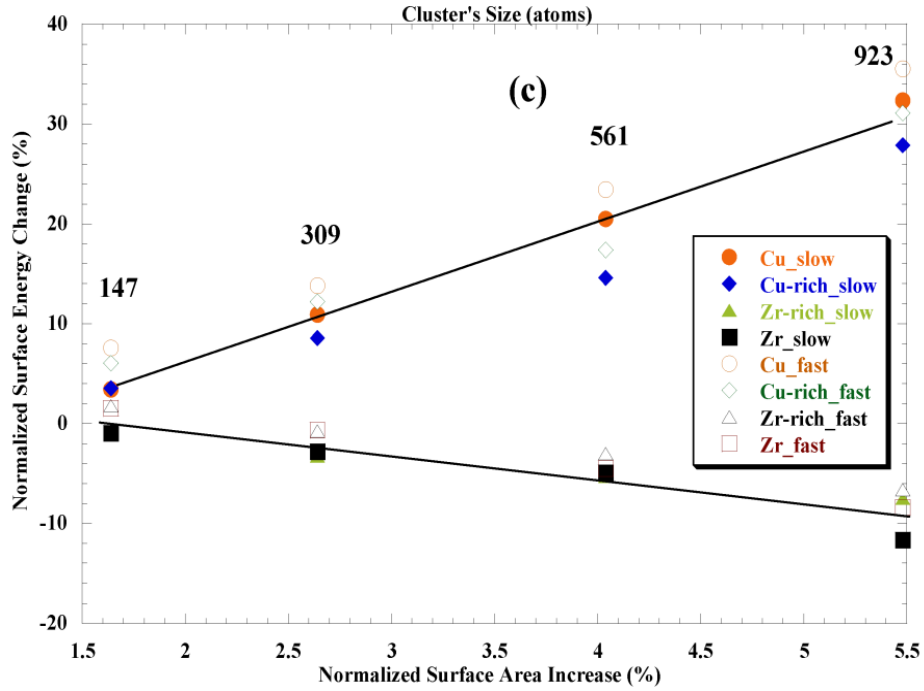


Fig.6.7. The % change in surface energy of the substrate and the deposited clusters versus the % normalized surface area increase for all systems prepared with different cooling rates.

In the same figure the results obtained with substrates equilibrated with the slow cooling rate also given, demonstrating that the different cooling rates do not alter the obtained results. As it can be seen clear linear dependence is found, with negative and positive slopes for the Zr-rich and Cu-rich ICOs, respectively. The degree of these correlations can be assessed by the Pearson-product moment correlation coefficient [55-57], according to which a sample correlation coefficient is written as:

$$r_{xy} = \frac{\sum_{i=1}^n (x_i - \bar{x})(y_i - \bar{y})}{(n-1)s_x s_y} \quad (6.4)$$

where \bar{x} and \bar{y} are the mean values of X and Y and s_x , s_y are the sample standard deviations of X and Y . Specifically, in Cu-based clusters the correlation coefficient is estimated to 0.98 and 0.96 for the Cu pure and Cu-rich clusters, respectively. The Pearson coefficient is negative for the Zr-pure and Zr-rich clusters and equals to 0.99, thus revealing a strong linear dependence between these two variables. It is important to note that a small change of only 3.5% of the active surface area is correlated with an increase of 35% in the surface energy, in the case of the large Cu ICO, while in the Zr ICO case this quantity is reduced by 10% when the surface area is increased by 5.5%. We note nevertheless, that in the present study we do not treat any liquid environment or electrostatic potential data, the correlation with catalysis being restricted to the cluster induced activation of the substrate. These findings may be used for the understanding of the activation of Cu-Zr MG catalysts. Depending on the catalytic application the same MG substrate may incur different pre-treatment. Indeed, activity enhancement of Cu-Zr MG-based catalysts is usually based on otherwise detrimental or degrading processes that include electrochemical treatment [58] selective dissolution/re-deposition of adsorbates on devitrified MG surface [59], oxidation, anodic activation, pre-treatment with hydrogen [60, 61], e.t.c. From these studies it is now accepted that independently of the variety of the mechanisms acting during these treatments, the Cu-Zr catalytic activation is closely related to the formation of clusters that are embedded in either an amorphous metallic or oxidized surface, depending on the process and the application. Although the catalytic reactions are governed by electronic redistributions and therefore a proper theoretical treatment would require quantum mechanical computations, the present results provide the initial guidelines for surface stability and reactivity.

In addition, the present results can be combined with the possibility of selective growth of amorphous or nanocrystalline thin film MGs [62] having improved catalytic activity and selectivity. Moreover, the present results can be considered in conjunction with the possibility of producing mixed metallic nanoclusters that can be deposited on various substrates, followed by a selective oxidation postgrowth treatment, for the production of metal-containing oxides, thus opening new pathway for the design of efficient catalysts.

6.4. Concluding remarks

We presented MD simulations results referring to the surface properties of $\text{Cu}_{50}\text{Zr}_{50}$ glassy substrate decorated with ICO Cu-Zr clusters of various sizes and compositions. For each cluster size we tested four different stoichiometries of $\text{Cu}_x\text{Zr}_{100-x}$ clusters. The structural changes of the clusters after their deposition were assessed by means of the % changes of the gyration radii, the equilibrated locations of the center masses, the percentages of the remaining ICO atoms above the surface along with their final stoichiometries. It came out that as the cluster size and the Zr content of the clusters were increased, the clusters remained more compact and their penetration depth into surface was smaller. In line with this trend, we found that upon Zr-rich ICO deposition, the active surface area was increased and surface energy was lowered, in contrast to Cu-rich ICO clusters depositions cases that resulted in less stable substrates.

6.5. References

- [1] D.B. Miracle, *Nat. Mater.* 3 (2004) 697.
- [2] H.W. Sheng, W.K. Luo, F.M. Alamgir, J.M. Bai, E. Ma, *Nature* 439 (2006) 419.
- [3] Ch.E. Lekka, A. Ibenskas, A.R. Yavari, G.A. Evangelakis, *Appl. Phys. Lett.* 91 (2007) 214103.
- [4] M.Wakeda, Y. Shibutani, S. Ogata, J. Park, *Intermetallics* 15 (2007) 139.
- [5] A.E. Lagogianni, G.A. Almyras, Ch.E. Lekka, D.G. Papageorgiou, and G.A. Evangelakis, *J. Alloys and Compd.* 483 ,(2009), 658
- [6] Jun Ding, Yong-Qiang Cheng, Evan Ma *Acta Mater* 2014, 69, 343-354
- [7] Z. W. Wu, M. Z. Li, W. H. Wang, K. X. Liu, *Physical Review B*, 2013, 88
- [8] Antonowicz J., Pietnoczka A., Drobiaz T., Almyras G.A., Papageorgiou D.G., and Evangelakis G.A., *Philosophical Magazine*, 92, 2012, 1865-75
- [9] Hirata A., Kang L.J, Fujita T., Klumov B., Matsue K., Kotani M., Yavari A.R., and Chen M.W. *Science*, 341, 2013, 376-9
- [10] Sha ZD, Xu B, Shen L, Zhang AH, Feng YP, Li Y *Journal of Applied Physics* 2010, 107.
- [11] Dong C, Wang Q, Qiang JB, Wang YM, Jiang N, Han G, Li YH, Wu J, Xia JH: *J Phys D-Appl Phys* 2007, 40:R273-R291.
- [12] Han G, Qiang JB, Li FW, Yuan L, Quan SG, Wang Q, Wang YM, Dong C, Haussler P *Acta Mater* 2011, 59:5917-5923.
- [13] Fan C, Liaw PK, Liu CT *Intermetallics* 2009, 17:86-87.
- [14] Fan C, Liaw PK, Wilson TW, Dmowski W, Choo H, Liu CT, Richardson JW, Proffen T, *Appl Phys Lett* 2006, 89.

- [15] Miracle DB, Greer AL, Kelton KF: *Journal of Non-Crystalline Solids* 2008, 354:4049-4055.
- [16] Almyras GA, Lekka CE, Mattern N, Evangelakis GA: *Scripta Materialia* 2010, 62:33-36.
- [17] Yang L, Yin S, Wang XD, Cao QP, Jiang JZ, Saksl K, Franz H: *Journal of Applied Physics* 2007, 102.
- [18] Antonowicz J, Pietnoczka A, Drobiazg T, Almyras GA, Papageorgiou DG, Evangelakis GA: *Philosophical Magazine* 2012, 92:1865-1875.
- [19] Antonowicz J, Pietnoczka A, Zalewski W, Bacewicz R, Stoica M, Georgarakis K, Yavari AR, *J Alloy Compd* 2011, 509:S34-S37.
- [20] Georgarakis K, Yavari AR, Louzguine-Luzgin DV, Antonowicz J, Stoica M, Li Y, Satta M, LeMoulec A, Vaughan G, Inoue A *Appl Phys Lett* 2009, 94.
- [21] Gleiter H *Journal of Applied Crystallography* 1991, 24:79-90.
- [22] Gleiter H *Metallurgical and Materials Transactions a-Physical Metallurgy and Materials Science* 2009, 40A:1499-1509.
- [23] Gleiter H *Beilstein Journal of Nanotechnology* 2013, 4:517-533.
- [24] Xie L, Brault P, Thomann AL, Bedra L *Applied Surface Science* 2013, 274:164-170.
- [25] Chen N, Frank R, Asao N, Louzguine-Luzgin DV, Sharma P, Wang JQ, Xie GQ, Ishikawa Y, Hatakeyama N, Lin YC, et al *Acta Mater* 2011, 59:6433-6440.
- [26] Chen N, Louzguine-Luzgin DV, Xie GQ, Sharma P, Perepezko JH, Esashi M, Yavari AR, Inoue A *Nanotechnology* 2013, 24.
- [27] C. Binns, *Curr. Opin. Solid State Mater. Sci.* 8, (2004).203
- [28] K. Shintani, Y. Taniguchi, and S. Kameoka, *J. Appl. Phys.* 95, (2004) 8207
- [29] S. Abbet, K. Judai, L. Klinger, U. Heiz, *Pure & Appl. Chem.* 74 (2002) 1527

- [30] H.-P. Cheng, U. Landman, *Science* 260 (1993) 1304
- [31] H.-P. Cheng, U. Landman, *J. Chem. Phys.* 98 (1994) 3527
- [32] Inoue, D. Kawase, A.P. Tsai, T. Zhang and T. Masumoto, *Mater. Sci. Eng. A* 178 (1994), 255
- [33] E. Kneller, Y. Khan, U. Gorres, *Z. Metallkd.*, 77, (1986) 152
- [34] G. Duan, D. Xu, Q. Zhang, G. Zhang, T. Cagin, W.L. Johnson, and W.A. Goddard III, *Phys. Rev. B* 71, (2005) 224208
- [35] D.B. Miracle, *Nature Mater.* 3 (2004) 697
- [36] M. Wakeda, Y. Shibutani, S. Ogata, J. Park, *Intermetallics* 15 (2007) 139-144
- [37] A.E. Lagogianni, G.A. Almyras, Ch.E. Lekka, D.G. Papageorgiou, and G.A. Evangelakis, *J. Alloys and Compd.* 483, (2009), 658
- [38] Ch.E. Lekka, A. Ibenskas, A.R. Yavari, G.A. Evangelakis, *Appl. Phys. Lett.*, 91 (2007) 214103
- [39] A.L. Mackay. *Acta Crystallogr.* 15 (1962) 916
- [40] H.B. Liu, R. Perez, G. Canizal, J.A. Ascencio, *Surf. Sci.* 518 (2002) 14.
- [41] F.M. Mulder, R.C. Thiel, L.J. de Jongh, P.C.M. Gubbens, *NanoStructured Mater.* 7 (1996) 269
- [42] C.R.A. Catlow, V.L. Bulatov, R.W. Grimes, *Nucl. Instr. Meth. Phys. Res. B* 122 (1997) 301.
- [43] Kara, T.S. Rahman, *Phys. Rev. Lett.* 81 (1998) 1453.
- [44] F. Baletto, C. Mottet, R. Ferrando, *Phys. Rev. B* 63 (2001) 155408 F
- [45] L. Wang, Y. Zhang, X. Bian, Y. Chen, *Phys. Lett. A* 310 (2003) 197
- [46] R. Singh, S. Prakash, *Surf. Sci.* 272 (2003). 532
- [47] Y. Qi, T. Cagin, W.L. Johnson, W.A. Goddard, *J. Chem. Phys.* 115(2001)385.
- [48] R. Ferrando, A. Fortunelli G. Rossi, *Phys. Rev. B* 72 (2005) 085449

- [49] D.G. Papageorgiou, G.A. Evangelakis, *Surf. Sci.* 602 (2008) 1486
- [50] H. Hsieh, R.S. Averback, *Phys. Rev. B* 42 (1990) 5365
- [51] M. I. Mendeleev, D. J. Sordet, M. J. Kramer, *J. Appl. Phys.* 102 (2007) 043501
- [52] H. L. Skriver, N. M. Rosengaard, *Phys. Rev. B* 46 (1992) 7157
- [53] W.R. Tyson, W.A. Miller, *Surf. Sci.* 62 (1977) 267
- [54] Q.-K. Li, M. Li, *J. Non-Cryst. Solids* 354 (2008) 2060
- [55] *Applied Statistics: Analysis of variance and regression*, eds. O.J. Dunn, V.A. Clark, Wiley, New York, (1974)
- [56] K. Pearson, *Philos. Trans. Royal Soc. London Ser. A*, 187 (1896) 253
- [57] J.L. Rodgers, W.A. Nicewander, *The Amer. Statistician*, 42 (1988) 59
- [58] Kudelski et al. , *Appl. Catal. A* 181 (1999) 123
- [59] M. Janik-Czachor, A. Szummer, A. Molnar, M. Dolata, A. Kudelski, M. Varga, J. Bukoeska, K. Sikorski, *Electrochim. Acta* **45** (2000) 3295
- [60] M. Janik-Czachor, A. Kudelski, M. Dolata, M. Varga, A. Szummer, A. Molnar and J. Bukowska, *Mater. Sci. & Eng. A* 267 (1999) 227
- [61] M. Janik-Czachor, A. Szummer, J. Bukowska, A. Molnar, P. Mack, S.M. Filipek, P. Kedzierzawski, A. Kudelski, M. Pisarek, M. Dolata, M. Varga, *Appl. Catal. A* 235 (2002) 157
- [62] G.A. Almyras, G.M. Matenoglou, P. Komninou, C. Kosmidis, P. Patsalas, G.A. Evangelakis, *J. Appl. Phys.* 107 (2010) 084313

Conclusions and Outlook

This chapter gathers the most important results (sorted thematically) of this dissertation along with some suggestions for future research.

Microstructure - Stoichiometry and Temperature

Concerning the role of the temperature and the systems' stoichiometry in the microstructure of metallic glasses, it came out that even at the highest temperatures of 2000K (well above the melting point) the basic structural unit of Metallic Glasses is the icosahedral-like clusters (ICO). The ICO number increases continuously in all stoichiometries, upon the solidification process, reaching a maximum value at RT.

Moreover, it was noticed that, with the exception of the Zr-richer system, these clusters were Cu-centered, while their number and their Cu content increases with Cu concentration, not only at RT but also at various temperatures around T_g , namely at 600K, 700K and 800K. Summarizing, we could say that upon cooling the solidification process is achieved via the formation and the evolution of these ICO clusters.

Microstructure - Tensile deformation; Bulk systems and systems with free surfaces.

The bulk systems exhibit higher Young moduli and yield strengths as the Cu content (%) in $\text{Cu}_x\text{Zr}_{1-x}$ increases, while they fail earlier upon tensile deformation under constant strain rate. This fact is highly correlated with the number of ICOs and their evolution. The richer stoichiometries in Cu (%) contain more ICOS, at equilibrium, but in all stoichiometries their number decreases and the evolution of their number matches with the corresponding stress strain curves. Regarding the influence of the strain rate on the mechanical behavior,

the bulk systems don't exhibit strain rate sensitivity, which means that for such high rates the produced stresses are almost identical, the phenomenon being reflected in the ICO's evolution.

The systems with free surfaces appear to have slightly higher Young moduli and yield strengths when Cu (%) content increases and higher ultimate tensile strengths. None of the stoichiometries fail till a strain value of 40%, however the stress starts decreasing after the strain value that corresponds to the ultimate stress. Focusing on the evolution of the ICO clusters, they evolve in a different way than in the bulk systems. More specifically, they remain almost constant in number till the elastic limit, thus permitting the reversibility of the deformation denoting that no changes took place in the free volume of the system. Beyond the elastic limit they decrease continuously, leading in increase of the free volume of the system, and thus higher stresses, while after a certain strain value they saturate around a mean value, similarly with the evolution of the stress. In the stoichiometries in which higher rate of decrease was found the ICOS exhibit a slight increase of their number (decrease of free volume).

Moreover, systems with free surfaces exhibit positive strain rate sensitivity which means greater resistance to necking, contrary to their bulk counterparts that display zero strain rate sensitivity. The evolution of the total number of clusters is directly correlated with the evolution of stress. Most of the changes in stress are accompanied by simultaneous changes in the number of clusters upon deformation.

Mechanical behaviour of 1D and 2D nanosized systems and microstructure Nanosized glassy foils exhibit larger plastic region than the glassy ribbons and the also the formers exhibit positive SRS. Moreover there is no significant change in stress-strain curves for thickness greater than 2.8 (nm) for both types of systems and they also appear to have same Young Modulus. In the case of the exhaustive study of the tensile deformation of a foil till fracture, it came out that the systems with this geometry exhibit extremely large ductility. The ICOs number remains constant till the elastic limit and then it decreases continuously until the strain value that corresponds to the ultimate strength. Beyond this strain it oscillates around a mean value of about 12% but it exhibits two significant steps not visible in the corresponding SSC. It came out by a 3D graphical representation of the system that the first remarkable step corresponds to the onset of necking and the second to that state of the system right before its failure. These results suggest that sometimes an exhaustive study of ICOS evolution gives more information about the deformation accommodation than the SSC itself.

Clusters as building blocks of MGs

Taking into account that ICO clusters are the main building blocks of MGs, we investigated whether a metallic glass could be created by direct deposition (soft-landing) of these clusters on a glassy substrate of $\text{Cu}_{50}\text{Zr}_{50}$. To this end, we first examined the changes in the geometrical characteristics of the deposited clusters, of various sizes and compositions, before and after the deposition. The structural changes of the clusters after their deposition were assessed by means of the % changes of the gyration radii, the equilibrated locations of the center masses, the percentages of the remaining ICO atoms above the surface along with their final stoichiometries. It came out that as the cluster size

and the Zr content of the clusters were increased, the clusters remained more compact and their penetration depth into surface was smaller.

Focusing on the consequences that may derive from the cluster deposition we calculated the changes induced in the surface energies. We found that upon Zr-rich ICO deposition, the active surface area was increased and the surface energy was lowered, in contrast to Cu-rich ICO clusters depositions cases that resulted in less stable substrates. In order to check the reliability of our results we examine some specific cases with another interatomic potential, namely with an embedded-atom potential (EAM). It came out that, despite the differences in the absolute values, both potential models yielded the same trends for the surface energies.

In addition, in our effort to ensure that the effect of the high cooling rate imposed by the MD simulations restrictions does not influence qualitatively the obtained results, we performed two additional simulations depositing the larger Zr ICO on two different substrates prepared with faster and slower by an order of magnitude cooling rates. We found that the different cooling rates alter the obtained results, which nevertheless differ only in the absolute values and not qualitatively, thus leading to the conclusion that despite the different cooling rates, the trends in all calculated quantities remain the same.

Future work

One of the most interesting issues for future study, could be the addition of a third element e.g Al for which it is known that a small amount in CuZr increases the ductility of the resulting alloy and enhances the Young Modulus compared with the binary counterpart. However the changes induced in the microstructure by the small Al additions resulting to the enhanced properties of the resulting alloy remain an open question. It could be useful to understand how the size of a third element and its electronic nature influences the microstructure and how the latter, in turn influences the mechanical properties of the alloy. Understanding the role of the addition could lead hopefully to the prediction of the mechanical properties of an alloy when a third element with similar or different size is added.

Concerning the deposition of icosahedral clusters as an alternative way to create a metallic glass from its building blocks, one could perform Density Functional Theory (DFT) calculations in order to gain deeper insight on the interactions between the deposited clusters due to their electronic nature, information that misses from MD calculations. Moreover it should be tested how the rate of deposition influences the stability of the deposited clusters. The information that could be gained from such calculations could define the appropriate size and the stoichiometry of the clusters that have to be deposited in order to end up with a fully glassy structure.

Another interesting issue that should be studied by means of Molecular Dynamic Simulations is how the nanocrystalline inclusions in a metallic glass enhance the ductility of the glass by suppressing the propagation of the shear bands. One should investigate the mechanism that takes place upon the suppression of the shear band by studying how the presence of crystalline phase affects the glassy environment.

Moreover concerning the Shear Bands which are narrow regions of the alloys with dimensions of 10-20 nm where the stress is localized and cause the failure of metallic glasses, one should calculate the atomic strains of the atoms upon tensile deformation and thus detect the plains where the atoms with highest atomic strains are concentrated. Additionally a structural analysis could reveal if the atoms of these plains belong to clusters and thus answer to the open question if shear bands are in fact networks of clusters.

Additionally it should be tested whether the high correlation existing between stress and ICO evolution upon tension occurs in other types of deformation, namely upon compression, indentation or shear deformation.

Publications

- 1) A.E. Lagogianni, G.A. Almyras, Ch.E. Lekka, D.G. Papageorgiou, and G.A. Evangelakis, *J. Alloys and Compd*, 483 ,(2009), 658
- 2) A.E. Lagogianni, D.G. Papageorgiou, G.A. Evangelakis, *Comput. Materials Science* 54, (2012), 145-149
- 3) G.B. Bokas, A.E. Lagogianni, G.A. Almyras, Ch.E. Lekka, D.G. Papageorgiou, G.A. Evangelakis, *Intermetallics*, 43, (2013),138

Conference contributions

- 1) A. Lagogianni, G.A. Evangelakis, “*Microstructure evolution in Cu_xZr_{100-x} metallic glasses under tensile deformation.*” XXV Panhellenic Conference on solid state physics and materials science” Thessaloniki, Greece, September 2009 (Poster)
- 2) A. Lagogianni, G.A Evangelakis, “*Molecular Dynamics Simulations of softly landed Cu, Zr and Cu_xZr_{1-x} icosahedral clusters on $Cu_{50}Zr_{50}$ glassy ribbon*”, 3rd International Conference on Advanced Plasma Technologies, Lake Bohinj, Slovenia, June 2010 (Poster)
- 3) A.E. Lagogianni, G.A Evangelakis, “*Surface Functionalization by means of softly landed Icosahedral Cu_xZr_{1-x} Clusters on $Cu_{50}Zr_{50}$ Metallic Glass* ”, XXVI Hellenic Conference of Solid State Physics and Materials , Ioannina, Greece, September 2010 (Poster)
- 4) A.E. Lagogianni, G.A Evangelakis, “*Mechanical properties of $Cu_{50}Zr_{50}$ glassy nano-ribbons and nano-foils*”, 18th International Symposium of Metastable and Amorphous Materials (ISMANAM), Gijón, Spain, June 2011 (Poster)

- 5) A.E. Lagogianni, G.A Evangelakis, “*Microstructure-Stress Correlations in Cu₅₀Zr₅₀ glassy Nano-Foils by Molecular Dynamics Simulations*”, 19th International Symposium of Metastable and Amorphous Materials (ISMANAM), Moscow, Russia, June 2012 (Poster)
- 6) A.E. Lagogianni and G.A Evangelakis, “*Microstructure And Tensile Response Of Cu₅₀Zr₅₀ Glassy Nano-Foils By Molecular Dynamics Simulations*”, XXVIII Hellenic Conference of Solid State Physics and Materials, Patra, Greece, September 2012, (oral)
- 7) A.E. Lagogianni, G.A. Evangelakis, “Microstructural alterations under tensile deformation of Cu-Zr model nanofoils by Molecular Dynamics Simulations.”, XIV International Conference on Intergranular And Interphase Boundaries In Materials (IIB 2013) Halikidiki, Greece, June 2013 (Poster)
- 8) J. Antonowicz, A. Pietnoczka, A.R. Yavari, A.E. Lagogianni, G.A. Evangelakis, O. Mathon, I. Kantor, S. Pascarelli, T. Shinmei, T. Irifune “*Short-range order in Zr₆₇Cu₃₃ metallic glass under high pressure*” 20th International Symposium of Metastable and Amorphous Materials (ISMANAM), Turin, Italy, July 2013 (Talk)
- 9) A.E. Lagogianni, G.A Evangelakis, “*Mechanical response and icosahedral clusters evolution in glassy Cu₅₀Zr₅₀ nanofoil and bulk systems by molecular dynamic simulations.*” 20th International Symposium of Metastable and Amorphous Materials (ISMANAM), Turin, Italy, July 2013 (Talk)
- 10) G.B. Bokas, A.E. Lagogianni, G.A. Almyras, Ch.E. Lekka, D.G. Papageorgiou, G.A. Evangelakis, “*On the role of Icosahedral-like clusters in the solidification and mechanical response of Cu-Zr metallic glasses by Density Functional Theory*”, 20th International Symposium of Metastable and Amorphous Materials (ISMANAM), Turin, Italy, July 2013 (Poster)

- 11) G. B. Bokas, A. E. Lagogianni, G. A. Almyras, Ch. E. Lekka, D. G. Papageorgiou, G. A. Evangelakis, “*On the role of Icosahedral-like clusters in the solidification and mechanical response of Cu-Zr metallic glasses by Density Functional Theory*” XXIX Hellenic Conference of Solid State Physics and Materials, Athens, Greece, September 2013 (Talk)